



## Deliverable D4.1.3 – Innovations on component level (final report)

Agreement n.:	308974
Duration	November 2012 – October 2017
Co-ordinator:	Danmarks Tekniske Universitet
Supported by:	



The research leading to these results has received funding from the European Community's Seventh Framework Programme FP7-ENERGY-2012-1-2STAGE under grant agreement No. 308974 (INNWIND.EU).

---

#### PROPRIETARY RIGHTS STATEMENT

This document contains information, which is proprietary to the "INNWIND.EU" Consortium. Neither this document nor the information contained herein shall be used, duplicated or communicated by any means to any third party, in whole or in parts, except with prior written consent of the "INNWIND.EU" consortium.

---

# Document information

<b>Document Name:</b>	Deliverable D4.1.3. – Innovations on component level (final report)
<b>Confidentiality Class:</b>	Public
<b>Document Number:</b>	Deliverable D 4.1.3
<b>Author:</b>	Niklas Scholle, Luka Radulović (LUH) Rogier Nijssen (WMC) Lars Bo Ibsen (AAU) Martin Kohlmeier, Aligi Foglia (FhG-H) Anand Natarajan (DTU) Jennifer Thiel (FhG-DA) Bernd Kuhnle, Martin Kraft, Martin Kühn (UOL) Phlipp Brosche (FhG-KS) Daniel Kaufer (RAW)
<b>Review:</b>	Niklas Scholle, Luka Radulović
<b>Date:</b>	2015-09-11
<b>WP:</b>	4 Offshore Foundations and Support Structures
<b>Task:</b>	4.1 Innovations on component level for bottom-based structures

## 1 TABLE OF CONTENTS

<b>1</b>	<b>TABLE OF CONTENTS .....</b>	<b>3</b>
<b>2</b>	<b>INTRODUCTION .....</b>	<b>7</b>
	References.....	8
<b>3</b>	<b>INNOVATIVE MATERIALS (LUH, WMC).....</b>	<b>9</b>
3.1	Sandwich material for tubes.....	10
3.1.1	Shell buckling design of sandwich components.....	10
	Optimized buckling capacity of steel shells under axial load .....	10
	Optimized buckling capacity of sandwich shells under axial load.....	12
	Buckling capacity under bending moment .....	13
3.1.2	Results of the performed studies of innovations on component level.....	14
3.1.3	Current TRL of innovations and recommendations for their further development .....	18
3.1.4	Cost reduction potential of innovations on component level .....	19
3.2	Sandwich material for connections and joints .....	20
3.2.1	Discussion of the considered innovations on component level .....	20
3.2.2	Description of the performed studies of innovations on component level.....	20
3.2.3	Results of the performed studies of innovations on component level.....	22
3.2.4	Current TRL of innovations and recommendations for their further development .....	22
3.2.5	Cost reduction potential of innovations on component level .....	23
3.3	Conclusions .....	24
	References.....	25
<b>4</b>	<b>SOIL &amp; FOUNDATION (AAU, FhG-H, DTU) .....</b>	<b>26</b>
4.1	Suction bucket foundations.....	27
4.1.1	Comparison of calculation methods for bearing capacity.....	27
	CASE STUDY OF COMPRESSIVE CAPACITY.....	31
	Soil Parameters .....	32
	Geometry of the Foundation .....	32
	Comparison.....	33
4.1.2	Comparison of calculation methods for tensile capacity .....	34
4.1.3	Test Equipment.....	35
	Sand box .....	36
	Bucket Models.....	37
	Loading and measuring systems.....	37
	Soil Description.....	38
	Soil preparation .....	38
	CPT tests .....	39
	<b>Test procedures.....</b>	<b>39</b>
	Test without membrane .....	40
	Test with membrane.....	40
4.1.4	Results presentation .....	41
	Static test without overburden pressure.....	41
	Cyclic test without overburden pressure .....	42
4.1.5	CPT based method installation methode.....	43
	DNV CPT-based installation method. ....	43

Senders (2008) CPT-based installation method. ....	44
Validation of installation CPT-based methods .....	45
Pull-out CPT-based method.....	46
Validation of pull-out CPT-based methods.....	46
4.1.6 Required experimental investigations on innovations on component level .....	49
4.1.7 Economical and technical advantages of Jacket with bucket foundation .....	49
4.2 Vibratory-driven piles for jacket sub-structures.....	52
4.2.1 Introduction and motivation .....	52
Introduction to piled foundation for offshore wind converters .....	52
Vibratory pile driving.....	53
Scope of the report.....	54
4.2.2 Tensile capacity of vibratory-driven piles .....	55
Introduction to CPT methods .....	55
Interpretation of the test results by means of CPT methods .....	55
4.2.3 Stiffness of vibratory-driven piles .....	58
2D-Axisymmetric numerical model.....	58
4.2.4 Current TRL and cost reduction potential of vibro-driven piles .....	62
4.3 Innovative foundations .....	64
4.3.1 Discussion of the considered innovations on component level .....	64
4.3.2 Description of the performed studies of innovations on component level.....	65
Mooring system .....	65
Universal joint .....	66
Reinforced concrete base.....	69
Design load cases .....	70
4.3.3 Results of the performed studies of innovations on component level.....	71
At component level.....	71
At the global level .....	72
Installation process .....	72
4.3.4 Current TRL of innovations and recommendations for their further development .....	74
4.3.5 Cost reduction potential of innovations on component level .....	74
4.3.6 Appendixes .....	75
Appendix 4.3-A: Preliminary design of catenary lines .....	75
4.3.7 Conclusions .....	76
4.4 Conclusions .....	77
References.....	77
<b>5 LOAD MITIGATION (FhG-DA, UOL, FhG-KS) .....</b>	<b>81</b>
5.1 Passive damping devices.....	82
5.1.1 Discussion of the considered innovations on component level .....	82
Simulation Model.....	82
Passive Vibration Absorber Design.....	83
5.1.2 Description of the performed studies of innovations on component level.....	84
Positioning .....	84
Numerical Analyses .....	85

5.1.3	Results of the performed studies of innovations on component level.....	85
	Results Modal Analysis .....	85
5.1.4	Current TRL of innovations and recommendations for their further development .....	87
5.1.5	Cost reduction potential of innovations on component level .....	87
5.1.6	Required further development of innovations (with a focus on challenges related to the upscaling from 10 MW to 20 MW wind turbine).....	88
5.2	Tuned Mass Dampers at Tower Top.....	89
5.2.1	Discussion of the considered innovations on component level .....	89
	Change of frequency relation.....	89
	Usage of speed exclusion window .....	90
5.2.2	Description of the performed studies of innovations on component level .....	90
	Boundary conditions.....	90
	Identification of critical components.....	90
	Structural damping by tuning the ratio between eigenfrequency and excitation frequency .....	91
	Parameter study for mass damper.....	91
5.2.3	Results of the performed studies of innovations on component level.....	92
	Optimization of the ratio between first eigenfrequency and rotor rotating frequency .....	92
	Parameter study on tuned mass dampers .....	95
5.2.4	Conclusion and assumed impact of innovations on component level.....	98
5.2.5	Required further development of innovations (with a focus on challenges related to the upscaling from 10 MW to 20 MW wind turbine).....	99
5.3	Semi-active and active damping devices.....	100
5.3.1	Discussion of the considered innovations on component level .....	100
	Implementation and analysis of the reference structure in GH Bladed.....	100
	Semi-active damper with liquid in a U-tube or multiple U-tube arrangements with control of the flow.....	100
	Semi active viscous dampers .....	100
	Active tower damping by Pitch or Torque Control.....	101
5.3.2	Description and results of the performed studies of innovations on component level	101
5.3.3	Conclusion and assumed impact of innovations on component level.....	101
5.3.4	Required further development of innovations (with a focus on challenges related to the upscaling from 10 MW to 20 MW wind turbine).....	101
5.3.5	Discussion of the considered innovations on component level .....	102
	Speed exclusion zone.....	102
	Peak Shaving .....	103
	Active tower damping.....	104
5.3.6	Description and results of the performed studies of innovations on component level	107
	In the following two of the concepts introduced before have been analysed by numerical investigations of the INN WIND.EU reference turbine. This includes the peak shaver and the active tower damping.....	107
	Peak Shaving .....	107
	Active tower damping.....	109
5.4	Conclusions and Recommendations .....	111

References .....	111
<b>6 MANUFACTURING (RAW) .....</b>	<b>114</b>
6.1 Jacket Transition Piece Concepts.....	115
6.1.1 Introduction.....	115
6.1.2 Overview.....	115
6.1.3 Design Study.....	120
Introduction.....	120
Design Procedure .....	120
Boundary Conditions .....	122
Load Description for the Advanced Finite Element Analysis of the TP.....	122
Discretization .....	123
Material Properties.....	125
Results of the TP Design Study.....	126
6.1.4 Cost Evaluation of TPs.....	130
6.1.5 Current TRL of Innovations and Recommendations for their further Development....	130
6.1.6 Conclusion .....	130
6.2 Jacket Assembly Concepts and Cost Optimization.....	132
6.2.1 Fabrication Cost Model .....	132
6.2.2 Assembly Concepts .....	133
6.2.3 Contribution to Cost Reduction.....	134
6.2.4 Technical Readiness Level.....	135
6.2.5 Conclusions .....	135
References.....	135
<b>7 Conclusions.....</b>	<b>136</b>

## 2 INTRODUCTION

Levelised cost of energy (LCOE) is one of the main decision drivers for or against offshore wind exploitation. Recent projects indicated actual LCOEs of around 165 € per MWh [2-01]. A reduction is highly desired, if not even necessary, for a further deployment of offshore wind energy. A study by the Crown Estate [2-01] indicates possible reduction up to under 100 € per MWh until 2020, which would be a reduction of 37.5%. Various fields were identified, which might contribute achieving this goal. Innovations regarding the support structure were one of those. Therefore, a reduction of costs of at least 20% is aimed for in the description of work during the course of this project [2-02] to significantly contribute to the realisation of the goal in cost reduction. Furthermore, risks and possibilities will be assessed.

The prospects of completely new concepts are expected to be minor, wherefore the focus in task 4.1. is on “Innovations on component level”. Relevant topics for future cost-effective, mass-producible designs were identified, such as new foundation types (without grout and/or piling), soil-structure-interaction of large piles or suction buckets, innovative transition piece designs or designs using hybrid materials never employed in wind energy before. In addition, design integration using jacket-specific controls and innovative fabrication and installation processes shall complete the overall cost saving potentials.

The following fields of interest, illustrated by Figure 2-1, are found in the sections of this report:

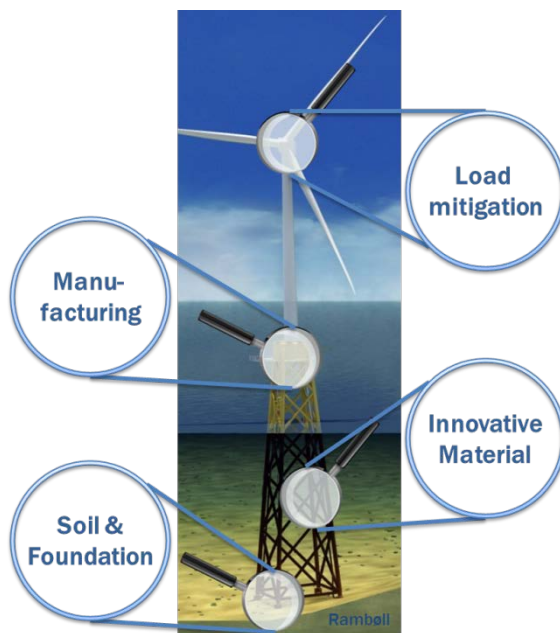


Figure 2-1: Subfields in task 4.1.

### **Innovative materials:**

Hybrid materials, such as sandwich structures are introduced in section 3 by the partners Leibniz University of Hannover (LUH) and Knowledge Centre Wind turbine Materials and Constructions (WMC).

### **Soil & foundation:**

Improvements in the modelling and numerical simulation of the soil structure interaction as well as innovative support structure and foundation designs are treated in section 4 by the Fraunhofer Institute IWES Hannover (FhG-H), the Danish Technical University (DTU) and Aalborg University (AAU).

### **Load mitigation:**

Concepts for load mitigation, such as jacket-specific and structural control are investigated in section 5 by the Fraunhofer Institutes LBF Darmstadt (FhG-DA) and IWES Kassel (FhG-KS), as well as by the Danish Technical University (DTU) and ForWind Oldenburg (UOL).

### **Manufacturing:**

Rambøll (RAMBOLL) is focusing on innovations in manufacturing, mass-production and installation in section 6.

The references used in the partners’ contributions are listed directly subsequent to the corresponding chapter.

In this report, the cost reduction potential and the current Technical Readiness Level (TRL) are discussed for the proposed innovations. In Table 7-1 in Chapter 7 several cost items are listed. Per innovation, a potential in cost reduction is expressed in percentages. The motivation for these numbers is discussed in the relevant chapters.

## References

- [2-01] The Crown Estate, "Offshore Wind Cost Reduction: Pathways Study", 2012.
- [2-02] InnWind.eu, "Annex I - "Description of Work"", Grant agreement no: 308974, 2012



### 3 INNOVATIVE MATERIALS (LUH, WMC)

The goal of section 3 is the investigation of innovative hybrid materials with the aim of cost reduction through reduced material use and reduced fabrication costs. Reducing material use requires optimization of material use and the use of materials with higher loading capacity. High strength steels can withstand higher stresses and enable the use of thinner walled members. However, the minimum wall thickness does not only depend on the allowable stress, but also on the resistance against buckling or wrinkling. A way to circumvent this limit is to move to a sandwich structure especially with regard to large water depths and longer span width of chords and braces.

Another challenge when moving to higher strength materials is to achieve sufficient joint strength. Often the joints are the critical parts in a truss structure, especially when considering fatigue loading. In a welded structure the fatigue life of the structure is commonly governed by the fatigue life of the welds. Welding also proposes a challenge in the use of high strength steels, as the weld fatigue strength hardly improved for higher strength steels. Therefore, to utilize the higher (fatigue) strength of such steels better joining methods have to be developed.

University of Hannover (LUH) is focusing on numerical and experimental investigation of sandwich tubes of as well as on developing pre-design methods for sandwich tubes and their application on the chords and braces of the INN WIND.EU reference jacket design [3-01] (Subchapter 3.1). In Deliverable 4.12 [3-02] the previously developed methods and performed tests for the estimation of bearing capacity of sandwich towers for wind energy converters are presented (see [3-03] & [3-04]). The existing methods and tests do not consider the combination of bending moment and axial force loading which represents a characteristic load situation in case of chords and braces of jacket substructure for OWEC. In the present deliverable the behavior of sandwich tubes under this specific loading will be investigated. To achieve this, a test plan has been created and specimens of sandwich components have been tested statically under eccentric compressive load [3-05]. These tests represent the starting point for investigation of the bearing capacity of chord and braces of the jacket in Innwind.eu project.

While sandwich tubular construction can provide a structurally efficient solution by circumventing buckling limits, joining of sandwich steel structures provides a challenge. The aim of the preliminary experimental program of WMC is to evaluate the potential of bonded joints for joining tubular steel sections. For this purpose static and fatigue experiments are performed on bonded steel specimens in Deliverable 4.12. An additional challenge is the combination of sandwich tubes with adhesive connections, since these results in relatively thin-walled structures, as well as potential interaction between the steel-adhesive-steel overlaps and the sandwich core, which might lead to unwanted fatigue damage. In the current report, the results of the test on the adhesive connection between sandwich tube and steel tube (see Deliverable 4.14 [3-05]) are discussed.

### 3.1 Sandwich material for tubes

To be suitable for use as structural components of supporting structures of OWT, sandwich tubes must have bearing capacity comparable to those of steel tubes. Considering that the present European and national codes are not covering fully this type of structural element, general methods for estimating the bearing capacity of different types of sandwich tubes developed in Keindorf [3-03] have been presented in Deliverable 4.12 [3-02]. The outcomes of these methods applied to a 90 m high tower for wind turbines with an outer diameter of 5.5 m, constructed with different types of sandwich tube (Figure 3.1-1) have been shown. Different types of core material (grout, elastomer, and concrete) and different steel grades (S235, S355, S460 and S690) of steel for the outer and inner face of sandwich tubes have been used. The aim was to determine which combination of core material and steel grade would lead to the greatest benefits in terms of bearing capacity (and afterwards stability) of the tower. The methods developed in Keindorf [3-02] represented the starting point for investigating bearing capacity of chord and braces of the jacket in Innwind.eu project.

In order to be able to use the bearing capacity according to the methods shown in [3-02] a potential shell buckling issues of the sandwich tubes must be avoided. In the present deliverable a proposal from Keindorf based on the EC3 1-6 and DIN 18800 has been presented.

Another important aspect of the sandwich material used for the chords and braces of a jacket sub-structures considers the bearing capacity of the tubes under a simultaneous action of axial force and bending moment. This kind of loading has not been studied before and for this reasons experimental tests have been performed. Namely, sandwich tubes with grout as core material have tested statically under eccentric compressive load in order determine their bearing capacity. Afterwards, a FE model of the tube have been created and calibrated according to the experimental results and a M-N interaction diagram have been obtained.

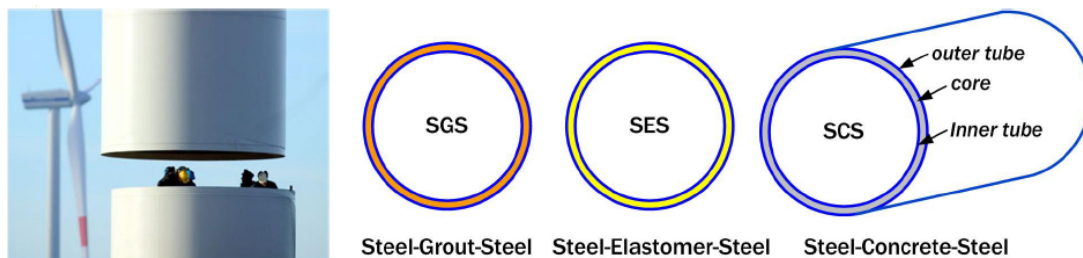


Figure 3.1-1 – Steel and different types of sandwich structures

#### 3.1.1 Shell buckling design of sandwich components

As already mentioned, the Deliverable 4.12 [3-02] describes methods for calculating bearing capacity of the sandwich tubes without considering shell buckling of such structural elements. The tubes shall be classified as shell structures and therefore a suitable design against buckling is also necessary. Here are presented the results from [3-03] for a 90 m high tower for wind turbines with an outer diameter of 5.5 m. Anyway, in the same way the following procedure can be used also from chords and braces of the jacket sub-structure for OWT.

##### Optimized buckling capacity of steel shells under axial load

According to EC3-1-6 and previously in Germany valid norm DIN 18800-4 shell steel structures made in steel have allowable characteristic or real buckling stress  $\sigma_{x,Rcr}$  (Eq. 3.1-2) which is usually lower than the yield stress  $f_{y,k}$ . This real buckling stress depends on the relative shell slenderness ( $\bar{\lambda}_s$ ) (Eq. 3.1-1), type of the loading and class of imperfection. In case of the axial compression the reduction factor according to EC3 Class 3 or DIN 18800-4 curve  $k_2$  has to be used (see Figure 3.1-2):

$$\bar{\lambda}_s = \sqrt{f_{yk}/\sigma_{x,Rcr}} \quad \text{Eq. 3.1-1}$$

$$\sigma_{x,Rcr} = \chi * f_{y,k} \quad \text{Eq. 3.1-2}$$

where:  $\chi = f(\bar{\lambda}_s)$

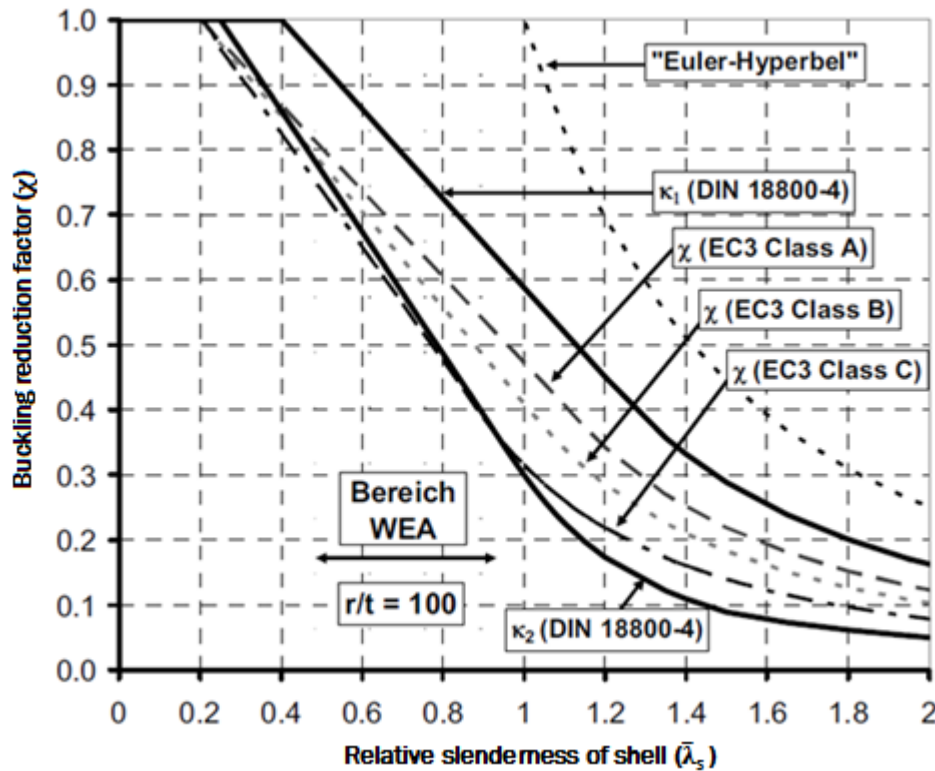


Figure 3.1-2 – Buckling reduction curves according to EC3-1-6 and DIN 18800-4 for shells loaded by axial compression

In order to avoid any shell buckling in elastic range, the shell can be optimized so that no reduction of the yield stress is necessary. This is achieved by reducing the relative slenderness below 0.2 according to EC3-1-6 and 0.25 according to DIN 18800-4. Thus:

$$\bar{\lambda}_s = \sqrt{\frac{f_{yk}}{\sigma_{x,Rcr}}} = 0.20 \text{ for } \chi = 1 \text{ acc. to EC3-1-6 (Class C)}$$

or

$$\bar{\lambda}_s = \sqrt{\frac{f_{yk}}{\sigma_{x,Rcr}}} = 0.25 \text{ for } k_2 = 1 \text{ acc. to DIN 18800-4}$$

Eq. 3.1-3

Knowing the necessary relative slenderness it is possible to calculate the optimized elastic critical buckling stress. In this case the results for steel shell with steel grade S235 and S460 will be given:

$$\sigma_{x,Rcr}(S235) = 3760 \text{ MPa}$$

$$\sigma_{x,Rcr}(S460) = 7360 \text{ MPa}$$

In this way the best configuration regarding the shell stability and utilization in the elastic range can be reached.

### Optimized buckling capacity of sandwich shells under axial load

A buckling linear analysis have been carried out in [3-03] for sandwich shells with different core thickness under axial load in order to get the optimized elastic critical buckling stress. In Figure 3.1-3 and Figure 3.1-4 the results of the parameter study for shells with steel grade S235 and S460 have been summarized. The critical buckling stress have been derived from numerical simulation as well as with the shell theories for composite shells presented by Vinson [3-06]. As already stated in [3-02] thickness of the outer and inner steel layers of the sandwich cylinder is 24mm for cylinder with steel S235 and 12mm for cylinder with steel S460. The thickness of the core is varied between 0mm and 80mm.

It can be observed that with an optimized core thickness the steel faces of sandwich shells can be utilize up to the yield stress (red dashed-line in Figure 3.1-3 and Figure 3.1-4 calculated according to Eq. 3.1-3) and no reduction due to shell buckling is necessary. The necessary thickness depends the core material used. In Figure 3.1-4 for SGS S460 where grout has been used as the core material the optimized elastic critical buckling stress has been reached with a core thickness of 70 mm. On the other hand for SCS S460 with concrete as the core material it was necessary a core thickens of 76 mm in order to reach the optimized elastic critical buckling stress. Regarding SES 460 with elastomer as core material, the optimized core thickens is almost 100 mm due to weaker mechanical characteristics of elastomer. By comparing Figure 3.1-3 and Figure 3.1-4 it can be noticed that the higher steel grade is used for the steel faces of sandwich shells, the greater must be also the thickness of the core material in order to reach the optimized elastic critical buckling stress.

Because the substructure for wind turbines (onshore and offshore) are normally designed in the elastic range it is not necessary to increase the buckling stress and core thickness over the optimized values. As previously stated, with the optimized core thickness the steel faces of sandwich shells can be utilize up to the yield stress and therefore no shell buckling in the elastic range should occur.

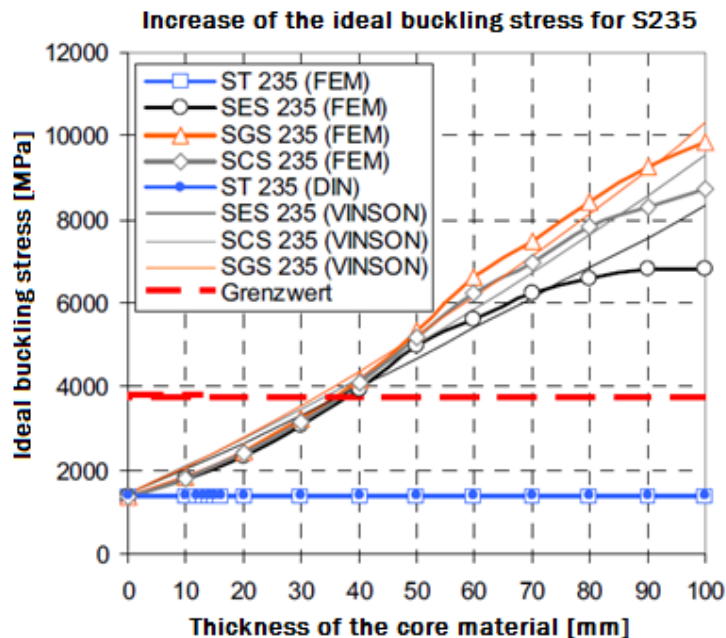


Figure 3.1-3 – Increase of the critical buckling stress under axial load for S235 depending on the core thickness (taken from [3-03])

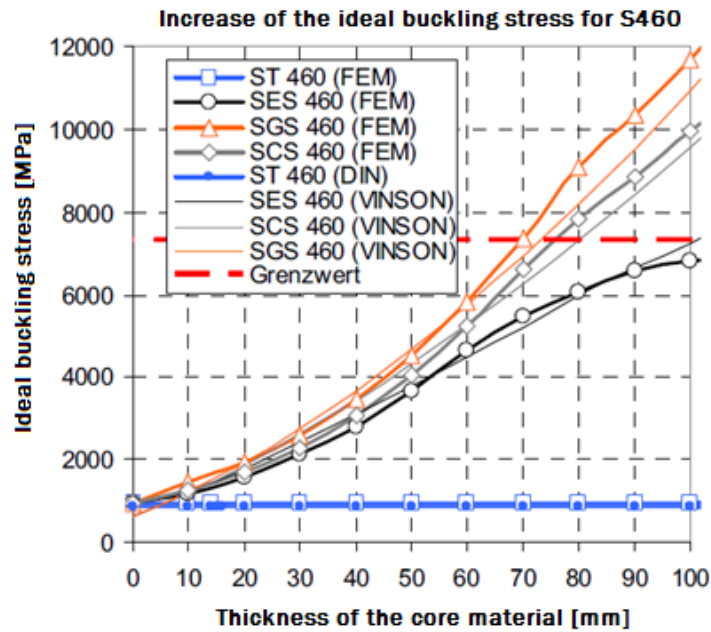


Figure 3.1-4 – Increase of the critical buckling stress under axial load for S460 depending on the core thickness (taken from [3-03])

#### Buckling capacity under bending moment

Additionally, a numerical analysis have been carried out in [3-03] for sandwich shells with different core thickness under bending moment in order to get the optimized elastic critical buckling stress. In Figure 3.1-5 and Figure 3.1-6 the results of the parameter study for shells with steel grade S235 and S460 have been summarized. As previously, the thickness of the outer and inner steel layers of the sandwich cylinder is 24mm for cylinder with steel S235 and 12mm for cylinder with steel S460. The thickness of the core is varied between 0mm and 80mm.

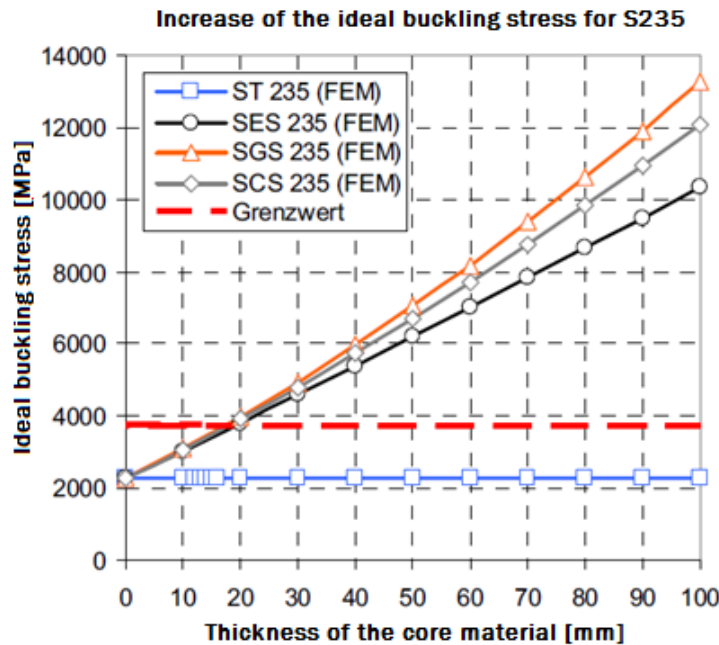


Figure 3.1-5 – Increase of the critical buckling stress under bending moment for S235 depending on the core thickness (taken from [3-03])



By comparing Figure 3.1-5 and Figure 3.1-6 with Figure 3.1-3 and Figure 3.1-4 it can be observed that the necessary core thickness is lower for a shell in case of bending moment compared to the axial loading case in order to reach optimized elastic critical buckling stress. For instance, in Figure 3.1-4 for SGS S460 where grout has been used as the core material, the optimized elastic critical buckling stress has been reached with a core thickness of 70 mm. In case of bending moment loading for the same type SGS S460 the necessary thickness is 54 mm.

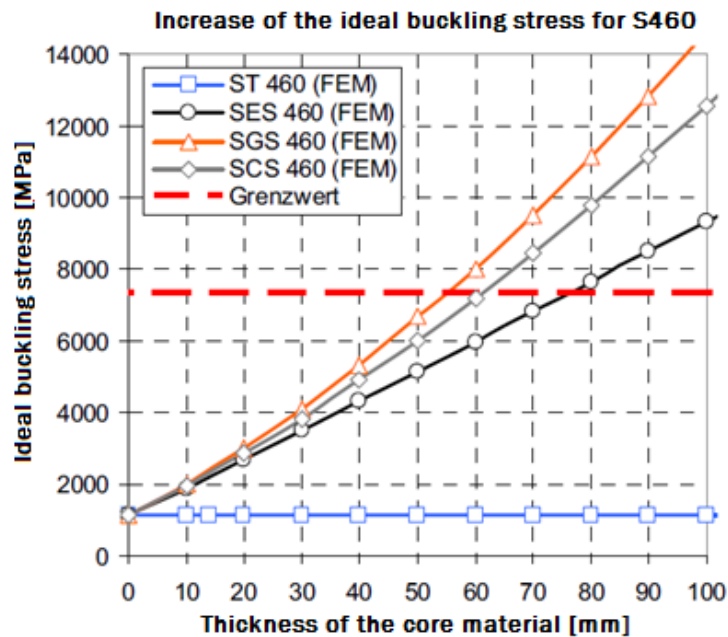


Figure 3.1-6 – Increase of the critical buckling stress under bending moment for S460 depending on the core thickness (taken from [3-03])

### 3.1.2 Results of the performed studies of innovations on component level

Numerical investigations of sandwich component consisting of UHPC as core material under eccentric compression load have been performed using a finite elements model. The model is realized in the commercial CAE software *ABAQUS* (version 6.14-1). The outer steel tube, the inner steel tube and the concrete core are modeled with 8-node brick elements with reduced integration (C3D8R) respectively which leads to a total of about 50.000 degrees of freedom, using the required mesh size that have been determined by a study of convergence.

The elements of the steel tube are implemented by an ideal elastic-plastic material model. The concrete core elements are modeled by a concrete damage plasticity constitutive model. Calibrations of all parameters of the concrete model have been performed upon experimental data. Interactions between the two steel tubes and the concrete core are implemented with general contact. Using surface smoothing assignments between steel tubes and concrete core the component's round characteristics are maintained throughout the discretization in finite elements during preprocessing.

A rigid body tie assignment of the nodes on the front faces represents the bearing condition. Being connected to a reference point which functions as load introduction point eccentricity can be simulated. The experiment's bearing conditions are represented by boundary conditions that prevent any movement and only allow rotation around an axis, while the upper face front's nodes execute a path-controlled moving downwards. The processing is performed by the 'Abaqus/Explicit' Solver with consideration of non-linear effects and large deformation.

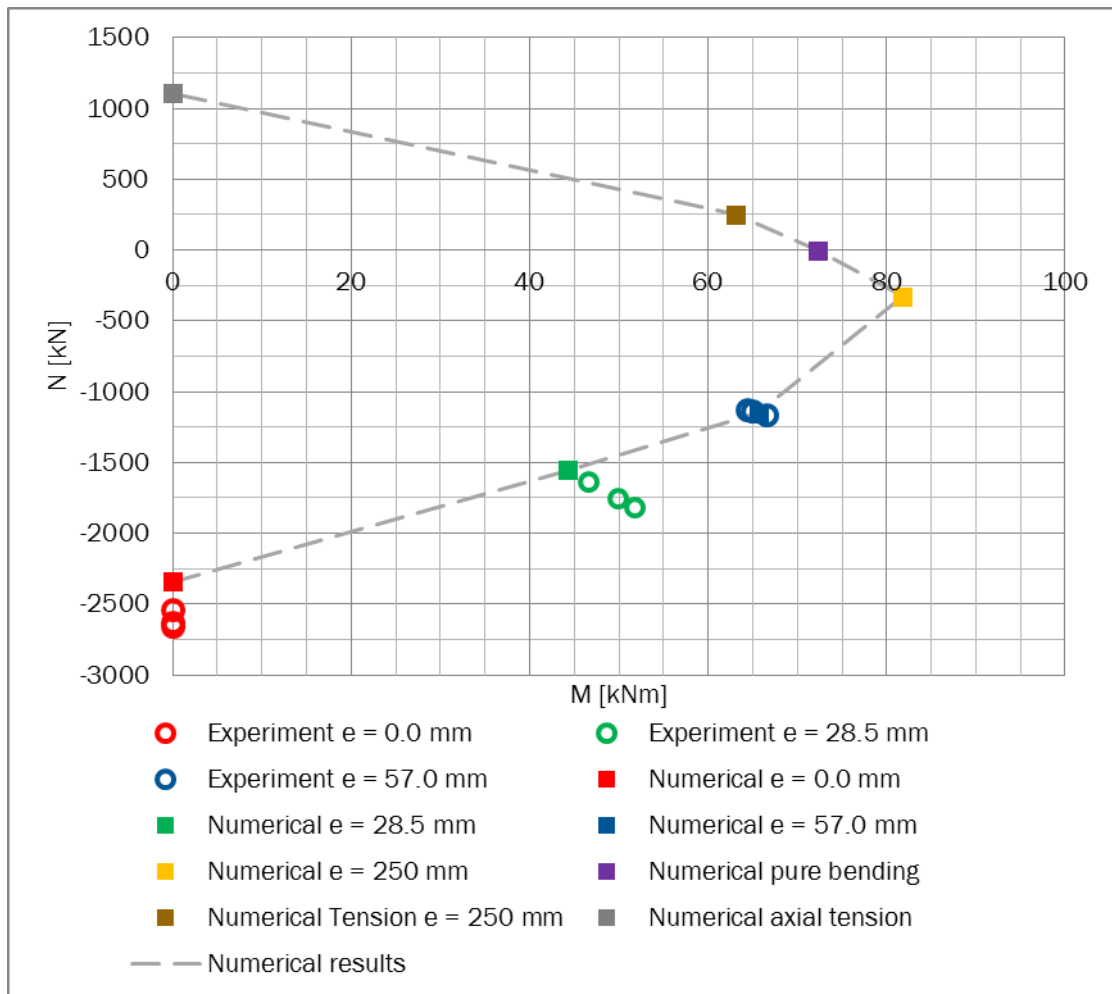


Figure 3.1-7 – Interaction of axial loading and bending

Figure 3.1-7 shows an interaction diagram for axial load and bending for the investigated representative sandwich component. Numerical results as well as the experimental results from Deliverable D4-1-4 [3-05] are included in the diagram. The numerical results show a very good consistency with the experimental results. Further extension of the eccentricities produce expected behaviour. Additional small compression load increases bending capacity whereas additional tension loading led to an approximately linear reduction in bending capacity. Furthermore, different capacities with respect to compressive and tensile loading are apparent from the diagram.

Figure 3.1-8 shows axial stress distribution in the cross section at center of the sandwich component for different eccentricities. In line with expectations, the localization process of compression stresses intensifies with increasing eccentricity due to the unequal strength of the core material in tensile and compression.

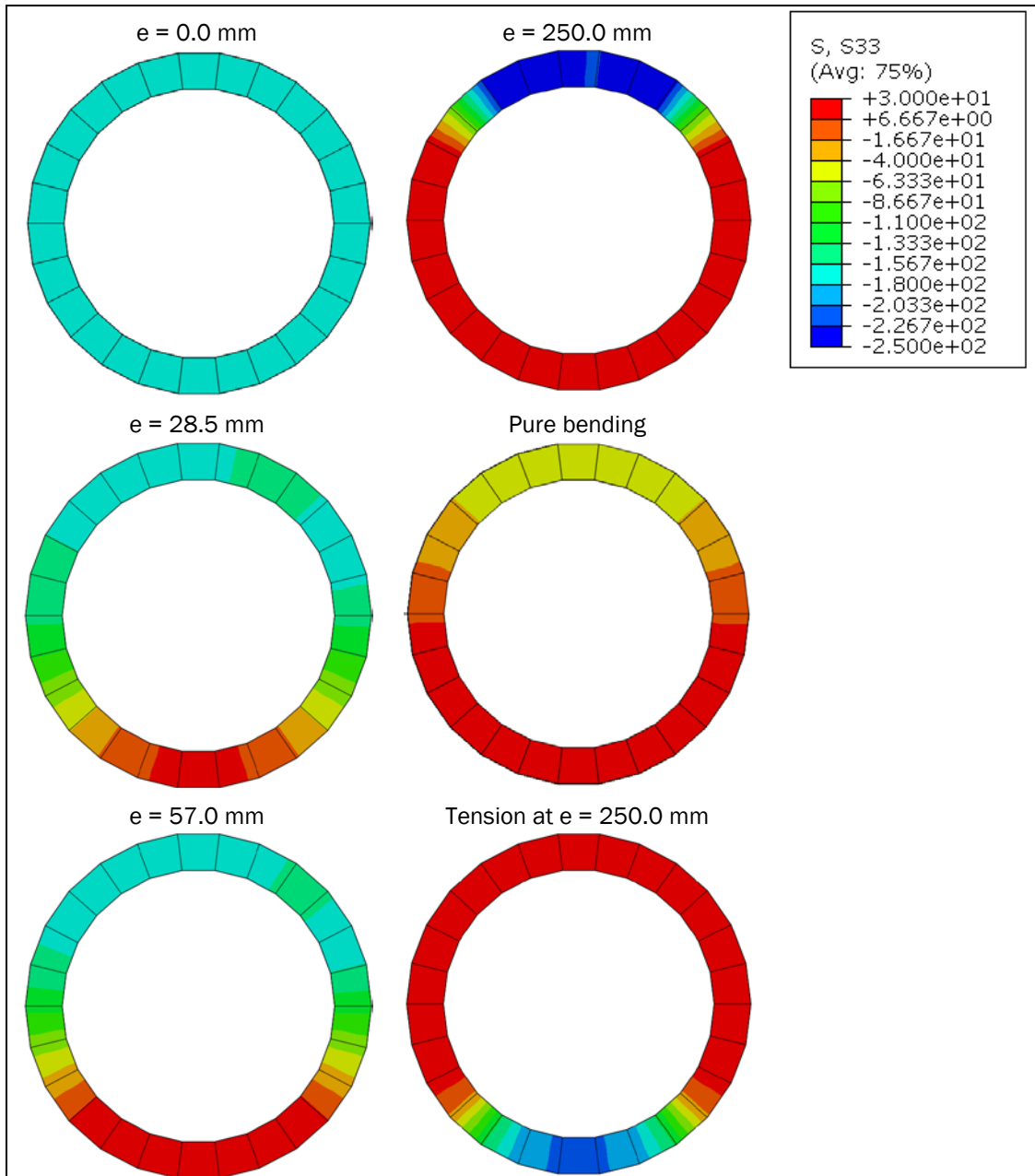


Figure 3.1-8 – Numerical results: axial stress distribution at center of sandwich component



Figure 3.1-9 and Figure 3.1-10 shows the absolute strain of the core material of the simulated sandwich components. Different failure mechanisms can be seen in dependence to the size of eccentricity. In a pure compression ( $e = 0.0$  mm) is a typical compression failure occurs. For small eccentricities ( $e = 28.5$  mm) a shear-induced failure mode can be observed. Increasing eccentricities at first generates mixed compression-tension failure modes until tension failure predominates.

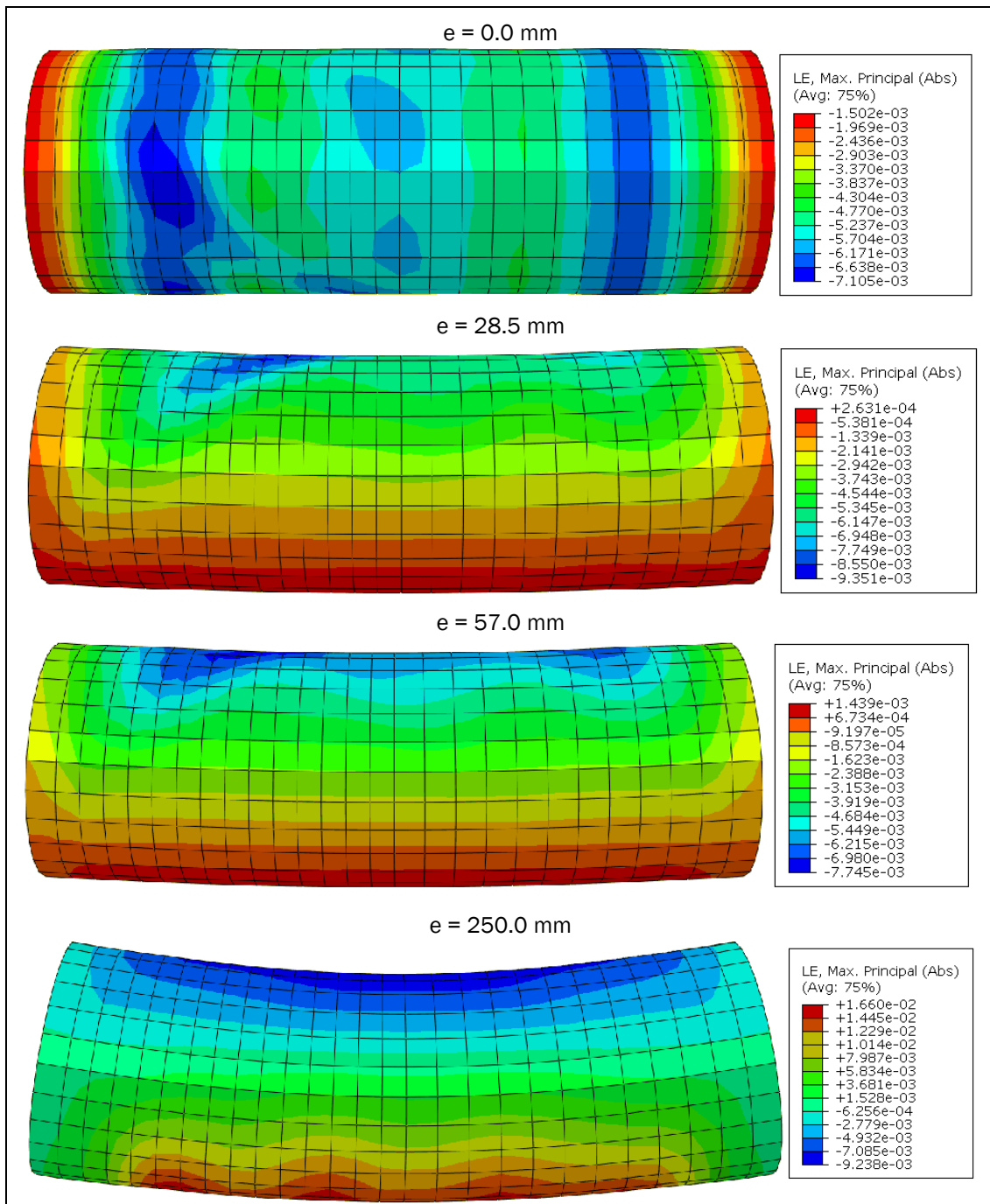
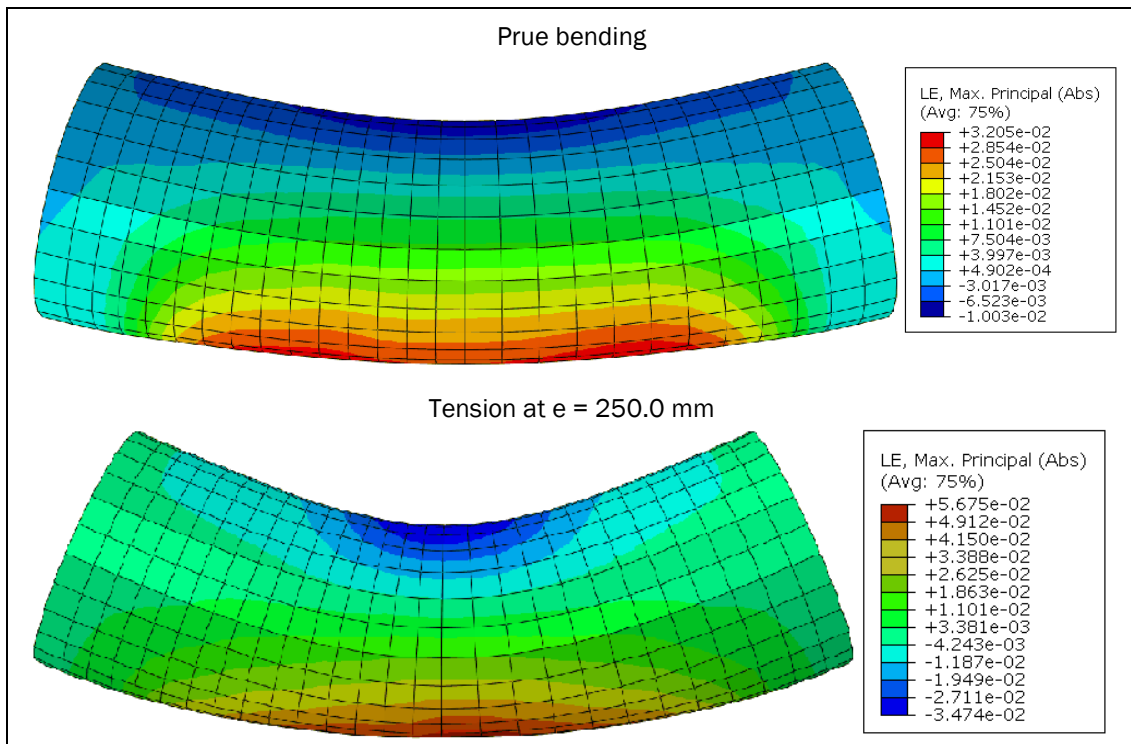


Figure 3.1-9 – Numerical results: absolute strain of core material of sandwich components



**Figure 3.1-10 – Numerical results: absolute strain of core material of sandwich components (continuation)**

The represented numerical results are very valuable. They are an extension of the state of knowledge on the behavior of sandwich components. These results allow an estimation of the influence of combinations of bending and axial load to the design of innovative sandwich components. To improve profitability, comparable studies with modified geometric cross-sectional configurations should be carried out in order to utilize the above-described advantages from lower steel sheet thicknesses of sandwich components as much as possible.

### 3.1.3 Current TRL of innovations and recommendations for their further development

As already stated in [3-02] the sandwich material for chords and braces of a jacket sub-structure has never been used in the offshore wind industry. The analytical solutions and the tests results in case of purely axial loading of the sandwich tubes have been reported in [3-03] and [3-04]. In the present deliverable the bearing capacity of the sandwich tubes under axial force – bending moment interaction (M-N interaction) have been investigated. The reported results are based on the test described in [3-05]. Considering this and according to the technology readiness level (TRL) definitions given by the INN WIND.EU Project, the TRL of sandwich tubes for jacket sub-structures is 3.

In order to reach the next TRL, further investigations on the component level are necessary. These investigations regard the influence of the variation of the thickness of the outer and inner steel tubes on the bearing capacity of the sandwich material components. In addition, the behavior of the sandwich tubes under consideration of the other core materials (elastomer) shall be experimentally tested.

Another important aspect that should be studied is the fatigue behavior of the sandwich tubes, as the fatigue represents a design driving parameter for jacket sub-structure. The most critical point of the sandwich tube represents the joint region, where the sandwich tube is connected with the steel node. The fatigue behavior of this critical connection region has been studied in Subchapter 3.2.

### 3.1.4 Cost reduction potential of innovations on component level

As it has been shown in the Deliverable 4.12 [3-02], the quantity of steel necessary for the sandwich tubes of the jacket varies significantly in relation to the strength of the used steel. In case of the reference steel jacket the stability problems may significantly reduce maximal capacity of the slender tubes made in high strength steel. This is not the case for sandwich tubes, for which the early buckling and wrinkling are circumvented due to the presence of the core material. Thus, with the reduced quantity of steel it can be achieved the same load capacity of the steel section. For the steel S460 this reduction can be estimated to up to 50 % [3-03].

On the other hand it has to be taken into account that in the case of the hybrid jacket the number of the necessary steel tubes is double (inner and outer steel tubes) with respect to the steel jacket. Accordingly, the necessary time for steel sandblasting doubles. The standard speed for sandblasting is between 0.6 and 1.0 m/min and the steel thickness does not have any influence. Regarding the necessary manufacturing time, although the number of tubes is doubled, the cutting and forming process require an additional time of only 50 % (in case of S460) [3-02]. The cutting and forming time does not double because the tubes have smaller thickness and flowingly the cutting and forming process of a single tube is faster. The maximal optimization according to [3-03] can be observed when using S460 where for the cutting process is estimated an additional time of 8% and for forming of about 45 %. The following phase in the manufacturing of tubes is welding of the formed cylindrical section. In this phase a substantial time gain of up to 25 % is expected due to the smaller thickness of the tubes [3-03]. The welding represents the most time consuming part of the manufacturing process and if the necessary manufacturing time is summed up, the steel tubes for hybrid jacket allow a saving of up to 50% in time in relation to the thicker tubes required for the reference steel jacket [3-02].

Finally, in case of the hybrid jacket, the core material and its injection represent additional costs which are not present in the standard steel jacket. These costs cannot be easily quantified because an industrial scale production of such sandwich tubes does not exist.

## 3.2 Sandwich material for connections and joints

One of the innovations considered in the INN WIND substructure work is the potential of adhesively bonding instead of welding. Below, a summary of the findings is given.

### 3.2.1 Discussion of the considered innovations on component level

On the component level (being the trusses connected to the main pillars in a jacket substructure, (see Figure 3.2-1) the innovation considered is to adhesively bond these connections. This innovation is combined with the innovative sandwich tubes discussed in the previous chapter. The main potential benefit is that an adhesively bonded connection can be less fatigue sensitive than a welded connection. On the other hand, potential disadvantages are issues during installation (can the adhesive be applied in a controlled manner), sensitivity to temperature and humidity influences during operation, sensitivity to multi-axial strains during operation.

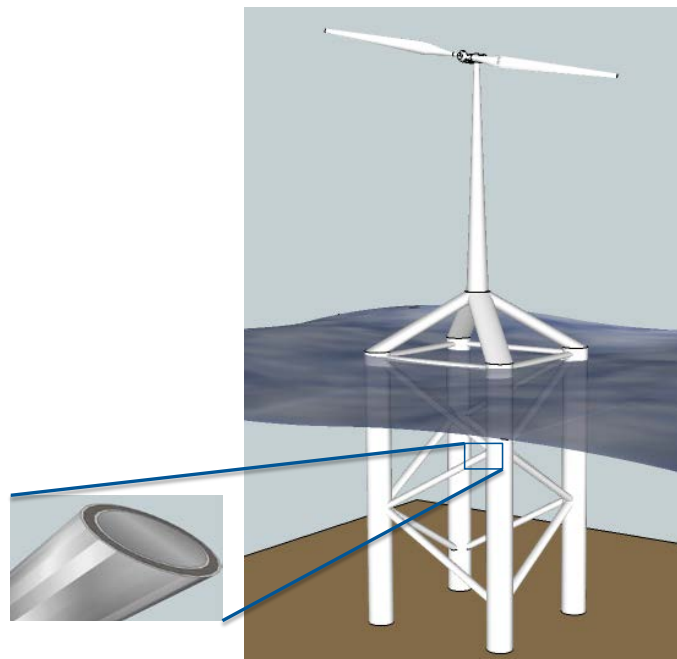


Figure 3.2-1: Innovative sandwich - adhesively bonded jacket trusses

An additional challenge is the combination of sandwich tubes with adhesive connections, since these results in relatively thin-walled structures as well as potential interaction between the steel-adhesive-steel overlaps and the sandwich core, which might lead to unwanted fatigue damage.

Several of the above topics were tackled in an experimental study. The scope of verifying this innovation is:

- Feasibility of installation
- Quasi-static strength of the steel-to-steel connection
- Fatigue performance of the connection in a scaled sandwich tube

### 3.2.2 Description of the performed studies of innovations on component level

In the framework of feasibility of installation, one of the main questions is, whether the adhesive can be inserted from the outside and still reach the inside of the overlap structure ('blind'

infusion). The feasibility of this was verified through a series of injection experiments, where three plexiglass panels were positioned with a gap of approximately the adhesive bondline thickness (5mm), and a hole in the middle panel. Adhesive bonding paste was then injected between panel 1 and 2, and the resulting infusion between all panels was monitored (Figure 3.2-2).

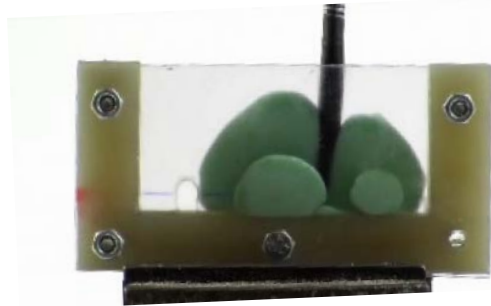


Figure 3.2-2: Adhesive injection experiments

Furthermore, quasi-static and fatigue experiments were carried out. First, adhesively bonded tubes were subjected to mechanical tests ([3-02]). All test specimens contained a single overlap region. Various adhesive overlap and fillet configurations were included in the test series. Axial compression loading was applied to the specimens, both to determine their maximum quasi-static loading capacity, and to determine their fatigue performance under  $R=10$  (minimum compression load equal to 10% of the maximum cyclic compression load, see Figure 3.2-3).

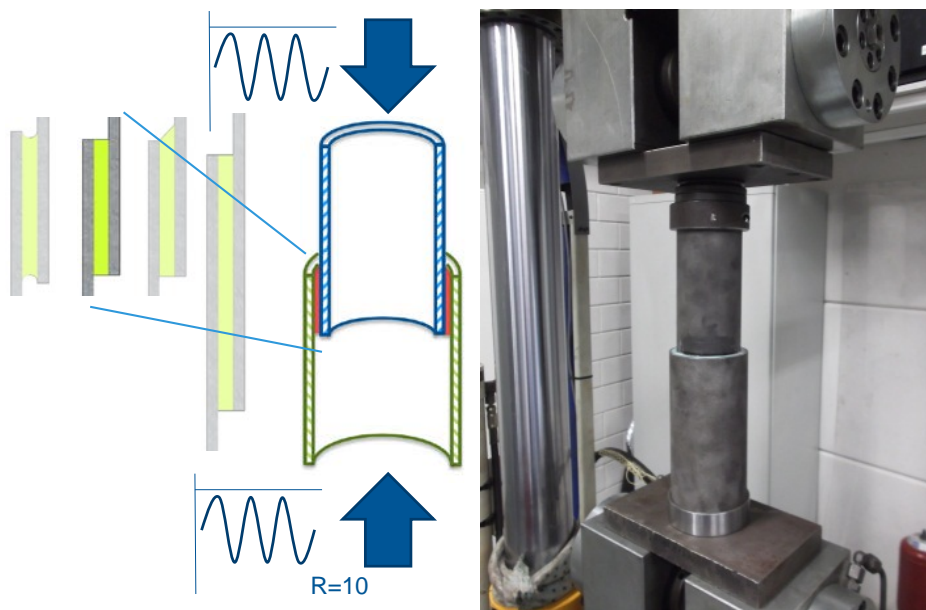


Figure 3.2-3: Mechanical tests on steel-adhesive single overlap tubular specimens

Furthermore, experimental verification was carried out on hybrid specimens, which were designed in collaboration between LUH and WMC ([3-05]). The specimens consisted of a sandwich tube (larger diameter than the previously described adhesively bonded tubes), with, on both ends, an adhesively bonded double overlap joint. These specimens were loaded in tension, as well as in  $R=-1$  fatigue (maximum cyclic tensile load equal and opposite to the maximum cyclic compressive load).



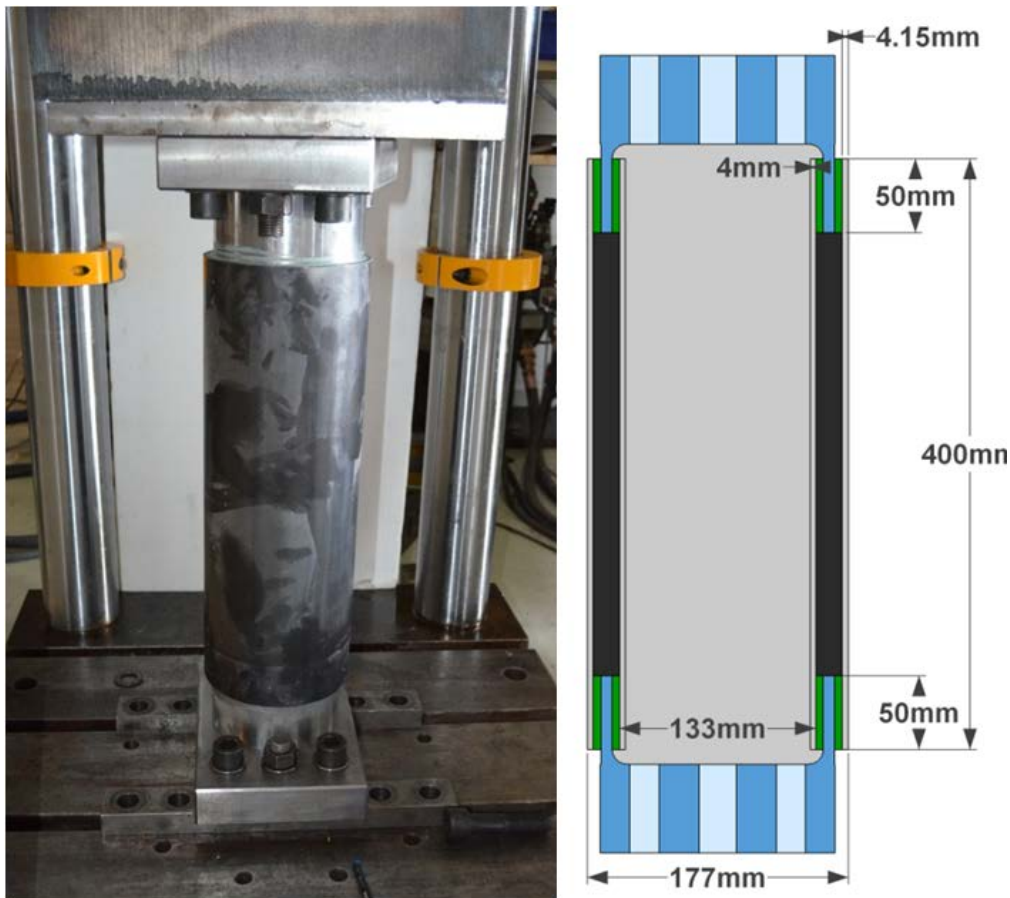


Figure 3.2-4: Sandwich - adhesive hybrid symmetrical joint

### 3.2.3 Results of the performed studies of innovations on component level

The adhesive injection experiments showed influence of the injection location, hole position and hole geometry, but the overall feasibility was satisfactorily demonstrated.

As for the experiments on the steel-to-adhesive connection, the results were promising, albeit that the strength of the connection depended significantly on overlap length and especially fillet.

In the hybrid joint quasi-static and fatigue tests, the applied loads were (in part) tensile as opposed to compressive in the tube-overlap tests. This may have resulted in transverse tensile stresses in the bondline, as opposed to (less disadvantageous) compressive transverse stresses in the bondline in the non-hybrid specimens. This resulted in strengths that were lower than expected based on the steel-to-adhesive connections. Several influences of test parameters were further investigated and some ruled out, but further numerical and experimental research is required to pin-point the cause for the lower-than-expected bondline strength.

### 3.2.4 Current TRL of innovations and recommendations for their further development

See Deliverable 4.12 [3-02] for a discussion on TRL level. The results of the hybrid joint tests indicated that the TRL level of this innovation might be lower than indicated in Deliverable 4.12 [3-02], as the results were lower than those for the non-hybrid specimens. One of the potential reasons for this is a larger influence of the biaxial stress state resulting in transverse tensile stresses in the hybrid specimen adhesive joint.

### 3.2.5 Cost reduction potential of innovations on component level

See Deliverable 4.12 [3-02] for the recommendations for further research to improve the insight in the cost reduction potential include the influence of humidity on the bondline quality, the need for periodic inspection of the bondline.

### 3.3 Conclusions

As already shown in the Deliverable 4.12 [3-02] and the first part of Chapter 4.1 of the present report, models/approaches describing the load bearing behaviour of sandwich structures already exist. However, they have been developed for thin-walled compression members [3-04] or tower sections [3-03] and do not consider any load combinations. The purposed application of the sandwich components in this research project as a brace or chord in a Jacket of a 10MW OWEC differs from the applications of the investigations of [3-03] and [3-04] and component-related load conditions have to be considered. The established structural models have to be checked considering the new purposed application. Namely, jacket as a substructure of an OWEC is characterized by special loading situations. Due to restraint moments a combination of moment and normal force appears in the brace and chord components. A model representing the bearing capacity of sandwich components under this specific load situation has not been established so far. As part of the project Innwind.eu such a model is investigated. To achieve this model, a test plan has been created and specimens of sandwich components are tested statically under eccentric compressive load [3-05]. Using selected experimental tests accompanied by numerical investigations the structural behaviour of sandwich components under eccentric compressive load is described and an interaction N-M diagram has been established. Further studies with modified geometric cross-sectional configurations and different core materials should be carried out in order to exploit the advantages from lower steel sheet thicknesses of sandwich components as much as possible.

In the experiments described in Deliverable 4.12 [3-02] and Deliverable 4.14 [3-05] the potential of bonding as a joining technique for tubular steel structures was evaluated. The results indicate that bonding could be a viable joining the technique but a large effort in the development of the bonding process and to select the adequate bonding paste needs to be done. In these experiments single walled specimens [3-02] were tested as well as sandwich tubes [3-05]. Sandwich tubes showed lower ratios of surface layer thickness to overlap length and a large scatter was recorded in the overall tests. A significant difference appears between the shear stresses of the different types of coupons in compression and tension.

The large scatter observed was due to the bonding process and type of adhesive and geometrical configuration. Unless this is further tackled, large safety factors in the design of this type of joints can be expected. Further research in the selection of the adhesive is required in order to ensure processability and stability of the mechanical properties. In addition, further research is recommended in relation with the manufacturing process aiming to ensure the stability of the bonding line properties and the surface treatment via automation.

In order to improve the adhesive properties and design allowable an adhesive benchmarking tests campaign is recommended for further research, in which static and fatigue properties are evaluated. In a later stage, also the fracture energy density of the adhesive-steel interface will need to be further investigated.



## References

- [3-01] INNWIND.EU Design report - Reference Jacket, "InnWind\_DesignReport\_ReferenceJacket\_Rev00.docx", Internal teamsite, uploaded 2014-01-16, accessed 2014-08-12.
- [3-02] INNWIND.EU: Innovations on component level (Interim report - Revision). Deliverable 4.1.2, 2015.
- [3-03] Keindorf, C., "Tragverhalten und Ermüdungsfestigkeit von Sandwichtürmen für Windenergieanlagen", Dissertation, Institute for Steel Construction, Leibniz University Hannover, 2010, (in German)
- [3-04] Lindschulte, N., "Drucktragverhalten von Rohren aus Ultrahochfestem Beton mit Stahlblechummantelung", Dissertation, Institute of Building Materials Science , Leibniz University Hannover, 2013, (in German).
- [3-05] INNWIND.EU: Validation of innovations by tests on component level. Deliverable 4.1.4, 2015.
- [3-06] Vinson, J.R. (1993): The behavior of shells composed of isotropic and composite materials, University of Delaware, USA, Kluwer Academic Publishers.

#### 4 SOIL & FOUNDATION (AAU, FHG-H, DTU)

To enable the transition to renewable energy in Europe, offshore wind energy will be necessary. Thus, it is of fundamental importance to reduce the costs related to this energy source. The cost of construction and installation of sub-structures may represent up to the 30% of the total investment of a wind farm. Furthermore, the necessity to exploit sea areas at larger water depths and to use wind turbines with larger nominal capacity, makes the need of innovations in the sub-structure of paramount importance. Jacket sub-structure for offshore wind turbines are founded on a set of foundations (usually three or four) which distribute the loads coming from wind and waves to the surrounding soil. The foundations employed to support jacket structures (piled, shallow or bucket) are mainly subjected to axial loading in tension or compression with secondary horizontal loading components. The peculiarity of the loading conditions concerning offshore wind turbines such as cyclic loading in tension and impact loading are not entirely explored in literature. Moreover, innovative installation methods for piles might solve the noise problem during installation and thereby become a valuable option for future installations.

This chapter includes three sub-chapters that address solutions for reducing the impact of the sub-structure on the total investment of an offshore wind farm. Bucket foundation supporting jacket structures is one of the solutions indicated. As opposite to monopiles, the installation process is theoretically fully reversible, meaning that the whole structure could be potentially recovered at the end of its life-time. In addition, it is claimed that installation and fabrication costs can be relevantly lower than those of other foundation types. In the contribution different methods regarding compressive and tensile capacity of bucket foundations are reviewed and novel tests are compared to existing empirical and numerical models. The second sub-chapter is about vibratory installed piles. This technology, though not new and potentially cost-effective, has never been used for offshore wind turbines. Vibratory-driven piles have the potential to be cost-reducing mainly for the smaller installation time needed and for the lower noise emission during installation. These undeniable advantages might be outweighed by a necessary increase in size due to weaker bearing behavior as a result of the installation method. In the sub-chapter dedicated to vibratory-driven piles a large-scale test of a vibro-driven pile is interpreted in order to gain information regarding its tensile bearing capacity and its initial axial stiffness. As a result of the analysis, more knowledge on the economic viability of this technology will be obtained. The last sub-chapter includes an advanced analysis on a semi-floater concept developed to be a cost-effective replacement for jacket sub-structures. The evaluation involves numerical and analytical methods to understand how the different elements of the sub-structure react to typical loading conditions. At the end of the contribution a discussion on cost analysis and technology readiness level is proposed.

## 4.1 Suction bucket foundations

Jacket structures are usually founded on piles, these foundations are of simple design but Bucket foundations are an option that can decrease the overall cost and increase the diffusion of wind turbine. Since wind turbine are dynamically sensitive structures where stiffness requirements have to be satisfied, an alternative design allowing to increase stiffness is multi-bucket configuration [4-01], wherein loading response changes significantly with respect to a mono bucket. The following work is focused on loading of multi-bucket foundation also referred to as multi-pod, where very little moment is taken by the bucket itself. The moment load is mainly resisted by push-pull load on the vertical axis of opposite buckets. For these reasons, it is important to understand behavior under tensile loading and improve the stiffness of foundation, so a correct design can be established. Among others, multi-pod foundations can be either tripod or tetrapod. Tripod has the advantage that it requires less material and it is easier to construct and install. This chapter has the purpose to analyze research on vertical loading of suction caisson installed in sand, focusing on works done in laboratory. Cyclic and monotonic pull-out tests are reported, specifying equipment used and test modality adopted in order to discuss and compare works of different authors. On the contrary to piles, there are no standard design methods for axially loaded bucket foundations. Oil and gas platforms transfer mainly compressive loads to the foundations. Tensile capacity is considered only for the short-term term events such as storms. Compared to the oil and gas platforms, wind turbines are very light. The foundation of a wind turbine has to sustain long-term tensile loads. It is recognized that the design of a wind turbine foundation is not driven by the ultimate capacity but it is governed by parameters as stiffness and behavior under cyclic loading, so particular attention has been given to these topics. Important matter is the enhancement in resistance to pull-out load given by pore pressure under the lid of the caisson. This resistance is a consequence of a complex interaction between permeability of the soil, drainage path and rate of loading, and is a resource on which can possibly contribute to peak load resistance. However studies needs to be done to have a more precise model of this phenomenon. This study also emphasises the need of standard guidelines for axially loaded bucket foundations by comparing and indicating the differences of the current design methods and latest research findings for axially loaded bucket foundations.



Figure 4.1-1: Jacket with bucket

Compared to the oil and gas platforms, wind turbines are very light. The foundation of a wind turbine has to sustain long-term tensile loads. It is recognized that the design of a wind turbine foundation is not driven by the ultimate capacity but it is governed by parameters as stiffness and behavior under cyclic loading, so particular attention has been given to these topics. Important matter is the enhancement in resistance to pull-out load given by pore pressure under the lid of the caisson. This resistance is a consequence of a complex interaction between permeability of the soil, drainage path and rate of loading, and is a resource on which can possibly contribute to peak load resistance. However studies needs to be done to have a more precise model of this phenomenon. This study also emphasises the need of standard guidelines for axially loaded bucket foundations by comparing and indicating the differences of the current design methods and latest research findings for axially loaded bucket foundations.

### 4.1.1 Comparison of calculation methods for bearing capacity

The compressive capacity of shallow foundations is calculated using the traditional Terzaghi [4-02] bearing capacity formula. The formula estimates capacity of shallow onshore strip foundations. It is also applied for offshore shallow foundation calculations when improved by various modification factors to convert the plain strain problem to axisymmetric problem. The bucket foundation is a skirted shallow offshore foundation of circular shape. The soil that is trapped inside makes the bucket behave as a gravity based structure. Thus, the bearing capacity of bucket can be estimated using the traditional formulae.

$$R_c = R_y + R_q + R_{c'} + R_{fric} \quad \text{Eq. 4.1-1}$$

Bucket compressive capacity  $R_c$  consists of four main parts: soil self-weight  $R_y$ , surcharge  $R_q$ , effective cohesion  $R_{c'}$  and skirt friction  $R_{fric}$ . Each of these parts can be estimated in various ways

which differ slightly from method to method. Factor for surcharge  $N_q$  increases exponentially with increasing soil friction angle  $\varphi$ . Most of the methods presented suggest  $N_q$  value derived by Prandtl [4-03], except Larsen [4-04] and Byrne [4-01]. Recently, Ibsen et al. [4-05], [4-06] has showed that  $N_q$  value for bucket foundations is influenced by surfaced roughness which was found by the finite element analysis. Bearing capacity factor for the self-weight  $N_\gamma$  depends on the values of  $N_q$ ,  $\varphi$  and surface roughness. However, it differs from method to method. Formulae for  $N_q$  and  $N_\gamma$  are provided in this paper. Most of the methods require modification factors for shape  $s$ , depth  $d$ , and inclination  $i$ . The specific formulae can be found in the references.

A large amount of laboratory tests on axially loaded bucket foundations was performed at Aalborg University. Vertical bearing capacities of rough circular surface footing and buckets of various shapes were tested and analyzed by Ibsen et al. ([4-05], [4-06], [4-07] and [4-09]). These results will be discussed later on in this report.

### DNV (1992)

DNV [4-10] provided guidelines for the geotechnical calculations of offshore foundations, such as gravity based and pile foundations. The application of bearing capacity for offshore foundation stability calculation is described as too rough, but a good estimate for the early stage of design.

$$R_c = A'(0.5\gamma'B'N_\gamma K_\gamma + q'N_q K_q + c'N_c K_c) \quad \text{Eq. 4.1-2}$$

$$N_q = \tan^2(45 + 0.5\varphi)e^{n \tan \varphi} \quad \text{Eq. 4.1-3}$$

$$N_c = (N_q - 1)^2 \cot \varphi \quad \text{Eq. 4.1-4}$$

$$K_q = s_q d_q i_q \quad \text{Eq. 4.1-5}$$

$$K_\gamma = s_\gamma d_\gamma i_\gamma \quad \text{Eq. 4.1-6}$$

$$K_c = s_c d_c i_c \quad \text{Eq. 4.1-7}$$

where  $c'$  effective cohesion,  $q'$  surcharge,  $A'$  effective bearing area of the foundation,  $B'$  effective width of the foundation,  $N_q$ ,  $N_\gamma$ ,  $N_c$  bearing capacity factors,  $K_q$ ,  $K_\gamma$ ,  $K_c$  modification factors to account for foundation shape, embedment, and load inclination.

DNV [4-10] suggests two methods for  $N_\gamma$ . The first one was found by Brinch-Hansen [4-11]:

$$N_\gamma = 1.5(N_q)\tan \varphi \quad \text{Eq. 4.1-8}$$

The second was suggested by Caquot and Kerisel [4-12]:

$$N_\gamma = 2(N_q)\tan \varphi \quad \text{Eq. 4.1-9}$$

Contribution of the friction on the out skirt is also considered by:

$$R_{fric} = \frac{\gamma' d^2}{2} K \tan(\delta \pi D) \quad \text{Eq. 4.1-10}$$

where  $\gamma'$  effective unit weight,  $D$  is outer diameter,  $d$  skirt length,  $\delta$  interface friction angle,  $K$  coefficient of horizontal stress.

### EC-7 (2004)

Eurocode 7 Geotechnical design (EC-7, [4-13]) provided guidelines for the geotechnical aspects of buildings and civil engineering structures. It adopts the same bearing capacity equation as DNV [4-10], and  $N_v$  is estimated only by Eq. 4.1-9. Moreover, the shape and depth factors differ from DNV [4-10]. The contribution of the friction on the outer skirt is not included in the formulae. For comparison reasons this guideline is included into consideration despite that it is intended for onshore foundation design.

### Byrne (2000)

Byrne [4-01] used the traditional drained bearing capacity of shallow foundations formula and included the contribution of friction force on the outer skirt. The bearing capacity factors  $N_q^*$  and  $N_\gamma^*$  are taken from Bolton and Lau [4-14]. These factors are estimated for the axisymmetric calculation:

$$R_c = A(0.5\gamma' DN_\gamma^* + qN_q^*) + \frac{\gamma' d^2}{2} K \tan(\delta\pi D) \quad \text{Eq. 4.1-11}$$

### Ibsen (2014)

Ibsen [4-06] derives a new theoretical relationship of the bucket bearing capacity:

$$\frac{R_c}{R_\gamma} = 1 + \frac{d}{D} \quad \text{Eq. 4.1-12}$$

$$R_\gamma = A(0.5\gamma' DN_\gamma)$$

In this formulation Larsen [4-04] derived new bearing capacity factors  $N_q$  and  $N_\gamma$  for the drained bearing capacity. The study was performed using an axisymmetric numerical model with bucket foundations and lead to equations Eq. 4.1-13 and Eq. 4.1-14. Detailed information is provided in Larsen [4-04] and Ibsen et al. [4-06].

$$N_c = c_3 e^{c_4 \pi t s \tan \varphi} \tan^2 \left( 45 + \frac{\varphi}{2} \right) \quad \text{Eq. 4.1-13}$$

$$N_\gamma = c_1 \left( (N_q - 1) + \cos \varphi \right)^{c_2} \quad \text{Eq. 4.1-14}$$

where  $c_i$  are available for circular and strip foundation with rough and smooth surface, as shown in Table 4.1-1.

**Table 4.1-1: Fitted values for constants in Eq. 4.1-12 and Eq. 4.1-13 for the bearing capacity factors.**

	Circular foundation		Strip foundation	
	Smooth	Rough	Smooth	Rough
$c_1$	0.1	0.16	0.12	0.25
$c_2$	1.33	1.33	1.51	1.5
$c_3$	0.715	0.8	1	1
$c_4$	1.42	1.5	1	1

### Randolph and Gourvenec (2011)

Randolph and Gourvenec [4-15] provide the classical approach for the drained bearing capacity of shallow foundations.  $N_q$  is estimated by Eq. 4.1-3.

$$R_c = A(0.5\gamma' B' N_\gamma K_\gamma + (q + a) N_q K_q - a) \quad \text{Eq. 4.1-15}$$

$$N_c = 1.5(N_q - 1) \tan(\tan\varphi) \quad \text{Eq. 4.1-16}$$

where  $a$  is soil attraction factor.

There is also a suggested solution for  $N_\gamma$  for rough foundation by Davis and Booker [4-16]:

$$N_\gamma = 0.1054e^{9.6\varphi} \quad \text{Eq. 4.1-17}$$

### Ovesen et al. (2012)

Geotechnical engineering textbook (Ovesen et al., [4-17]) provides a general bearing capacity equation based on Terzaghi [4-02]. The main equation is Eq. 4.1-2,  $N_q$  is estimated by Eq. 4.1-3.

$$N_\gamma = 0.25 \left( (N_q - 1) \cos\varphi \right)^{1.5} \quad \text{Eq. 4.1-18}$$

$$N_\gamma = \frac{(N_q - 1)}{\tan\varphi} \quad \text{Eq. 4.1-19}$$

### Finite Element Modelling

Plaxis is a commercial geotechnical design program which is based on finite element method. Depending on the complexity of the structure, the design can be two-dimensional or three-dimensional. User-friendly interface allows design of various geotechnical structures, easy boundary set-up, loading application in steps and etc. Subsequently, a number of soil constitutive models are available which estimate the soil response when the soil properties are well known. Obviously, the quality of the solution increases if the soil properties are estimated well. Plaxis 2D axisymmetric model provides a relatively fast estimate of the bearing capacity and displacements of axially loaded bucket foundations.

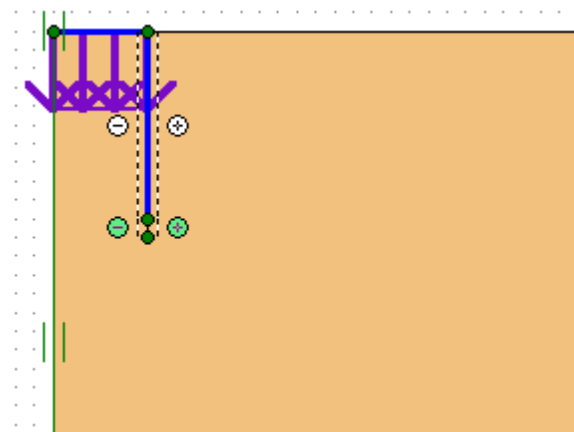


Figure 4.1-2: A fragment of Plaxis 2D model for bucket foundation with geometric ratio of  $d/D=1$

Two models, Mohr-Coulomb and Hardening-Soil, were chosen for the research. The first one is rather simple, because it requires only the main soil parameters which are rather easy to get from the soil classification data and cone penetration test (CPT). For drained soil a rather rapid calculation can be performed only knowing friction angle  $\varphi$ , dilation angle  $\psi$ , effective cohesion  $c'$ , Poisson's ratio  $\nu$  and effective Young's modulus  $E'$ . On the contrary, the Hardening-Soil model

requires knowledge about the advanced soil properties, such as triaxial loading stiffness  $E_{50}^{ref}$ , triaxial unloading stiffness  $E_{ur}^{ref}$ , and oedometer stiffness  $E_{oed}^{ref}$ . The parameters serve to describe the non-linearity in stress-strain curve as well as stress level dependency. The advanced parameters can be estimated using triaxial testing or calculated by the formulae provided in Schanz et. al. [4-18].

**Table 4.1-2: Methods used for ultimate capacity analysis**

No.	Method	Variables
M1	Plaxis 2D, Hardening-Soil	$d, \gamma', \delta, \varphi_{triax}$ .
M2	Plaxis 2D, Mohr-Coulomb	$d, \gamma', \delta, \varphi_{triax}$ .
M3	Randolph and Gourvenec [4-15] and Davis and Booker [4-16]	$d, \gamma', \varphi_{red,pl}$ .
M4	Randolph and Gourvenec [4-15]	$d, \gamma', \varphi_{red,pl}$ .
M5	Eurocode 7: Geotechnical Design	$d, \gamma', \varphi_{red,pl}$ .
M6	Byrne [4-01]	$d, \gamma', \delta, \varphi_{red,triax}$ .
M7	Ibsen [4-06]	$d, \gamma', \varphi_{red,triax}$ .
M8	DNV [4-10] and Caquot and Kerisel (1953)	$d, \gamma', \delta, \varphi_{red,pl}$ .
M9	DNV [4-10] and Brinch-Hansen [4-11]	$d, \gamma', \delta, \varphi_{red,pl}$ .
M10	Ovesen et al. [4-17]	$d, \gamma', \varphi_{red,pl}$ .
M11	Senders [4-19]	$d, \delta, q_c (\epsilon \gamma', l_D)$
M12	Houlsby et al. [4-20]	$d, \gamma', \delta$
M13	DNV [4-10] tensile loading	$d, \gamma', \delta$

## CASE STUDY OF COMPRESSIVE CAPACITY

In order to compare and visualize the differences of these design tools, an idealized case study is created. Table 4.1-2 provides the numbered marking for the previously mentioned methods which is used in the comparison. Moreover, the main variables are given in the table to avoid any possible confusion. In this study, two bucket foundations of different geometries are compared. The seabed contains ideal uniform dense sand, and the water depth is 15 meters. Soil parameters are given in Table 4.1-3. A jacket structure is supported by bucket foundations; therefore, the critical loads are axial tensile and axial compressive load. It does not matter how many buckets there are, because the comparison will be done for the pure axial capacity of a single foundation.

**Table 4.1-3: Geotechnical soil parameters**

Parameter	Units	Value
Triaxial friction angle $\varphi_{triax}$	[°]	38.8
Plane friction angle $\varphi_p = 1.1\varphi_{triax}$	[°]	42.7
Interface friction angle $\delta$	[°]	32.2
Angle of dilation $\psi$	[°]	9
Density ratio $l_D$	[%]	80
Soil unit weight $\gamma$	[kN/m <sup>3</sup> ]	20.25
Effective unit weight $\gamma'$	[kN/m <sup>3</sup> ]	10.25



Effective cohesion $c'$	[kPa]	0 1 (in Plaxis)
Effective Young's modulus $E'$	[MPa]	39.3
Triaxial unloading stiffness $E_{ur}^{ref}$	[MPa]	260.9
Oedometer stiffness $E_{oed}^{ref}$	[MPa]	43.7
Triaxial loading stiffness $E_{50}^{ref}$	[MPa]	87
Poisson's ratio $\nu'$	[-]	0.2
Plaxis interface factor $R$	[-]	0.78
Plaxis factor $m$	[-]	0.58
Reference pressure $p$	[kPa]	100
Over consolidation ratio $OCR$	[-]	1
Horizontal stress parameter $K$	[-]	0.37
Cone penetration $q_c$ at 5 m depth	[kPa]	10297
Cone penetration $q_c$ at 5 m depth	[kPa]	15075

### Soil Parameters

Horizontal soil stress parameter  $K$  is often recommended to be in the range of 0.5-0.8 (DNV, [4-10], and Byrne and Houlsby, [4-23]). This recommendation originates from the offshore pile design criteria. Hammering of piles into the seabed strengthens the soil properties; therefore, the factor  $K$  can be higher. However, suction bucket installation is slightly different and  $K_0=1-\sin\phi_{triax}$  is used instead in this study according to Larsen [4-04]. For the analytical solutions, the reduced friction angle is used. It is calculated using the plane friction angle and the dilation angle in order to reduce the possibility of overestimated axial capacity. The parameter is analyzed in details by Ibsen et al. [4-07]. This technique was adopted by several authors, such as Larsen [4-04] and Vaitkunaite et al. [4-24].

$$\tan\phi_{red} = \frac{\sin\phi\cos\psi}{1 - \sin\phi\cos\psi} \quad \text{Eq. 4.1-20}$$

where  $\phi_{red}$  is reduced friction angle,  $\phi$  friction angle equal and  $\psi$  angle of dilation.

Moreover, in the compressive capacity calculations, where the formulae are based on plain strain solution, the plane friction angle to  $\phi_{pl}=1.1\phi_{triax}$  was introduced.

### Geometry of the Foundation

Two weightless bucket foundations are considered for the analysis. Both of them have a diameter  $D$  of 10 m. The skirt lengths  $d$  are 5 m and 10 m. During the comparison they are identified by the geometric ratio  $d/D$ , which is 0.5 and 1 correspondingly. Foundation surface is rough. The foundations are illustrated by Figure 4.1-2.



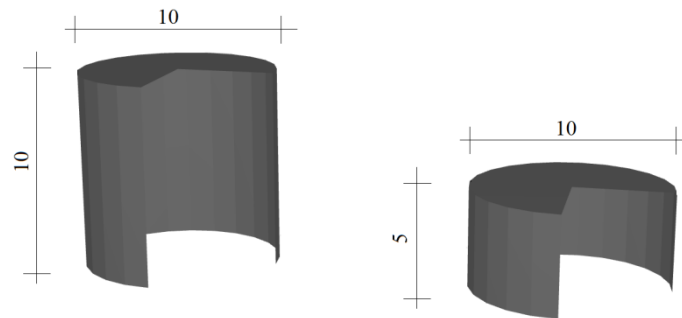


Figure 4.1-3: Buckets dimensions in meters

### Comparison

During the case study, the vertical bearing capacity was estimated according to previously presented analytical and numerical methods. The 10 bearing capacities were estimated for each of the bucket foundations. It was showed that Ibsen [4-06] has derived a good match for the laboratory test performed and described in the next section. Consequently, the bearing capacities were therefor normalized by the Ibsen [4-06] estimation (M7). Figure 4.1-4 presents the normalized bearing capacities. It can be seen that the values deviate slightly and the tendencies depend on the embedment ratio. However, Byrne [4-01] provides the highest estimate of the compressive bearing capacity (M6). On the contrary, the most conservative values are computed using Ovesen et al. [4-17] expression (M10). The estimation of  $R_q$ ,  $R_v$  and  $R_{fric}$  differ from method to method depending on the bearing capacity factors. Skirt friction is sometimes not even included into the calculation, because it is considered to be too small, see methods M3, M4, M5 and M10. When analyzing the analytical methods, it is found that  $R_q$  value increases approximately twice if the skirt is two times longer. However, it increases 2.27 times using M10 while two times using M5, M6 and M7. The frictional part  $R_{fric}$  becomes even four times larger if the larger bucket is used. Obviously  $R_v$  is equal, independent of the skirt length, as it depends only on the foundation area.

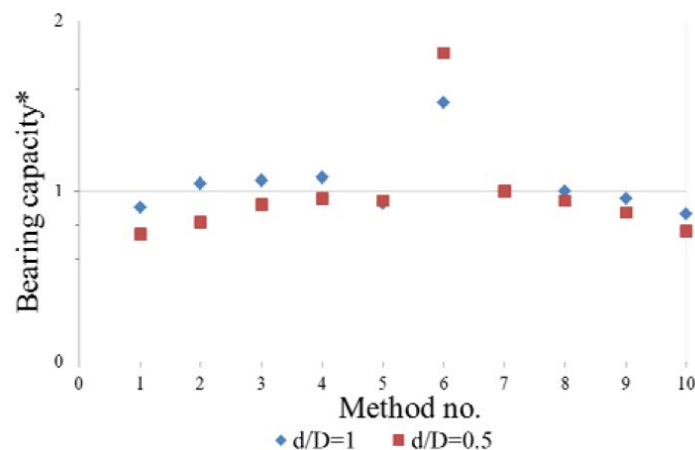


Figure 4.1-4: Compressive capacity normalized by Ibsen[4-06], see method no. 7 in the Table 4.1-2

#### 4.1.2 Comparison of calculation methods for tensile capacity

Applying the theory of anchoring systems, three failure modes for tensile loading on bucket foundation can be considered. When the tensile load is applied rapidly, suction under the lid is generated creating the reverse bearing capacity. In long-term loading conditions, two components resist the tensile load: friction on the outer skirt, and the lower value of the soil plug weight and friction on the inner skirt. Obviously, foundation self-weight is a favorable component, but it is not considered in this study as mentioned earlier. This study considers only long-term tensile loading.

##### DNV (1992)

DNV [4-10] is a widely used standard for offshore foundations. It provides the design principles for gravity based and monopole foundations as well as jack up platforms. Open ended offshore steel piles are of circular tube shape and in this way similar to bucket foundations. Therefore, the recommendations for axially loaded offshore piles will be considered in this report:

$$R_t = ((K\tan\delta)_o D_o + (K\tan\delta)_i D_i) \pi \frac{\gamma' d^2}{2} \quad \text{Eq. 4.1-21}$$

where  $i$  and  $o$  are indications for the inner and outer skirt correspondingly.

##### Houlsby et al. (2005)

Houlsby et al. [4-20]-[4-22] have proposed to take into account the reduced vertical stress down the bucket. The authors described that if the reduction is not included into the tensile capacity calculations, bucket strength is overestimated.

$$R_t = -\gamma' Z_o y \left( \frac{d}{Z_o} \right) (K\tan\delta)_o (\pi D_o) - \gamma' Z_i y \left( \frac{d}{Z_i} \right) (K\tan\delta)_i (\pi D_i) \quad \text{Eq. 4.1-22}$$

$$y \left( \frac{d}{Z_x} \right) = \exp \left( -\frac{d}{Z_x} \right) - 1 + \left( \frac{d}{Z_x} \right) \quad \text{Eq. 4.1-23}$$

$$Z_i = \frac{D_i}{4(K\tan\delta)_i} \quad \text{Eq. 4.1-24}$$

$$Z_o = \frac{D_o(m^2 - 1)}{4(K\tan\delta)_o} \quad \text{Eq. 4.1-25}$$

where  $Z_{i/o}$  is interface parameter, and  $m=1.5$ .

##### Senders (2008)

Senders [4-19] used cone resistance for the estimation of the tensile bucket capacity. Foundation resistance is expressed as the sum of the inner friction and the outer friction of the skirt.

$$R_t = F_{i,t} + F_{o,t} \quad \text{Eq. 4.1-26}$$

$$F_{i,t} = \pi D_i k_{f,t} \int_0^d q_c(z) dz \quad \text{Eq. 4.1-27}$$

$$F_{0,t} = \pi D_0 k_{f,t} \int_0^d q_c(z) dz \quad \text{Eq. 4.1-28}$$

$$k_{f,t} = -0.375C \left[ 1 - \left( \frac{D_i}{D_0} \right)^2 \right]^{0.3} \tan \delta \quad \text{Eq. 4.1-29}$$

where  $q_c$  is cone resistance from a CPT test,  $k$  coefficient,  $C$  coefficient equal to 0.012.

Five different static pull-out capacities were estimated for each of the bucket foundations. It was shown that Senders [4-19] has derived a good match for the Performed laboratory test (M11). Consequently, the bearing capacities were normalized with this CPT based method. Cone resistance highly depends on location and sand properties. However, an idealized profile was assumed which corresponds to possible cone penetration values for dense sands, as shown in Table 4.1-3. Figure X4 presents the normalized pull-out capacities. It can be seen that the values deviate significantly and the tendencies depend on the embedment ratio. Tensile capacity for the smaller bucket is very similar, but for the smaller bucket methods M1 and M2 estimate much higher capacity than the rest of the methods. On the contrary, the most conservative estimate of the bearing capacity was estimated by M11.

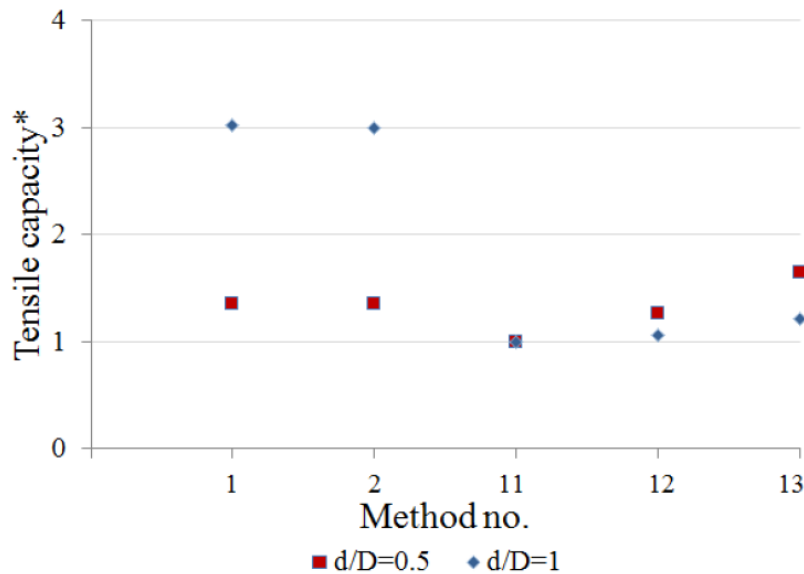


Figure 4.1-5: Tensile capacity normalized by Senders [4-19], see M11 in the Table 4.1-2

The intension of this article was to collect up-to-date methodology for the compressive and the tensile bucket bearing capacity estimation. Ten different expressions were used for the estimation of the compressive capacity and five for the tensile capacity. Quite some scatter between the compressive and tensile capacities was seen, which indicates that more testing and analysis would be favourable to clarify the design of the bucket foundations

### 4.1.3 Test Equipment

Therefore large model tests are carried out in the geotechnical laboratory of Aalborg University, see Figure 4.1-6 where the testing rig is shown.



Figure 4.1-6: The test set-up of axially loaded bucket foundations

The equipment used for testing of axial loaded bucket foundation is shown schematically in Figure 4.1-7. The testing rig includes a rigid circular box, a movable loading frame equipped with two movable hydraulic pistons, a signal transducers box and a measuring system described in the following.

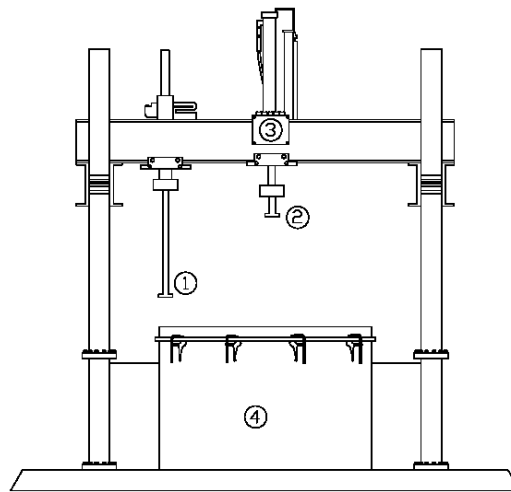


Figure 4.1-7: Equipment used testing bucket foundation: loading piston (1), installation piston (2), signal transducers box (3) and sand box (4)

### Sand box

The sand box is a steel made cylinder with a diameter of 250 cm and a total height of 152 cm. A 30 cm thick layer of gravel with high permeability is placed at the bottom, in order to provide a uniform distribution of water and create uniform water pressure, avoiding piping problems. A geotextile sheet is placed on top of the gravel layer, to avoid sand infiltration and thus maintain drainage property unaltered. The top layer is composed of Aalborg University Sand No.1 and has a thickness of 120 cm. Water is led into the box by a system of perforated pipes, uniformly placed on the bottom. To supply water a tank of 1 m<sup>3</sup> is filled of water and placed in a higher position with respect to the sand box. This allows having an upward gradient in the sand box, needed to loosen the sand. The in and out flow of water is controlled by a system of valves by regulating the inflow valve, the gradient in the sand box is controlled.

### Bucket Models.

Two cylindrical shaped models of bucket foundation have been built to be tested. Both models have an outer diameter of 1000 mm, and a wall thickness of 3 mm, the skirt length is 500 mm (aspect ratio  $d/D=0,5$ ), and 1000 mm ( $d/D=1$ ). Models are approximately scaled of 1:10. To simulate overburden pressure the sand is compressed by a suction system that create a depression inside the sand box. Hermetic isolation is provided by a membrane made of nonporous latex rubber. The membrane has been cut so that can fit with the bucket model, it has thicknesses that allow it to adapt to the sand surface. Four connections for suction pipes and one connection for surface pressure transducer are installed on the membrane. Hermetic isolation along the perimeter of the sand box is provided by a groove where a circular rubber gasket is inserted. The membrane is stretched on the rubber gasket and the steel frame is placed on it and fixed with clamps as shown in Figure 4.1-6.



Figure 4.1-8: Bucket model of  $d/D=0.5$

### Loading and measuring systems.

Two hydraulic pistons are connected on the frame placed above the sand box: the installation piston and the loading piston as shown in Figure 4.1-7. The installation piston is used to run CPT tests and to install the bucket. It has a capacity of 200 kN and is actuated by a control, while speed has to be settled by the control panel in a range of 0.01-5 mm/s. Vertical displacement is measured by a displacement transducer connected to the transducers box, applied force is measured by a load cell. The signals are recorded by a computer with the program Catman. Loading piston can apply a vertical force of 250 kN and has a maximum displacement range of 40 cm. Force or forced displacement for static and cyclic loading are applied with loading piston, controlled by the MOOG system whereby data are recorded and test are programmed. A wide range of options are available for cyclic loading in terms of frequencies and load modalities. Displacements are measured by two 125 mm displacement transducers. As shown in Figure 7, six pressure transducers are installed at different levels inside and outside the bucket. Installation valves and connection for pressure transducers are installed on top of the lid. Cable of pressure transducers are connected to the signal transducers box and through the signal amplifier MGCplus and Spider 8, the signal is elaborated by Catman. A pressure sensor is placed outside and connected to MGCplus system, in order to have a measurement of ambient pressure.

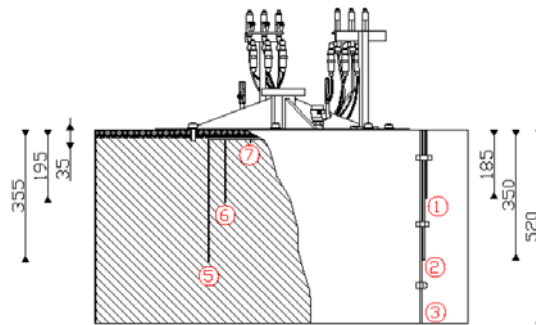


Figure 4.1-9: Section of the test bucket  $d/D = 0.5$ . Distances and position of pressure transducers inside and outside the bucket are shown. Connection for pressure transducers (1) and installation valves (2)

### Soil Description

Sand utilized is Aalborg University Sand No. 1. The main part of sand is quarts, but it also contains feldspar and biotit. The classifications parameters is given in Table 4.1-4

Table 4.1-4: Classifications parameters of Aalborg University Sand No. 1

50% quantile	$d_{50}$	0.14 mm
Uniformity coefficient	$d_{60}/d_{10}$	1.78
Specific grain density	$d_s$	2.64
Maximum void ratio	$e_{max}$	0.854
Minimum void ratio	$e_{min}$	0.549
Permeability	$K_{e=0.612}$	$6.89 \cdot 10^{-12} \text{ m}^2$

### Soil preparation

To obtain homogeneity of the soil and so ensure comparability between tests, the procedure described in the following has been settled, based on previous experiences (Fisker, L.B., and Kromann, K. [4-25]). First the groove along the perimeter of the sand box is cleaned by compress air and paper, then the rubber gasket is placed and aluminum frame is fixed by clamps. To loosen the sand, an upward gradient of 0.9 is applied opening gradually the inflow valve. To avoid air infiltration during vibration, water is set to rise approximately 8 cm above the sand surface. To reach this level, the inflow valve is closed and additionally water has to be poured from the top, placing a small panel on the area of interest so as soil in the surface do not move. A wooden panel with symmetrically distributed holes is placed on the box, as shown in Figure 4.1-10. Then rod vibrator is systematically pushed and pulled in the sand. After vibration the outflow valve is opened and water level is lowered till one centimeter above the sand surface, then the wooden plates are removed and the surface is first cleaned manually, then leveled using a specific shaped aluminum beam.





Figure 4.1-10: Vibration starts inserting the rod vibrator in the hole marked in yellow

### CPT tests

Cone penetration tests are carried out to have complete information about compaction and homogeneity of the soil. CPT probe used is shown in Figure 4.1-11. It has a diameter of 15 mm, tip area of 176.7 mm<sup>2</sup>, cone angle of 60° and penetration length of 120mm. It is connected to the installation pistons then force transducer is plugged in the signal transducer box. Afterwards four CPT tests in four different positions are run. The penetration velocity is set to 5 mm/s. The penetration resistance  $q_c$ , time and vertical displacement is measured. The CPT test is performed to a depth of 110 mm. Figure 4.1-11 shows the typical results of cone penetration test made in the four positions of the test rig. Trend of the curves shows a cone resistance that uniformly increases with depth. Figure 4.1-11 shows also the variation in relative density  $D_r$  with respect to depth. An iterative process described in Ibsen et al. [4-07] is used to calculate  $D_r$  based on the CPT tests.

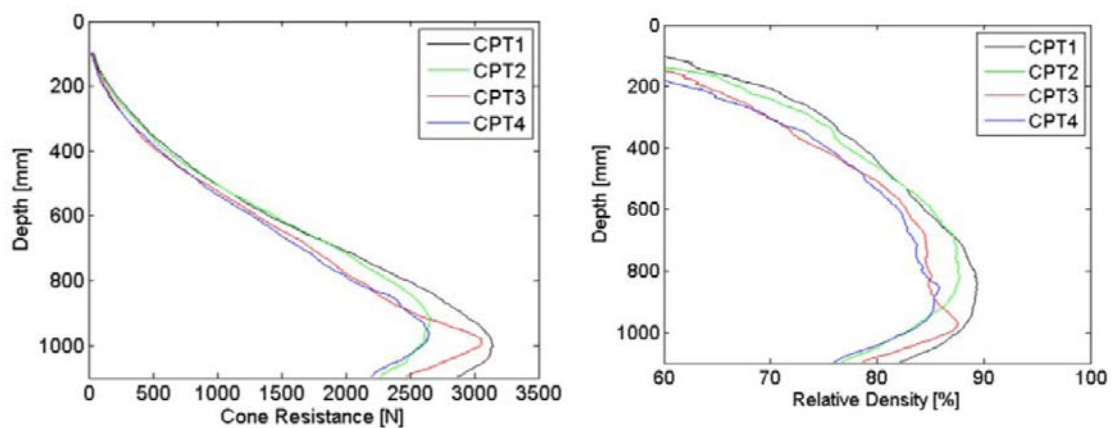


Figure 4.1-11: CPT test results for test no 5

### Test procedures

In the following, steps on how to run tests are described. Soil preparation is common for both tests with and without membrane. Steps of installation are the same for both long and short bucket. Only differences are the longer time and greater installation force required in the installation of long bucket.

### Test without membrane

The water level is raised to 5-8 cm above the surface level and is kept while tests are run. The bucket is connected to the installation piston and installed with a speed of 0.2 mm/s. To ensure comparability between different tests, a preloading load of 70 kPa is reached before to close the two valves of the lid. An indicator of a good installation is water flowing out from the two valves of the lid, since no air is trapped between lid and soil. Figure 14 is showing installation loading curve that is similar for all tests, since sand and sand properties like relative density and saturation are uniformed by soil preparation. In the first part of the curve it can be seen the increase of resistance due to skin friction of the sand adjacent to the caisson. When the lid touches the surface, the load is increase to 70 kN.

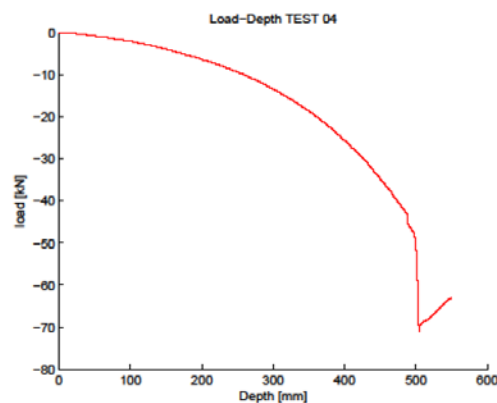


Figure 4.1-12: Installation load curve for static test

Once installation has been completed, installation piston is disconnected and the loading piston is positioned in the central position of the horizontal beam and fixed. Pressure sensors are connected to the signal transducers box. Data of pressures, load and displacement are registered by both MOOG and Catman.

### Test with membrane

Test with membrane is performed in order to simulate overburden pressure. Overburden pressure is used in order to have a greater stress level along the skirt. This allows simulating higher friction ratios. Preparation and installation of the bucket are then the same as described in for the tests without a membrane. After the bucket is penetrated into sand, the filter is laid on the sand and the membrane is outstretched so that overlay the rubber gasket placed on the perimeter. A metal ring is positioned and fixed with clamps. Installation piston is then removed and load piston is connected as indicated in the procedure of without membrane test. Suction pipes are connected to the membrane and the suction system is activated. The pressure level is measured by Catman and, once reached the required value, has to be kept constant for at least 12 hours.

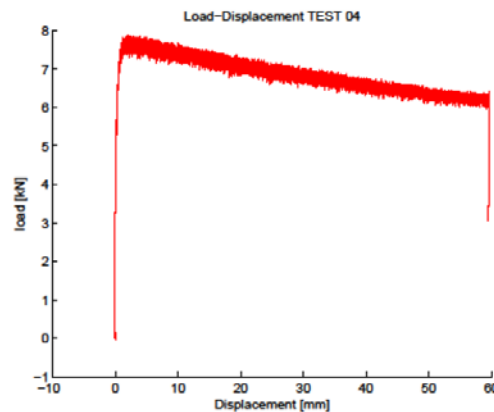
#### 4.1.4 Results presentation

Tests carried out until now are summarized in Table 4.1-5

**Table 4.1-5: Test overview**

Test	L/D	Load	Overburden pressure [kPa]	Displacement [mm]	Amplitude [kN]
13.02.06	0.5	Static	0	3.8	-
13.02.08	0.5	Static	0	4	-
13.02.09	0.5	Static	40	8.8	-
13.02.10	1	Static	0	3.9	-
13.02.11	0.5	Static	20	4	-
13.02.12	0.5	Static	40	6	-
13.02.14	1	Static	0	6.5	-
13.02.15	0.5	Static	0	4	-
13.03.02	0.5	Cyclic	0	-	1.925
13.03.03	0.5	Cyclic	0	-	3.85

In the following typical test results are presented. All tests presented are carried out with the bucket model ( $d/D=0.5$ ) numbers. In Figure 4.1-9 are shown the corresponding positions of pressure measurements.



**Figure 4.1-13: Load-Displacement curve for static test without overburden pressure**

#### Static test without overburden pressure

Figure 4.1-13 is shown the expected trend for a static load – displacement curve. In this case in MOOG it has been set up to reach a maximal vertical pullout displacement of 60 mm. That has

to be reached in 3000 seconds. The load – displacement curve is very steep until it reaches the maximal value of 7.8 kN, than is slightly decreasing until a residual value of 6.2 kN before to drop in correspondence of the end of the test. To show pressure measurements, it has been chosen to split the results in two graphs.

Figure 4.1-14 shows the pore pressured measured on the inside and outside of the bucket. The positions of the pore pressure measurement are shown on Figure 4.1-9. Measurement of atmospheric pressure given by “p6a” and shown in both graphs, this is made in order to have a reference point and allow a better comparison between results.

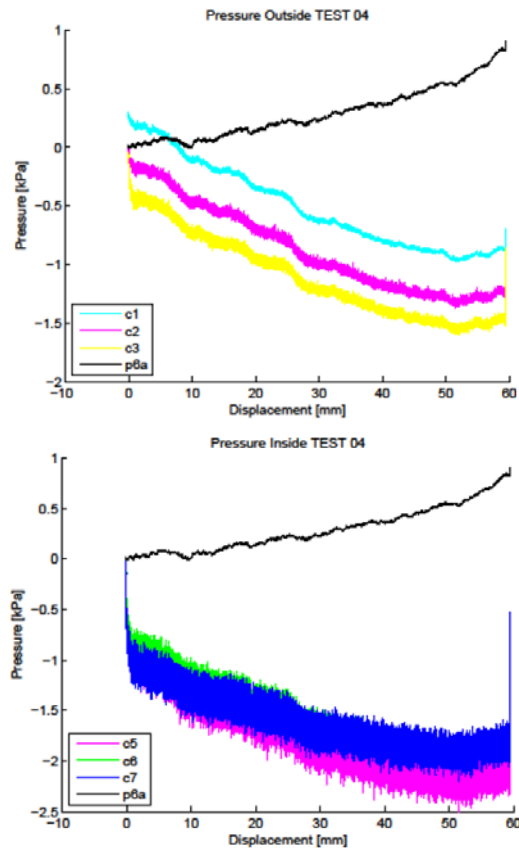


Figure 4.1-14: Pressure measurements at the outside and inside of the bucket

#### Cyclic test without overburden pressure

Figure 4.1-15 shows a load-displacement curve for a cyclic test. Considering results of static test, for the cyclic test 40000 cycles has been settled with a frequency of 0.1 Hz and an amplitude of 50% of the static maximum load. Before of the cyclic load, the bucket is loaded with a static tensional load of 50% of the static maximum load, by “round ramp” mode.

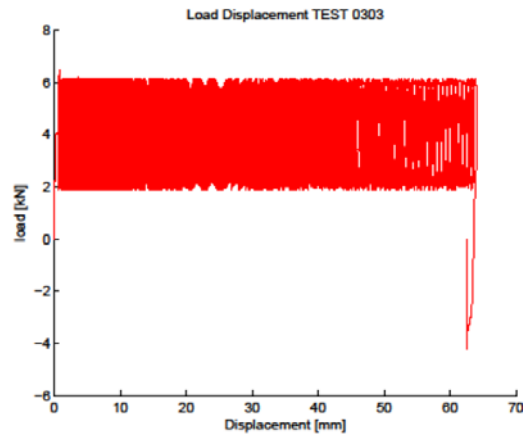


Figure 4.1-15: Load-Displacement curve for cyclic test without overburden pressure

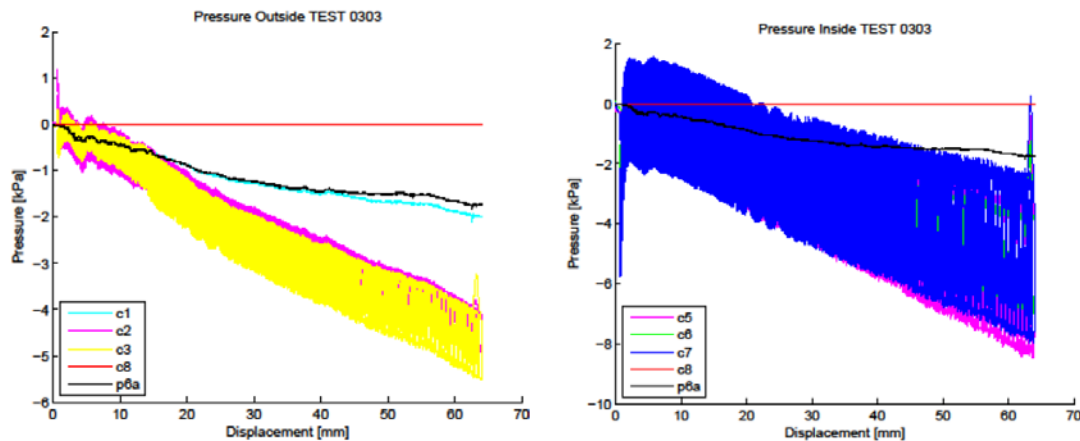


Figure 4.1-16: Pressure measurements at the outside and inside of the bucket

Pressure results are presented in the same way as for the static test, as it can be seen in Figure 4.1-16.

#### 4.1.5 CPT based method installation method

In this section the tests are analysed with CPT based methods both for the installation and the pull-out face of the tests. In order to compare results, load and displacements are plotted in dimensionless form, respectively as  $V/(D^3 \cdot \gamma)$  and  $h/D$ , according to Kelly et al. [4-26]. In the following study, parameters are evaluated from responses of test 6, test 9, and test 11, carried out with overburden pressure of respectively 0kPa, 40kPa, and 20kPa.

#### DNV CPT-based installation method.

DNV presents a method to estimate the installation resistance of steel caisson based on the average cone resistance  $q_c$ . Installation resistance is calculated summing friction forces and end-bearing resistance by Eq. 4.1-30. End bearing resistance and friction resistance on the skirt, are related to  $q_c$  respectively by constants  $k_p$  and  $k_f$ , of which suggested ranges are listed in Table 4.1-6.

$$R_t = F_i + F_o Q_{tip} \quad \text{Eq. 4.1-30}$$

$$F_i = \pi D_i k_f \int_0^d q_c(z) dz \quad \text{Eq. 4.1-31}$$

$$F_0 = \pi D_0 k_f \int_0^d q_c(z) dz \quad \text{Eq. 4.1-32}$$

$$F_0 = \pi D_0 k_0 q_c \quad \text{Eq. 4.1-33}$$

**Table 4.1-6: Parameters suggested by DNV**

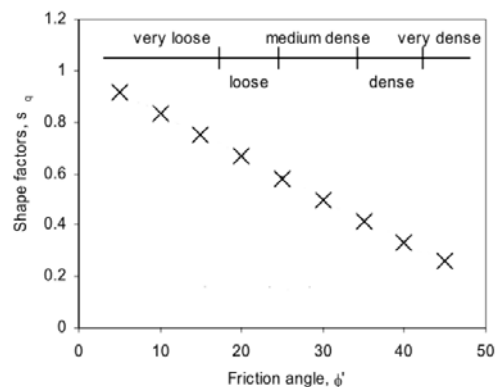
$k_p$		$k_f$	
Most probable	Highest expected	Most probable	Highest expected
0.3	0.6	0.001	0.003

#### Senders (2008) CPT-based installation method.

Senders [4-19] suggests to modify CPT-based method presented in DNV using a different  $k_p$  and evaluating  $k_f$  with Formula 22.

$$k_f = C \left[ 1 - \left( \frac{D_i}{D_0} \right)^{2 \cdot 0.3} \right] \tan \delta \quad \text{Eq. 4.1-34}$$

where  $C=0.21$  is a constant suggested by Lehane et al. [4-27].  $k_p$  factor is taking into account differences in shape between the circular cone and the strip geometry of the caisson rim. Values of the shape factor  $s_q$ , giving the ratio between  $N_q$  for circular and strip footing, have been extrapolated and are showed in Figure 4.1-17, where are plotted with respect to the friction angle. In Senders [4-19] it was noticed that  $s_q$  factor is in line with the range of  $k_p$  factor suggested by DNV, and  $s_q$  was therefore substituted to  $k_p$  in the calculation. In the present work it is chosen to use  $k_p = s_q = 1 - 0.016f' = 0.1536$ .



**Figure 4.1-17: Theoretical shape factor (Randolph [4-28])**



### Validation of installation CPT-based methods

In order to show how different value of  $k_f$  are affecting results of CPT-based methods, in Figure 4.1-18 are plotted responses keeping constant  $k_p=0.3$ , while  $k_f$  is varying on the range proposed in DNV Table 4.1-6.

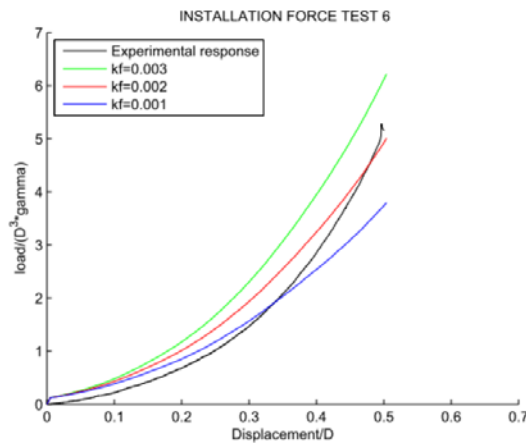


Figure 4.1-18: DNV method with constant  $k_p=0.3$  while  $k_f$  is varying

Figure 4.1-19 is showing the effect on the response varying  $k_p$  in the range suggested by DNV, and maintaining constant  $k_f=0.002$ . As can be noticed from Figure 4.1-18 and Figure 4.1-19, increase of the response is directly proportional to  $k_f$  and  $k_p$ .

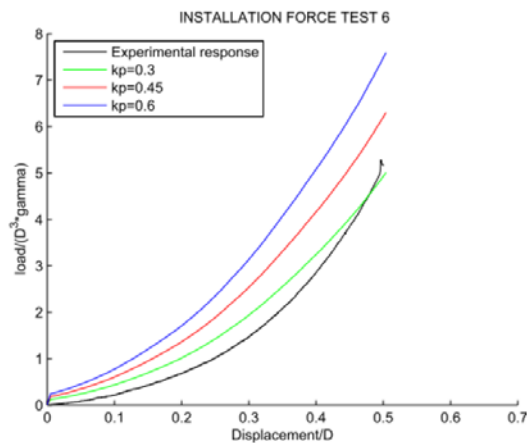


Figure 4.1-19: DNV method with constant  $k_f=0.002$  while  $k_p$  is varying

Parameters of method suggested by Senders [4-19] are evaluated as  $k_f=0.0032$  (Eq. 4.1-34), and  $k_p=0.1536$  Figure 4.1-17. Best fit of parameters in DNV method is obtained with  $k_f=0.002$  and  $k_p=0.3$ . Responses are shown in Figure 4.1-20. Both CPT-based methods are giving a good approximation of the experimental response, as it can be seen in Figure 4.1-20. Peak of the experimental response is  $4.92D^3\gamma'$ , peaks in Senders [4-19] and DNV methods are, respectively,  $5.1D^3\gamma'$  and  $5.0D^3\gamma'$ . Method proposed by Senders [4-19] has a better slope, since the response is lower at the beginning and steeper at the end of the installation, therefore is following the experimental trend.

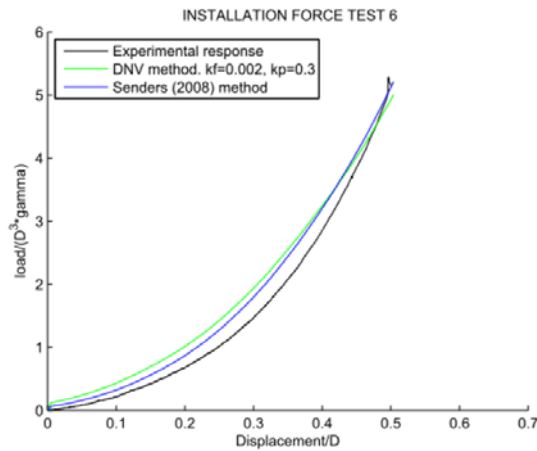


Figure 4.1-20: Comparison of DNV and Senders [4-19] CPT based methods

#### Pull-out CPT-based method.

Method suggested by CUR introduces a constant  $k_f=0.004$  to evaluate the frictional pull-out resistance from  $q_c$ . In CUR is also presented a CPT based method to evaluate penetration resistance, where higher value of  $k_f$  is utilized. In CUR it is pointed out that friction resistance in compression is higher than friction resistance in tension. Frictional resistance in drained condition is calculated by Eq. 4.1-26). In the method suggested by CUR, internal and external frictions are given respectively by Eq. 4.1-27 and Eq. 4.1-28.

Senders [4-19] proposed that the friction resistance is calculated following CUR procedure, but a different value of  $k_f$  is introduced in Eq. 4.1-29. This ratio was extrapolated from experimental results in centrifuge tests by Senders [4-19], as -0.375, In the present work, the ratio between tensile and compressive friction is evaluated from back-calculation the experimental responses as -0.1652, and is substituted into Eq. 4.1-35.

$$k_{f,t} = -0.1652C \left[ 1 - \left( \frac{D_i}{D_0} \right)^2 \right]^{0.3} \tan \delta \quad \text{Eq. 4.1-35}$$

#### Validation of pull-out CPT-based methods.

CPT-based method proposed in CUR is using a  $k_f = 0.004$ . This heavily overestimating of the experimental response is shown in Figure 4.1-21. CUR also present an installation method where  $k_f$  is greater than the one fitted in the previous section. Therefore the methods presented by CUR are overestimating both installation and pull-out responses.

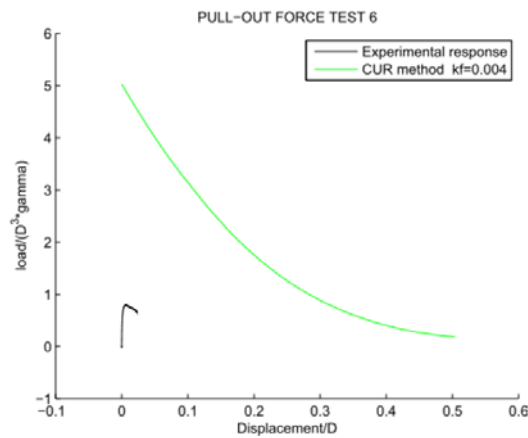


Figure 4.1-21: Pull-out method presented by CUR, heavily overestimate the pull-out resistance

By fitting CUR to the test result  $k_f = 0.00049$ . This gives a good approximation of the pull-out load for tests without overburden pressure. Figure 4.1-22 shows that the modified CUR method has a peak value of  $0.785D^3\gamma'$  where the experimental result is  $0.795D^3\gamma'$ .

In test with 0kPa overburden pressure, CPT-based method proposed by Senders [4-19] gives a slight overestimation of the pull-out resistance, due to the greater value of  $k_f=0.00053$ . Figure 4.1-22 shows that Senders [4-19] reaches a peak value of  $0.832D^3\gamma'$ . This result is slightly unconservative but, since the method does not need any fitting of parameters, the method presented in Senders [4-19] is considered the most reliable CPT-based method to evaluate pull-out resistance.

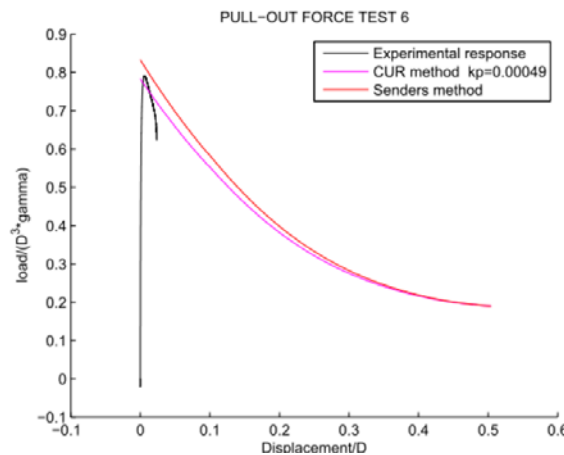


Figure 4.1-22: CPT-based method for test without overburden pressure

In the tests where overburden pressure is applied, values of cone resistance are evaluated before of the installation phase. After the application of overburden pressure, it is not possible to carry out CPT tests. In the tests with overburden pressure of 20kPa and 40kPa,  $k_f$  are evaluated as, 4.5 and 5.7 times the  $k_f$  measured with zero overburden pressure. Function is fitted in order to evaluate  $k_f$  with different overburden pressures, see Figure 4.1-23. The slope progressively decreases with the increase of overburden pressure, showing that  $k_f$  is not constant but dependent on the applied overburden pressure. As overburden pressure is applied, a decrease of the friction angle will occur, therefore it is suggested that  $k_f$  could be dependent on the stress stage in the same way as the friction angle. To find this relationship more tests must be performed to confirm this theory.

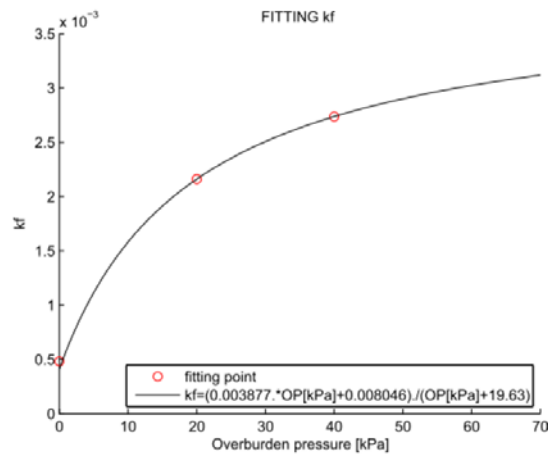


Figure 4.1-23: Function relating  $k_f$  and overburden pressure

In Figure 4.1-24 and Figure 4.1-25 the experimental responses are compared to the results calculated with  $k_f$  defined by Figure 4.1-23. Figure 4.1-24 and shows that CUR and Senders methods are respectively underestimating and overestimating the response. Therefore the same trend as observed with zero overburden pressure is maintained.

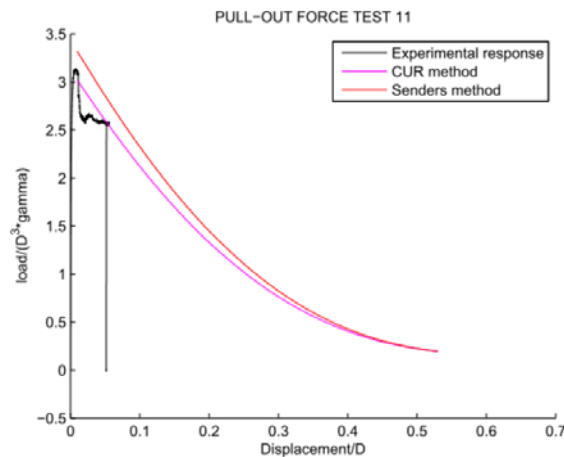


Figure 4.1-24: CPT-based methods for 20kPa overburden pressure

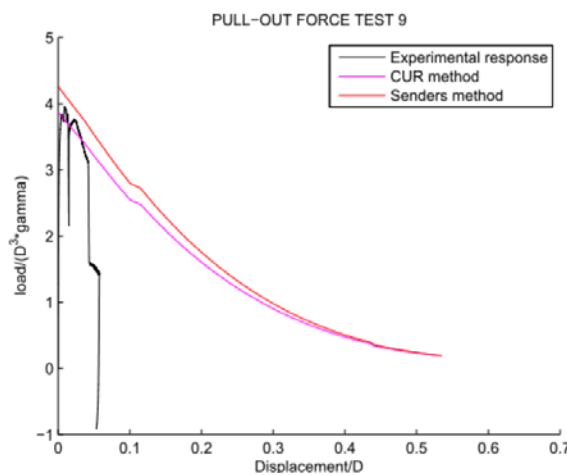


Figure 4.1-25: CPT-based methods for 40kPa overburden pressure

#### 4.1.6 Required experimental investigations on innovations on component level

This chapter presents a new developed testing rig of Aalborg University, and the procedure followed to carry out tests. Responses obtained are considered of high reliability, given the large model test with scaling factor adopted (1:10) and the standardized procedure followed in each test. The possibility to apply overburden pressure allows examining a wide range of friction ratios simulating different skirt length. This allows extending the possibility of study to configurations otherwise not reachable. Methods to evaluate pull-out and installation forces are validated, relying on responses obtained from tests described. More tests are needed in order to reach a better definition of parameters on which the designs methods are based. Since in installation measurements is not well defined where the lid makes contact with soil, an approximation on this value has been done. It is believed that more precise data can be obtained installing for a depth of 50cm the bucket model M2 ( $L/D=1$ ). Following this expedient ensures that only frictional forces and end-bearing resistance Dependence of  $k_r$  to overburden pressure has been demonstrated, however a better definition of parameters used in CPT based method is needed. The foundation of a wind turbine has to sustain long-term tensile loads. It is recognized that the design of a wind turbine foundation is not only driven by the ultimate capacity but it is governed by parameters as stiffness and behaviour under cyclic loading, so particular attention has been given to these topics. The new test rig has the capability to study this effects and a test program is under execution. Important matter is the enhancement in resistance to pull-out load given by pore pressure under the lid of the caisson. This resistance is a consequence of a complex interaction between permeability of the soil, drainage path and rate of loading, and is a resource on which can possibly contribute to peak load resistance. However, studies need to be done to have a more precise model to describe this phenomenon.

#### 4.1.7 Economical and technical advantages of Jacket with bucket foundation

A jacket with bucket foundations might be economically and technically advantageous for the following reasons:


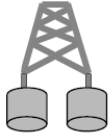
- 1 There is no noise during the suction installation of the buckets. Enabler to operate for noise regulated projects (especially in Germany) as the concept solves noise regulation issue and associated noise mitigation costs.
- 2 The bucket foundation can be fully decommissioned and leave the seabed intact after decommissioned the wind park.
- 3 The installation can be performed faster Installation time for a jacket buckets 1-3 days where as installation of a jacket with piles is 5-6 days. This saves time and therefore costs during the installation operations.
- 4 Possibility to install from a floating DP2 vessel

In Table 4.1-7 the cost structure assumption for key cost elements are compared for a piled jacket and a jacket with bucket foundations. It is seen that the cost of the buckets are higher compared with standard piles but the advantages come from the faster and thereby cheaper installation. The time used to install a jacket with buckets is less than half the time used for installing a Jacket with piles.

In Figure 4.1-26 a study of cost down potential for the suction bucket jacket is presented by Dong energy, see Mørch C.B [4-29]. It is seen that the suction bucket jacket is more expensive to fabricate compared with a piled jacket but 1 mill EUR/ Foundation cheaper to install. The cost down potential is 15 -20 % if using a suction bucket jacket compared with a standard jacket with piles.

The technology readiness level (TRL) of the Suction Bucket Jacket, according to the definition given by the INN WIND.EU Project is between 6 and 7.

**Table 4.1-7: Key cost elements based on actual values witnessed in offshore wind projects after Jensen J, Jain S. Fehler! Verweisquelle konnte nicht gefunden werden.**

	Material Cost	Seabed Preparation	Vessel requirements (Feeder Concept)	Vessel requirements (Installation Vessel)	Other
<p><b>Jacket</b></p> 	<p>Steel of jacket body: 3.200 EUR/tonne</p> <p>Secondary Structure steel: 7.800 EUR/tonne</p> <p>Transition piece steel: 5.000 EUR/tonne</p> <p>Primary steel for piles ect: 1..600 EUR/tonne</p> <p>Manufacturing Costs: 400 EUR/tonne</p>	<p>Scour protection: not needed</p>	<p>Barge: 10.000 EUR/Day (3.000T payload) to 25.000 EUR/Day (7000T payload)</p> <p>Heavy lifting cranes: 150.000 EUR/Day (for 8.200T lifting capacity)</p> <p>Drilling equipment: 79.000 EUR/Day. 1.6 days/foundation</p> <p>Piling equipment: 11.000 EUR/Day. 1.6 days/foundation</p> <p>Days required for installation: 5-6 days required (Jacket + TP+ Piles).</p>	<p>Heavy lifting/jack up vessel: 84.00 t0 290.000 EUR/day as lifting capacity increases from 800 tonne to &gt; 2000 tonne.</p> <p>4 foundation can be installed/trip</p> <p>Drilling equipment: 79.000 EUR/Day. 1.6 days/foundation</p> <p>Piling equipment: 11.000 EUR/Day. 1.6 days/foundation</p> <p>Days required for installation: 5-6 days required (Jacket + TP+ Piles).</p>	<p>Cost (Grouting material + vessel): 90.00 EUR/foundation</p> <p>Surface treatment: 110 EUR/m<sup>2</sup> for 1000 m<sup>2</sup></p> <p>Noise mitigation: 200.000 – 300.00 EUR/Foundation</p>
<p><b>Suction Bucket Jacket</b></p> 	<p>Steel of jacket body: 3.200 EUR/tonne</p> <p>Secondary Structure steel: 7.800 EUR/tonne</p> <p>Transition piece steel: 5.000 EUR/tonne</p> <p>Suction buckets steel: 3.200 EUR/tonne</p> <p>Manufacturing Costs: 400 EUR/tonne</p>	<p>Scour protection: 200.000 EUR/tonne</p>	<p>Barge: 10.000 EUR/Day (3.000T payload) to 25.000 EUR/Day (7000T payload)</p> <p>Heavy lifting cranes: 150.000 EUR/Day (for 8.200T lifting capacity)</p> <p>Tugboats : 17.000 EUR/Day (waves&lt;4mheight) 27.000 EUR/Day (waves&gt; 4mheight) 1 Tugboat required for 1 day/foundation</p> <p>Suction Pump: 8.000 EUR/ foundation</p> <p>Days required for installation: 1 - 3 days required.</p>	<p>Heavy lifting/jack up vessel: 84.00 t0 290.000 EUR/day as lifting capacity increases from 800 tonne to &gt; 2000 tonne.</p> <p>2 foundation can be installed/trip</p> <p>Suction Pump: 8.000 EUR/ foundation</p> <p>Days required for installation: 1 - 3 days required.</p>	<p>Surface treatment: 110 EUR/m<sup>2</sup> for 1000 m<sup>2</sup></p>



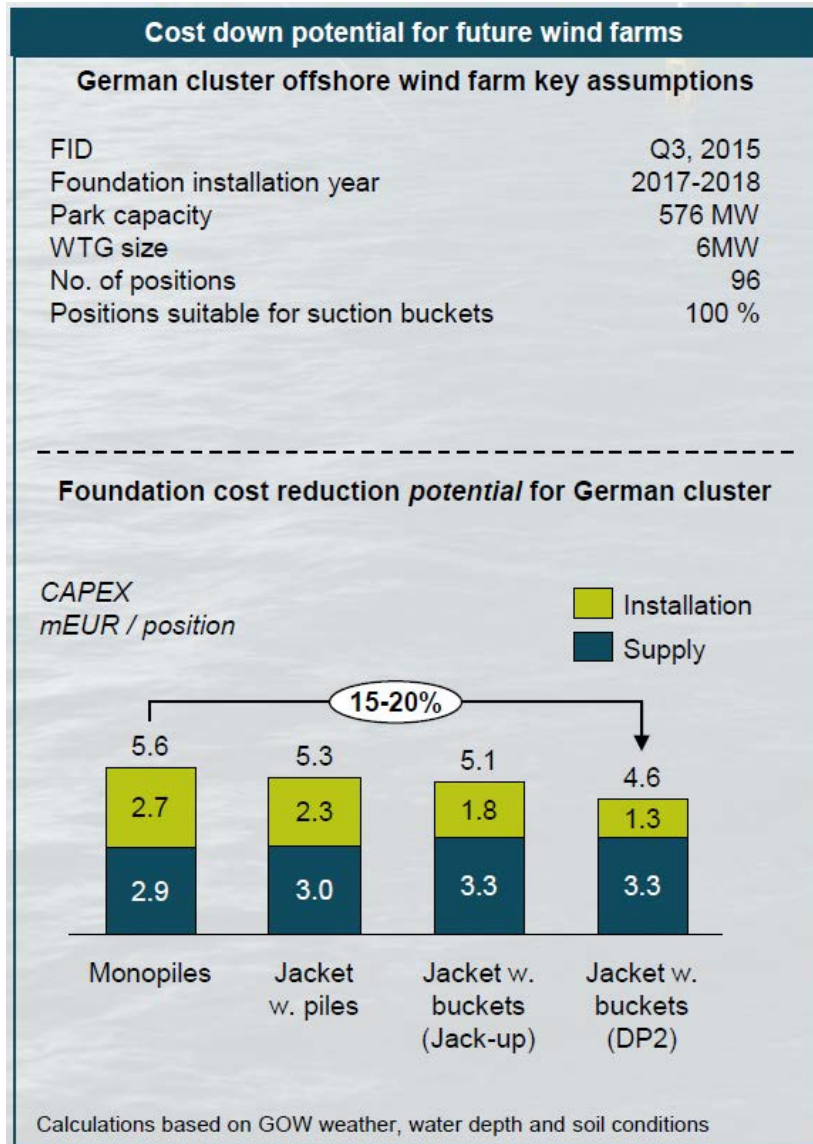


Figure 4.1-26: Cost down potential for future wind farms after Mørch C.B [4-29]

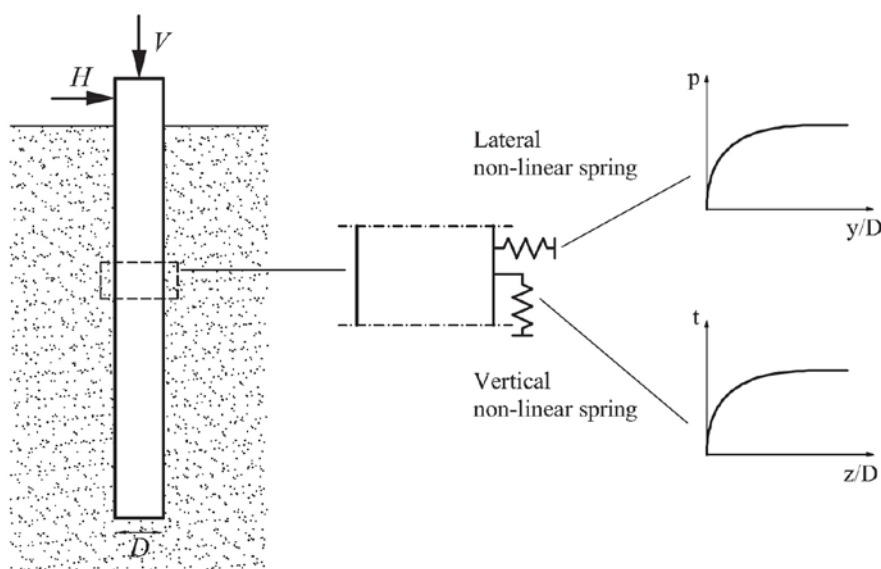
## 4.2 Vibratory-driven piles for jacket sub-structures

In this sub-chapter, the possibility of using vibro-driven piles as foundations for jacket sub-structures is explored by interpreting the experimental data obtained during the experimental campaign thoroughly described in [4-01]. In Section 4.2.1 deep foundations are introduced, a brief literature review of vibratory driven piles is given and the underlying motivations of the contribution are outlined. In Section 4.2.2 attention is given to the ultimate capacity prediction of vibro-driven piles. In Section 4.2.3 the initial stiffness of axially loaded piles is the research focus and a numerical model is calibrated on the base of the experimental results. In Section 4.2.4 conclusions are drawn and economic benefits as well as next research steps for vibro-piles are discussed.

### 4.2.1 Introduction and motivation

#### Introduction to piled foundation for offshore wind converters

Piled foundations can be subdivided into large diameter piles (between 4 and 8 m in diameter), for sub-structures with monopod foundations, and small diameter piles (from 2 to 4 m in diameter), for sub-structures with multipod foundations. Piled foundations are the best option for offshore structures when the shallow soil encountered is soft or when there is the likelihood of foundation slide problems due to large horizontal loads. Most piles are driven into the soil with hydraulic hammers. Piles supporting jackets are driven into the seabed through the sleeves integrated at the jacket base (post-piling) or through mobile piling templates transported by jackup vessels (pre-piling). Large diameter piles are hammered down through a frame leaning out from the installation vessel. To model the load transferred to the soil, the soil-pile interaction is schematised with non-linear springs (see Figure 4.2-1).  $t$ - $z$  curves describe the relationship between mobilised shear stress and vertical displacement of axially loaded piles.  $p$ - $y$  curves describe the relationship between soil resistance and lateral displacement of laterally loaded piles.



**Figure 4.2-1 – Simplified scheme of soil-structure interaction for axially loaded piles and horizontally loaded piles. After [4-31].**

As depicted in Figure 4.2-2, monopiles (large diameter piles) have to bear large lateral loads in terms of combined moment and horizontal load. The current design base for laterally loaded piles is the well-known p-y curves approach. This method was developed some decades ago for slender piles. Whether this design method is appropriate for very large diameter (and thus stiffer) piles or not is a controversial and ongoing topic of discussion among researchers and industry players [4-32].

Piles supporting jacket structures (small diameter piles) are mainly subjected to vertical loading in tension and compression (see Figure 4.2-3). The axial capacity of a piled foundation under compressive loads has two contributions: the base resistance and the shaft resistance. In sandy soils the shaft resistance is assessed based on the CPT cone resistance whereas in clayey soils it is quantified as a function of the undrained shear strength. The ultimate base resistance is defined with an allowable vertical displacement criterion and is calculated by summing the contributions of external pile shaft resistance, base resistance and either soil plug or internal pile shaft resistance. Obviously, in case of tensile loading, the base resistance has no influence on the pile capacity. As emphasized in recent publications ([4-35], [4-36]) tensile loading for piles supporting multipod sub-structures are very important and can in some cases be the design driver.

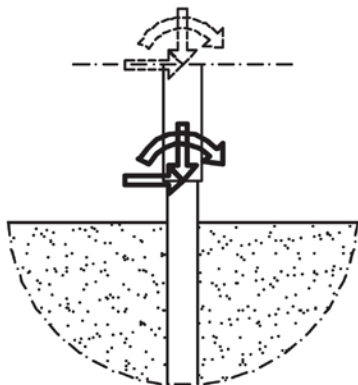


Figure 4.2-2 – Load configuration of a sub-structure with monopod foundation.

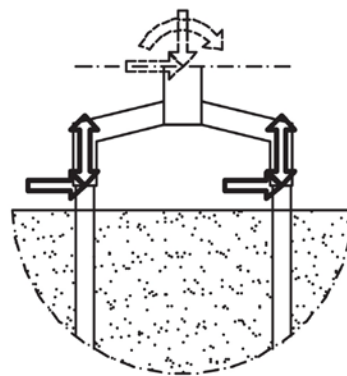


Figure 4.2-3 – Load configuration of a sub-structure with multipod foundation.

### Vibratory pile driving

Important studies on vibratory-driven piles include: [4-34], [4-37], [4-38], [4-39], [4-40] and [4-41].

Viking [4-37] conducted field tests to investigate the main geotechnical mechanisms intervening when installing steel structures in the soil with vibratory hammer. He argued that only after having understood the installation process, can the bearing behaviour also be understood. Not surprisingly he argues that the prime factors affecting vibro-driveability can be divided in three categories: vibratory-rig related, structure related and soil related. Rather interestingly he explains that during the structure penetration the soil grains undergo an abrupt reduction of the effective stresses making the inter-granular contact forces very weak. He also points out that in case of water-saturated soil the process described is accelerated.

Lammertz [4-38] examines the axial compressive bearing capacity of vibratory-driven piles. Field tests were performed and compared with various existing prediction methods. A parameter study was conducted taking into consideration soil properties and pile dimensions. Finally, a method for predicting the pile capacity was proposed on the base of the experimental results.

A literature study elaborated within Lammertz [4-38] reveals that vibro-driven piles have generally lower capacity and stiffness in comparison to impact-driven piles. In addition, high penetration

rates results in lower pile capacity. According to the literature review, the only tensile capacity of hollow piles tests were those of Braaker [4-39] in which 10 to 40% lower resistance was found.

Borel et al. [4-40] report a comprehensive experimental campaign of vibratory- and impact-driven piles under compressive axial loading. The bearing capacity of vibratory driven piles is found to be smaller than that of impact-driven piles (shaft resistance between 5 and 75% while base resistance between 10 and 75%).

In the offshore wind energy industry vibratory-driven piles have never been employed for real. Currently, the German regulation [4-42] requires that vibratory-driven piles must be impact driven at the end of the installation until a specific depth (dynamic testing), in order to make sure they have adequate capacity. This makes project developers reluctant on choosing this installation technique since the final impact drive phase considerably raise the project costs. Recently, two important research projects on vibro-piles for offshore wind sub-structures were conducted. In LeBlanc et al. [4-41] two prototypes of vibro-driven monopiles were installed and laterally tested. Lateral stiffness and capacity did not show any particular difference than those predicted with standard methods for impact-driven piles.

In Matlock [4-34] a comprehensive large scale experimental campaign was successfully carried through. The aim was to compare lateral capacity of vibro-driven and impact-drive piles. Results of the campaign are for the time being not publically available.

### Scope of the report

Jacket sub-structures for offshore wind turbines are normally founded on impact-driven piles. As already mentioned in INN WIND.EU [4-33], and as also presented in Matlock [4-34], vibro-driven piles offer the following advantages with respect to impact-driven piles:

- No noise mitigation system required when installing
- Faster installation
- No fatigue induced by ramming (potential saving in steel for piles)

These advantages might bring cost savings in the range of 5% to 10% of foundation fabrication and installation costs [4-34].

As stated in the brief literature review above, information on tensile capacity of vibro-piles are very limited.

Research on vibro-driven piles has so far focused on installation analysis, onshore piles subjected to compressive loading and offshore piles subjected to overturning moment. Therefore, it is not clear whether the economic advantages mentioned above would be able to outweigh a potential increase in pile dimension due to limitations in bearing capacity. In other words, the cost reduction outlined can have an impact on the project economics only if vibro-driven piles have similar capacity to the traditionally adopted impact-driven piles. Thus, the first specific aim of this study is to prove whether the ultimate tensile capacity predicted with the standard CPT-methods gives comparable results to the large scale test data presented in INN WIND.EU [4-01].

Another crucial analysis for the complete understanding of the soil–structure interaction concerns the initial axial stiffness of the geotechnical system. The second specific aim of the contribution focuses on this aspect of the axially loaded pile. A 2D axisymmetric finite element model with a simplified pile is validated in terms of initial stiffness against the test results. As reported in INN WIND.EU [4-01], two piles were vibro-installed for the INN WIND.EU project (see also Figure 4.2-4). In the present contribution only Pile 2 will be interpreted. Pile 1 will be used for a further model validation in the final deliverable of the project.

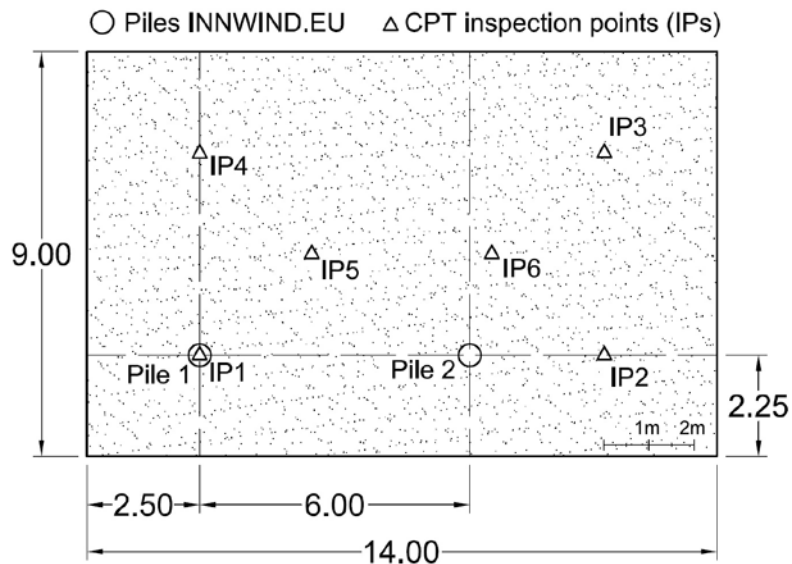


Figure 4.2-4 – Plan view of the sand pit with indication of the inspection points (IPs) for CPT and the piles (Pile 1 and Pile 2) installed for the INNWIND.EU project.

#### 4.2.2 Tensile capacity of vibratory-driven piles

In this section the first specific aim of this contribution is achieved. The ultimate tensile capacity of the vibratory-driven pile tested is compared to the design CPT-based methods.

##### Introduction to CPT methods

CPT methods for axially loaded piles are empirical formulas developed by four different research groups (Imperial College, London (ICP); University of Western Australia, Perth (UWA); Norwegian Geotechnical Institute, Oslo (NGI); Fugro) which relate CPT measurements with the axial capacity in tension and in compression of purely axially loaded piles. A comprehensive and comparative review of the methods is given in Lehane et al. [4-44]. The methods are also included in the offshore foundation standard [4-45] with the names ICP-05, UWA-05, Fugro-05 and NGI-05. This nomenclature will be retained in this report as well. The calculations presented in this report were performed with the IGtHPile software developed by the Institute of Geotechnical Engineering (IGtH), Leibniz Universität Hannover, Germany.

##### Interpretation of the test results by means of CPT methods

Usually, the input data for CPT methods are an average of raw CPT data calculated over a specified distance step. The distance step chosen was 0.5 m. The average of raw CPT data taken each 0.5 m (design idealization of  $q_c$ ) is plotted in Figure 4.2-5 against the real  $q_c$  measurements. It should be noted that the input curve starts from 0.6 m. This is why the first 60 cm of sand were taken out from the sand pit since sand cementation occurred superficially in the sand pit. A cone

resistance equal to 0 in correspondence of 0.6 m depth was assumed (see Figure 4.2-5 at 0.6 m depth).

In Figure 4.2-6 the experimental load displacement curve is plotted. It can immediately be observed that a general failure of the system did not occur since no particular discontinuity followed by hardening or softening behavior can be seen on the curve. A specific criterion to figure out the ultimate capacity (Criterion 1) of the pile consists on drawing the tangent curves to the

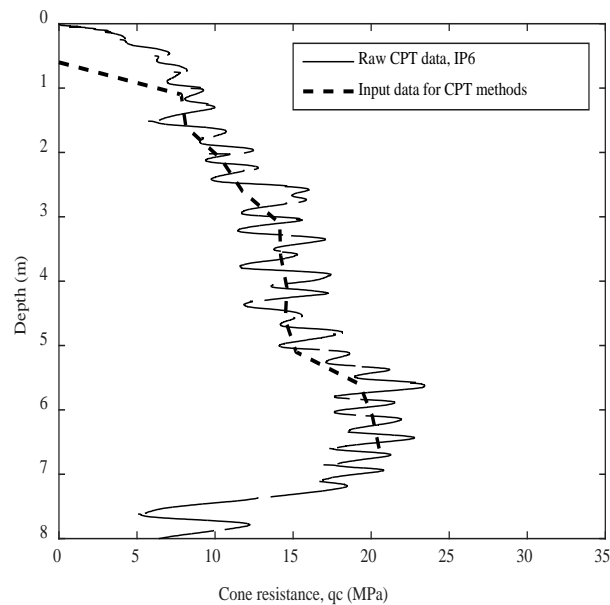


Figure 4.2-5 – Design idealization of  $q_c$ . Input  $q_c$  data for CPT methods together with raw CPT data of IP6.

Table 4.2-1 – Summary of ultimate capacity prediction in comparison to the experimental data.

Method	Ultimate capacity (kN)	Experimental result / CPT method prediction
ICP-05	316	0.364
UWA-05	286	0.402
Fugro-05	398	0.289
NGI-05	648	0.177
Experimental data	115.1	1

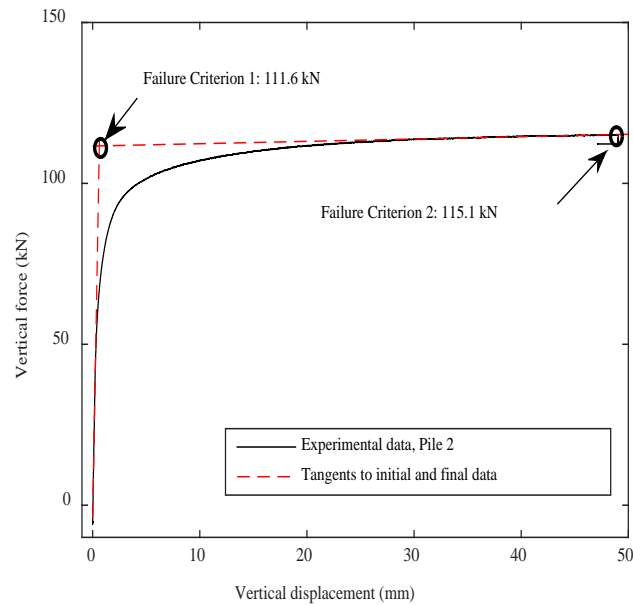
initial and final stiffness of the curve. The intersection point of these two tangents can then be taken as ultimate capacity.

The ultimate capacity of the pile obtained with Criterion 1 is 111.6 kN. A much more often adopted criterion for tensile capacity of piles (Criterion 2) defines the ultimate load as that load reached at a displacement equal to a tenth of the pile diameter ( $D/10$ ). A vertical displacement of  $D/10$  was strictly speaking not reached during the test. However the maximum displacement achieved equals the 98% of the limit defined by Criterion 2 and was therefore judged to be representative of the ultimate capacity. According to Criterion 2, the ultimate tensile loading is 115.1 kN. The two criteria described above are shown together with the experimental data in Figure 4.2-6. The second criterion is from now on considered for the interpretation.

Table 4.2-1 gives an overview of the CPT based methods prediction in comparison with the tensile capacity test. It is immediately apparent that the experimental tensile capacity is overpredicted by



all the CPT methods. The experimental result is in proportion between 17 and 40% of the CPT methods prediction. The same information is visually presented in Figure 4.2-7 where the NGI-05 method is omitted to allow appropriate representation of the experimental data. In accordance to [4-43] the most suitable approaches for open-ended piles in tension seem to be the ICP-05 and the UWA-05. This seems to be confirmed also by the test data of this study, which show the smaller deviation for the ICP-05 and UWA-05 methods. The quite relevant discrepancy between



**Figure 4.2-6 – Experimental data with ultimate capacity identifications through tangent lines of initial and final data.**

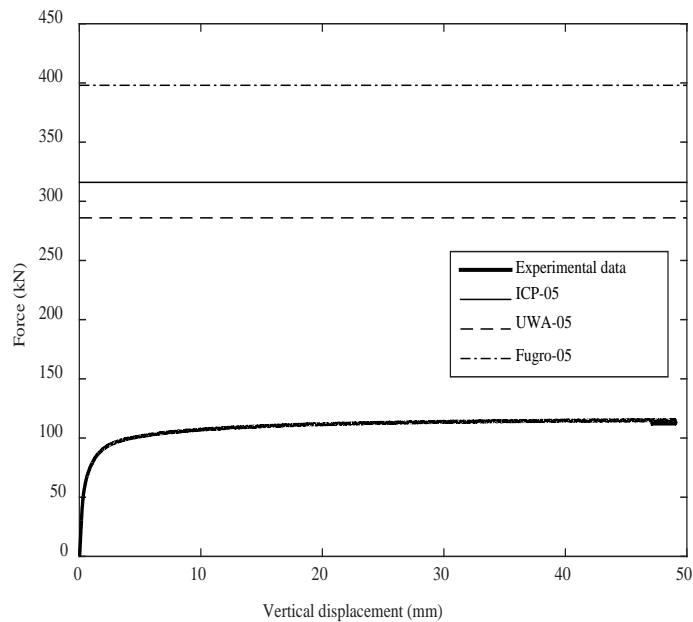


Figure 4.2-7 – Experimental data in comparison to CPT methods prediction.

CPT-based estimation and experimental result is to be ascribed to the installation method used. As already mentioned, CPT-based approaches were developed with impact-driven and pressed piles data. The test performed corroborates the previous finding of other researchers; the shaft resistance of vibro-driven piles is smaller than that of impact-driven piles. It remains though to be seen whether Pile 1, which underwent relevant pre-loading sessions and had time after the installation to grow set-up effects, will show a similar behavioral pattern.

### 4.2.3 Stiffness of vibratory-driven piles

In this section the second specific aim of the contribution is achieved. Two numerical models are described and are validated in terms of initial pile stiffness against the experimental results.

#### 2D-Axisymmetric numerical model

In INN WIND.EU [4-01] a 3D numerical model for the soil-foundation interaction was presented. However in this study a 2D numerical model is used to interpret the numerical data. The geometry of the geotechnical system allows the pile-soil interaction to be properly modelled also by means of a 2D axisymmetric model. The choice of adopting a simplified 2D model at this stage was deliberately made and was driven by the possibility, offered by 2D axisymmetric models, of running faster simulations. As a result of that, parametric studies can more easily be conducted and the complex soil-structure interaction more thoroughly analysed. In the final deliverable of the INN WIND.EU project the 3D model will be compared to the 2D model.

The numerical model was created with the finite element program ABAQUS [4-46]. The 2D-axisymmetric model is formed by axisymmetric elements of the type CAX4. The laboratory physical situation is recreated in the model. In the numerical model the distance between the pile center and the retaining wall (boundary condition) was taken as the minimum distance present in the laboratory (5 pile diameters). This is not properly realistic since the boundaries in all the other

directions are not so close to the pile. The effect of this will however be estimated by comparing the 2D-axisymmetric model with the 3D model. The discretization of the model is shown in Figure 4.2-8. A very fine mesh was created in the vicinity of the pile. The pile was modelled with a linear-elastic material behavior with Young's Modulus  $E=2.1 \cdot 10^8$  kPa and Poisson's ratio of  $\nu=0.3$ . For the soil the Mohr-Coulomb failure criterion is adopted. The stiffness modulus,  $E$ , was derived with two methods:

1. Oedometric tests carried out on the sand used
2. CPT data were averaged over the embedded depth of the pile

A value of 11 MPa was calculated with oedometric tests, and a value of 17 MPa was calculated with CPT data.

The soil is fully saturated except for the most superficial 20 cm. Despite of that, only one soil strata with effective unit weight,  $\gamma' = 10.15$  kN/m<sup>3</sup>, was considered. A Poisson's ratio of 0.27 was used. The friction angle,  $\phi'$ , was chosen as the critical friction angle characteristic for the sand with that particular compaction state. A value of  $\phi = 33^\circ$  was chosen on the base of a calculated peak friction angle according to [4-47] and assuming a dilation angle of  $10^\circ$ .

The hypothesis of pile wished in place was made. The coefficient of lateral earth pressure at rest was traditionally calculated as  $K_0 = 1 - \phi'$ .

The model was constructed so that the pile is a solid section with equivalent weight and  $E$  modulus to the real system (pile plus saturated soil inside). As a result of that, only the self-weight of a plugged pile plus the external shaft resistance contribute to the tensile resistance. For modelling the pile-soil contact an elasto-plastic contact interaction was considered. The friction coefficient was calculated with the well-known equation  $\mu = \tan(\delta) = \tan(2/3 \phi')$ . The displacement at which full frictional stress mobilization occurs (elastic slip) was set to 2 mm. A list of the parameter used is listed below in Table 4.2-1.

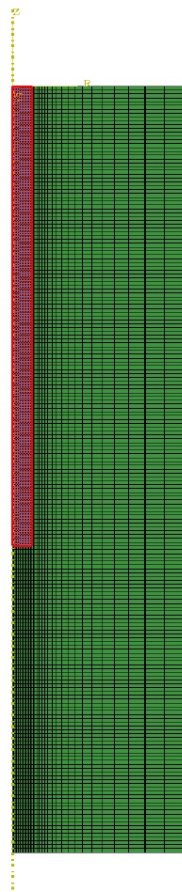


Figure 4.2-8 – Discretization of the 2D - axisymmetric model. Pile emphasized in red color.

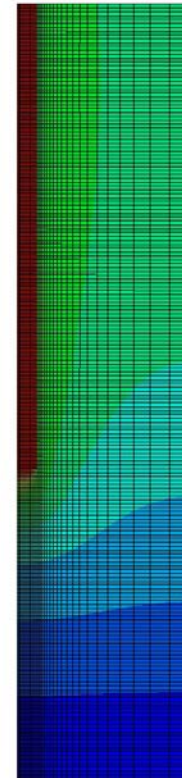
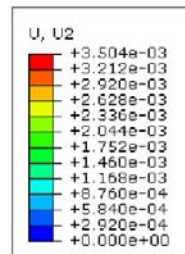


Figure 4.2-9 – Vertical displacement during the tensile test. Legend in (m).

Table 4.2 – Parameters used for sand and contact model

Property	Symbol	Unit	Value
Friction angle	$\phi'$	(°)	33
Soil-pile interface friction angle	$\delta$	(°)	22
Effective unit weight	$\gamma'$	(kN/m <sup>3</sup> )	10.15
Poisson ratio	$\nu$	(-)	0.27
Dilation angle	$\psi$	(°)	10
Young's moduli	$E$	MPa	11, 17 120

In Figure 4.2-8 the contour graph of the vertical displacement during the tensile loading are shown. The model was carefully checked by applying different loads to the pile in tension and compression and by calculating thereafter equilibrium between forces applied and resultant stresses. To enable the achievement of a clear plastic plateau at the end of the curves and also to simulate the physical experiment, the simulations were run displacement-controlled and thus by defining a particular displacement. A considerable number of parameter studies were carried out in order to have a clear understanding of the model parameters.

The model responds as expected to the parameter change. The displacement-force curves relative to three different  $E$  moduli are shown in Figure 4.2-10. As expected, the three curves present equal ultimate capacity and significantly different initial stiffness. The change in initial stiffness is consistent with the different values of the  $E$  moduli. A further study was conducted on the effect of the friction angle between soil and structure,  $\delta$ . In Figure 4.2-11 three simulations with different soil-structure friction angles were performed. Again the model responds realistically to the parameter change. It can be noticed that the parameter  $\delta$  has an effect on the ultimate capacity of the curve but not on the initial stiffness.

The numerical model is validated in terms of initial stiffness by fitting the initial load-displacement curves of model and test. The region of the curve of interest is that which goes approximately up to the 50% of the ultimate capacity. In Figure 4.2-12 it can immediately be seen that the load-displacement behavior of the model calculated with  $E = 17$  MPa is considerably off the trajectory of the test curve. The physical model indeed shows a much higher initial stiffness. In order to have reasonable match with the experimental curve the  $E$  modulus of the sand has to be increased to 120 MPa, as shown in Figure 4.2-12. This value of  $E$  is undoubtedly out of the normally used range. The consequence of such a discovery is that care must be taken in the choice of  $E$  when modelling piles under tensile loading.

The model validation proposed is not ultimate and will have to be corroborated by the more sophisticated 3D numerical model where the  $E$  modulus is more realistically defined as a function of the depth. In addition, the information provided by the second experimental test will also be necessary to corroborate the model calibration and to see how the parameters of the numerical model should be changed when effects such as set-up and pre-loading are to be modelled.

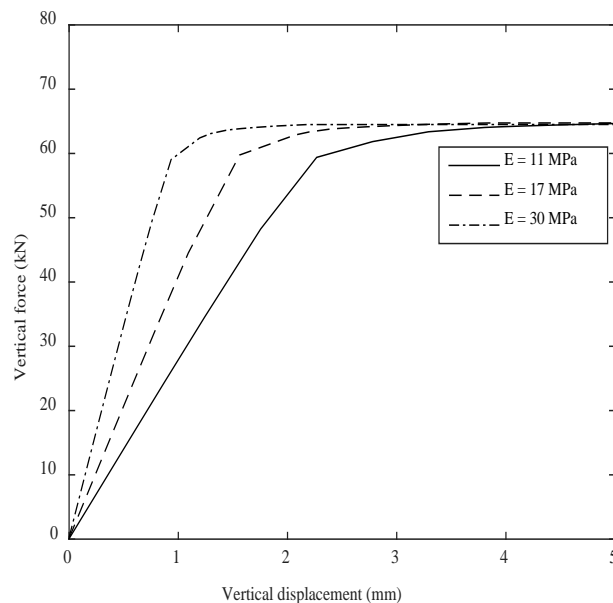


Figure 4.2-10 – Load-displacement curves of the 2D axisymmetric model with three different  $E$  moduli.

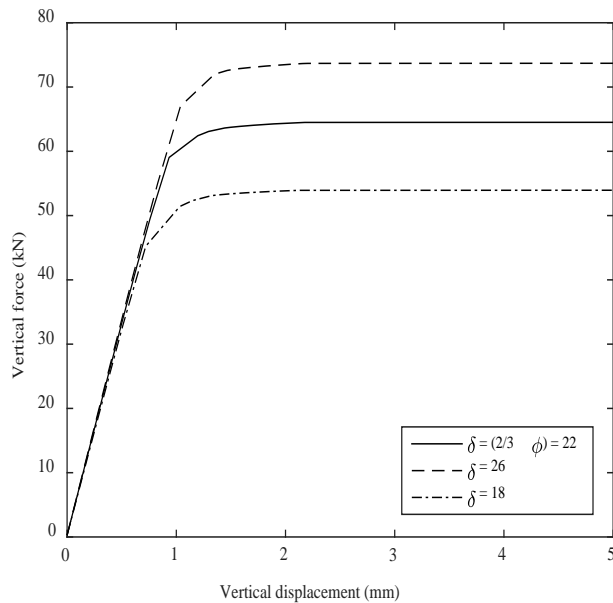


Figure 4.2-11 – Load-displacement curves of the 2D axisymmetric model with three different values of  $\delta$

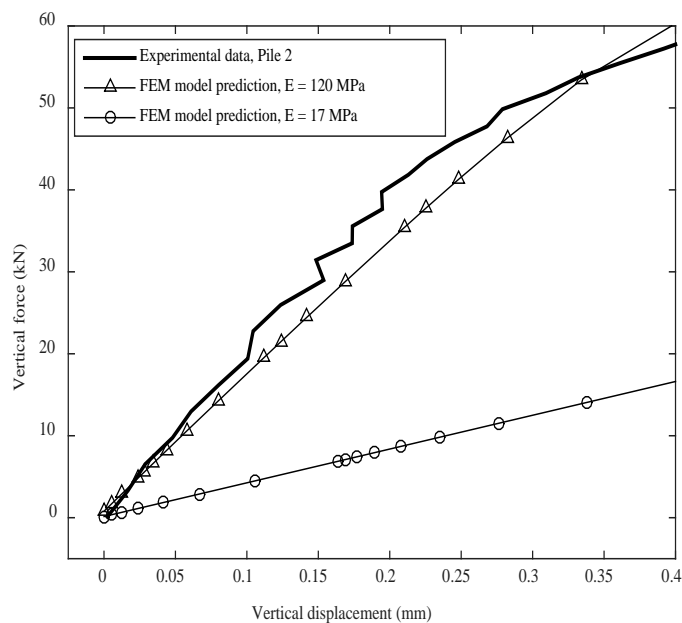


Figure 4.2-12 – Comparison of load-displacement curves of numerical model and experimental test

#### 4.2.4 Current TRL and cost reduction potential of vibro-driven piles

As explained in the previous section, the behaviour of vibro-driven piles under tensile loading is by far unexplored. In the context of the INNWIND.EU project large scale tests are conducted on this particular kind of foundation. All the details concerning the experimental campaign are described



in [4-01]. In more specific terms, two piles with same dimensions are tested for the following purposes:

- to understand whether vibro-driven piles have similar bearing capacity to that prognosticated by standard CPT methods used for impact-driven and jacked piles
- to calibrate a numerical model on the base of the experimental results
- to understand whether relevant pre-loading, scour and set-up effects influence the tensile bearing capacity of vibro-driven piles

Research concerning the last bullet point will be developed for another deliverable of the project. The present contribution proposes discussions on the first two bullet points.

According to the definition given by the INN WIND.EU Project, the technology readiness level of vibro-driven piles for jacket sub-structures is 7. That means that the next development step should be the integration of this technology in a prototype of the commercial turbine design in order to perform field testing.

The results of the test campaign on vibro-driven monopiles conducted by [4-34] highlighted very promising potential saving. Considering a 50 turbine wind park with 6MW turbine and 30 m water depth the cost reduction of foundation fabrication and installation costs can be summarized as follows:

- The absence of noise mitigation system when vibrating amounts to 12,5 M€
- The reduced installation time gives 1,25 M€ saving
- The fatigue induced during installation with impact hammer is avoided bringing steel reduction in the piles for a saving of 0.75 M€

Again [4-34] states that the overall savings might be between 5 and 10% of fabrication and installation costs. However, the experimental test conducted so far within this project highlights a considerable lower ultimate capacity and therefore a deficit of this foundation technology when designing a pile in ultimate limit states (ULS). This means that if the design is driven by ULS design the potential savings should be carefully estimated with an *ad-hoc* cost analysis considering both logistic and fabrication. It remains also to be seen how set-up effects and pre-loading (Pile 1) will affect the bearing behavior of impact-driven piles

The calibration of the numerical model revealed that the initial stiffness of the pile seems to be rather underpredicted by the numerical analysis with standard parameters. The stiffness parameter calculated with standard methods (in particular the  $E$  modulus) should be increased by a factor 7 for the numerical and experimental curves to match.

### 4.3 Innovative foundations

Advances in components' design are proposed for the semi-floater concept. Attention is given to main parts of this concept; they are mooring system and universal joint founded on a reinforced concrete base. Design processes are presented in details and the results are enriched with detailed figures. The resulting performance of the turbine is investigated and recommendations are given for further developments. Cost analysis permits comparison with other possible solutions.

#### 4.3.1 Discussion of the considered innovations on component level

A novel semi-floater support for a 10 MW wind turbine was introduced in the previous deliverables ([4-48] and [4-49]). It is mainly made of (i) a universal joint mounted on a base placed at the sea bed; (ii) a buoyant system; and (iii) a mooring system. Figure 4.3-1 depicts the geometry of this concept at the previous study stage. A detailed description is given in [4-50]. There are presented some characteristic curves describing operational conditions, representative loads for operating and storm cases, and structural displacements. In particular, it has been determined representative loads applied at the joint. They are as summarized in Table 4.3-1.

In the present design phase, closer look is given to the mooring lines, to the universal joint and to the base. The mooring lines will be designed such that they can allow a maximum of 10 m sway, and develop a yaw counter-moment thanks to their delta connections.

This last feature arises the possibility to free the universal joint in torsion such that it is not transmitted any torque. However, it should be able to deform under roll and pitch moments. Consequently, a torque-free mechanism is proposed. Finite element method is used to design the universal joint. Its equivalent matrices (stiffness, damping and mass) with coupled actions in all directions are used in hydro-aero-servo-elastic simulations. The universal joint transmits loads to the reinforced concrete base which is designed or justified with respect to various failure modes (overturning, bearing, sliding and punching).

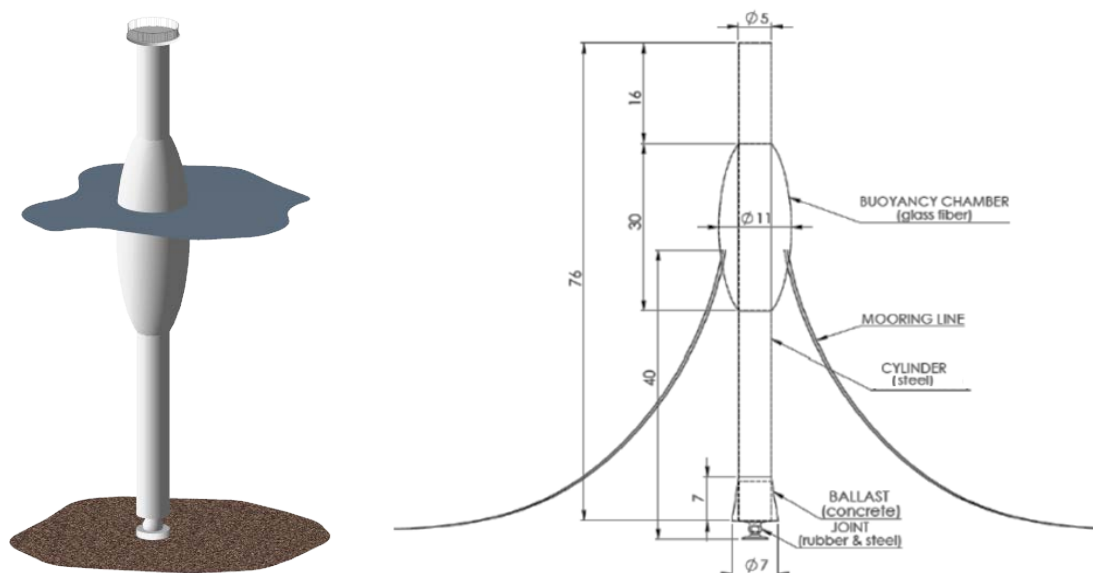


Figure 4.3-1 – Semi-floater concept

**Table 4.3-1 – Representative loads at the universal joint as per previous design stage**

		DLC	F <sub>x</sub> [kN]	F <sub>y</sub> [kN]	F <sub>z</sub> [kN]	F <sub>res</sub> [kN]	M <sub>x</sub> [kNm]	M <sub>y</sub> [kNm]	M <sub>z</sub> [kNm]	M <sub>res</sub> [kNm]
F <sub>x</sub>	Max	6.2a	5.70E+03	2.00E+02	1.00E+04	5.70E+03	-7.90E+04	2.30E+05	-1.10E+04	2.40E+05
	Min	6.2a	-6.00E+03	1.80E+03	9.20E+03	6.30E+03	1.10E+05	2.30E+05	-5.80E+04	2.50E+05
F <sub>y</sub>	Max	6.2a	-7.50E+02	6.40E+03	1.00E+04	6.40E+03	2.40E+05	1.50E+05	8.50E+03	2.80E+05
	Min	6.2a	1.50E+03	-6.80E+03	8.30E+03	6.90E+03	-9.10E+04	-1.30E+04	8.80E+04	9.20E+04
F <sub>z</sub>	Max	6.2a	5.50E+02	-3.20E+02	1.80E+04	6.40E+02	2.00E+05	-4.30E+04	9.90E+04	2.00E+05
	Min	6.2a	3.70E+02	-1.60E+02	4.40E+03	4.10E+02	3.00E+05	-1.00E+05	-1.00E+04	3.10E+05
F <sub>res</sub>	Max	6.2a	-5.50E+03	-4.50E+03	1.10E+04	7.10E+03	5.60E+04	5.50E+04	-1.60E+05	7.80E+04
	Min	1.2	1.10E-01	-1.40E-01	1.10E+04	1.80E-01	1.60E+05	1.60E+04	-3.40E+03	1.60E+05
M <sub>x</sub>	Max	6.2a	7.10E+01	1.10E+02	1.30E+04	1.30E+02	4.60E+05	-2.20E+05	8.40E+03	5.10E+05
	Min	6.2a	-6.60E+02	-5.60E+02	9.90E+03	8.70E+02	-4.80E+05	7.80E+04	1.90E+04	4.90E+05
M <sub>y</sub>	Max	6.2a	-1.70E+02	8.80E+02	1.00E+04	9.00E+02	1.10E+04	5.30E+05	-1.20E+04	5.30E+05
	Min	6.2a	2.90E+03	7.40E+01	9.50E+03	2.90E+03	-2.10E+04	-5.40E+05	4.80E+03	5.40E+05
M <sub>z</sub>	Max	6.2a	3.60E+03	2.20E+03	7.20E+03	4.20E+03	1.10E+05	-1.80E+05	2.20E+05	2.10E+05
	Min	6.2a	-2.70E+03	3.90E+03	1.00E+04	4.80E+03	4.30E+04	-5.00E+04	-2.00E+05	6.60E+04
M <sub>res</sub>	Max	6.2a	3.20E+02	3.00E+02	1.20E+04	4.40E+02	3.80E+05	-4.30E+05	1.40E+04	5.70E+05
	Min	1.3	-1.00E+02	-1.20E+03	1.10E+04	1.20E+03	1.50E+02	-9.10E+01	-3.20E+03	1.80E+02

### 4.3.2 Description of the performed studies of innovations on component level

#### Mooring system

The mooring system is made of six catenary lines attached to the buoyant chamber through delta connections. Line anchorages at the sea bed are assumed fixed, i.e. restrained for all translational and rotational directions.

Bulder et al (2002) [4-51] and Lefebvre and Callu (2012) [4-52] respectively considered maximum offset for comparable floating structures to be 10.10 m and 10.00 m at 50 m and 40 m water depth. 10.00 m is chosen for this design stage as the maximum admissible offset.

At 50 m water depth, Benaissai et al (2014) [4-53] showed that it was not feasible to design a wire rope mooring system under an assumption of 10 m assigned as admissible offset. Therefore stud link R5 chain type is selected for the lines in the rest of the present study.

**Table 4.3-2 – Chain properties (Stud Link R5)**

Properties	Reference	General values	Actual values
Effective Elastic Modulus [N/m <sup>2</sup> ]	DNV OS E301, 2013 [4-54]	$E_{eff} > 5.6 \times 10^{10}$	$5.6 \times 10^{10}$
Nominal Diameter [mm]	DNV OS E302, 2008 [4-55]	$74 < d < 210$	124
Linear Density in air [kg/m]	DNV OS E302, 2008 [4-55]	$m_a = 0.0219 d^2$	336.7344
Linear Density in water [kg/m]	Benassai et al, 2014 [4-53]	$m_w = 0.87 m_a$	292.9589
Breaking load [kN]	DNV OS E302, 2008 [4-55]	$Q = 0.032(44-0.08d) d^2$	16768.45
Drag Coefficient [-]	DT Brown, 2005 [4-56]	$C_d = 2.6$	2.6

Under the assumptions of maximum admissible offset of 10 m and the representative axial load  $T_2 = 4000$  kN on the critical line after load application i.e. after deformation, a three-step algorithm has been proposed to find the line length and the horizontal anchorage distance from the fairlead. It has been found a radius of about 320 m. It should be noted that attention has been taken to ensure that the critical line never gets taut by setting a laid cable fraction on the seabed. Appendix 4.3-A provides details of the algorithm.

After load simulation, it is obtained representative mean and dynamic loads,  $T_{mean}$  and  $T_{dyn}$ , respectively. Considering a Class 2 mooring system, Ref [4-54] recommends 1.40 and 2.10 for

mean and dynamic load factors, respectively. The characteristic line strength is taken as 95% of the nominal breaking load [4-53]. Therefore the utilization factor,  $u$  is calculated:

$$u = \frac{1.40T_{mean} + 2.10T_{dyn}}{0.95Q} \quad \text{Eq. 4.3-1}$$

### Universal joint

Adapted from Ref [4-57], the universal joint is roughly made of three main parts: a spherical ball, a coating of elastomeric pads and a socket. Each of these main parts can be exploded into subparts as annotated in Figure 4.3-2. Spherical ball and socket are fabricated using steel shell.

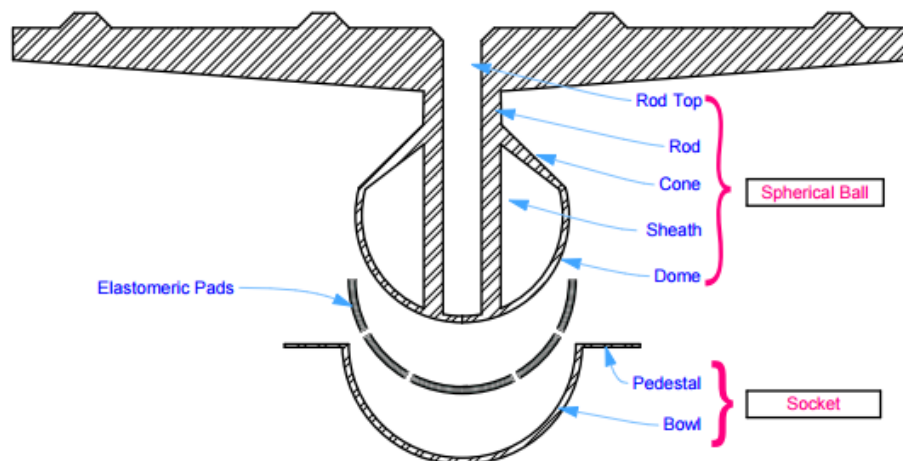


Figure 4.3-2 - Universal joint parts

The elastomeric pads are made of laminated rubbers placed between two external steel plates. These plates are respectively bolted to the dome and to the bowl. During roll and pitch, joint rotations induce shear deformations within the rubber layers.

The universal joint is also capable to withstand forces from the three principal directions but no torque is applied on it. In order to achieve a torque-free mechanism, passive connection is required between the floater cylinder and the joint. Two configurations were thought about: (i) Configuration 1 with a shaft going from the floater cylinder into the spherical ball; and (ii) Configuration 2 with a short cylinder originating from the joint platform plugged into the floater cylinder. Figure 4.3-3 presents both configurations. Configuration 1 has been found to be better performing than Configuration 2 in reason of the following criteria:

1. **Construction:** the construction of Configuration 2 requires detailed manufacturing of circular rails.
2. **Installation:** in case of non-automatic installation, plugging the shaft of Configuration 1 into the spherical ball is easier than adjusting the floating cylinder around the short cylinder of Configuration 2. The difficulty is augmented due to the lateral rails with prevent the floater cylinder from a smooth slide.
3. **Stress distribution:** with Configuration 2, all the five direction loads are applied to the joint through the rod top. This causes excessive stresses at its connection with the conical part. However, in Configuration 1, the bending moments are transmitted as pressure applied to the shaft sheath and resulting stresses are distributed to the whole ball.

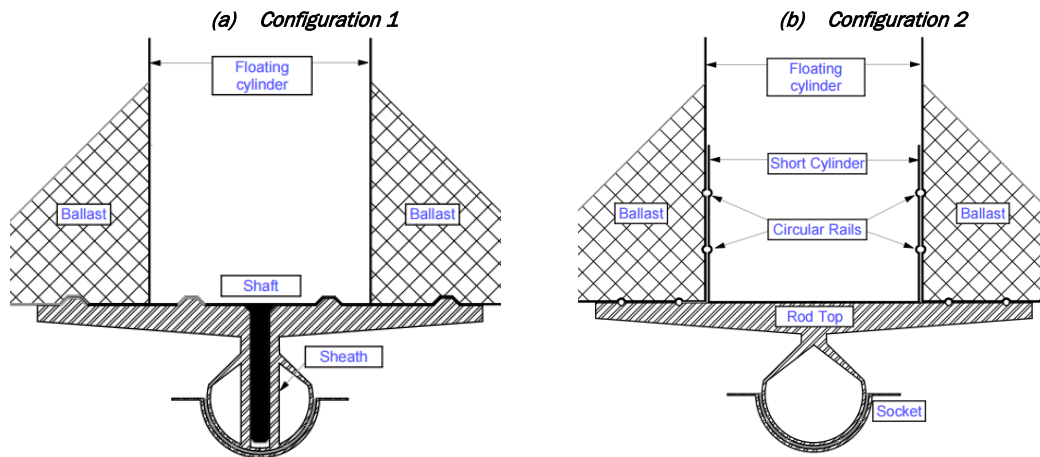


Figure 4.3-3 – Torque-free mechanisms

The steel used for shell is of type NV (Normal strength steel – NS) as designated by Ref [4-58]. It has a specified minimum yield stress of 235 MPa. Ref [4-59] recommends as steel density 7800 kg/m<sup>3</sup>, as elastic modulus 210 GPa and as Poisson's ratio 0.31.

The elastomeric pads consist of layers of steel shims sandwiched by rubber layers. The shim steel has the same properties as those of the one used for shells. With a density of 1250 kg/m<sup>3</sup>, the rubber has a bulk modulus of 1500 MPa as given by Sedillot and. Stevenson (1983) [4-57]. Ref [4-60] strongly recommends initialising Poisson's ratio of 0.495 for hyperelastic material when performing stress analysis in the commercial software package Abaqus [4-61]. South J.T (2001) [4-62] pointed out that there are no literature values of the shear strength of rubber. He performed a series of test on many rubber specimens with variable specifications, compositions and at different temperatures. He obtained shear strengths ranging between 35 and 55 MPa. In this study, a value of 30 MPa is opted; this corresponds to linear strain limit of 1.32.

Ref [4-57] derived the resisting moment of the joint as given by:

$$M_{resisting} = \frac{4\alpha}{3} \gamma G \frac{R_i^3 R_e}{n t} \quad \text{Eq. 4.3-2}$$

From which it can be deduced that:

$$\frac{R_i^3 R_e}{n t} \geq \frac{3M_{driving}}{4\gamma G\alpha} \quad \text{Eq. 4.3-3}$$

where

- $R_i$  and  $R_e$  are respectively the internal and external radii of the ball joint;
- $\gamma$  is the heel angle of the tower. It is estimated to be maximized by  $11.31^\circ = 0.197$  rad;
- $G$  is the shear modulus of rubber;
- $\alpha$  is the angular spread of the articulation. Considering the blank spaces between the pads,  $\alpha = 5\pi/18$  rad;
- $n$  is the number of rubber layers, and  $t$  is the thickness of each rubber layer.

Fehler! Verweisquelle konnte nicht gefunden werden. is evaluated at  $\frac{R_i^3 R_e}{n t} \geq 164.619$  m<sup>3</sup>. A

possible solution set of this equation is  $R_i = 1.715$  m,  $R_e = 1.84$  m,  $n = 3$  and  $t = 15$  mm:  $\frac{R_i^3 R_e}{n t} = 206.252$  m<sup>3</sup>.



AASHTO Specifications [4-63] recommend that the reinforcement shims should have at service limit state a total thickness of:  $hs \geq \max(0.1587 m; \frac{3t\sigma_s}{f_y})$  where  $\sigma_s$  is the axial stress on a pad; and  $f_y$  is the steel yield stress. Assuming the extreme case where the whole axial load is only supported by the central pad:  $\sigma_s = 2.145 MPa$ . Therefore,  $hs \geq \max(0.16 cm; 0.04 cm)$ . Two shim layers of 5.0 mm each are selected for  $hs = 1.00 cm$ .

Based on these dimensions, a finite element model is built in Abaqus. The model uses shell elements for the spherical ball and the socket, and solid elements for the elastomeric pads. The outer face of the socket is restrained for the six degrees of freedom. Figure 4.3-4 illustrates the finite element model as implemented in Abaqus.

The elastomeric coating is modeled as a unique set with equivalent properties in shear deformation mode. It is discretized with solid element C3D20H (20-node quadratic brick, hybrid with linear pressure). The ball is implemented as shell with 4-node quadrilateral element S4. The socket is also input as shell of type S8R which accounts for thick shell problem since its thickness is much larger than the distance between supports. Further details can be found in Ref [4-61].

On the model, a master node is created at the top rod center. It is solidary with all the point forming the top rod. Only forces (not moments) are applied at the said master node. The sheath is divided into two parts about the pedestal plane. Bending moments are modeled as force couple by applying opposite forces to each part (above and below the separating plane).

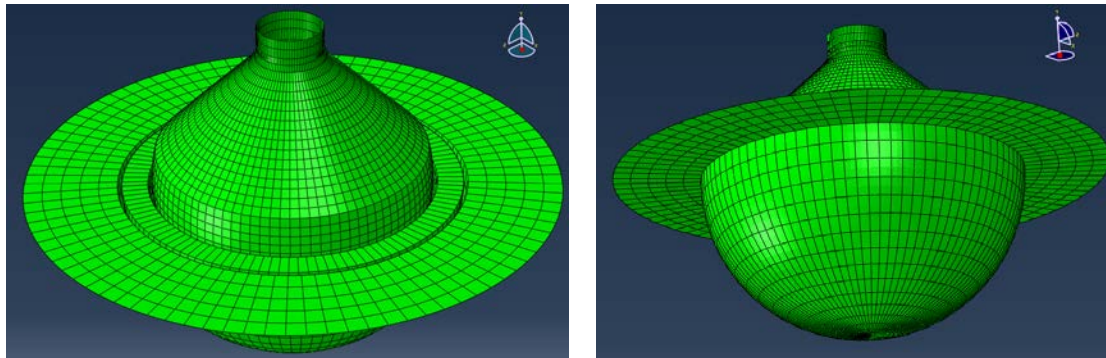


Figure 4.3-4 – Finite element model of the universal joint

A 6x6 equivalent stiffness matrix related to the rod top is obtained after elastic analysis of the universal joint. A Rayleigh damping matrix is determined to comply with the finding of Kim et al (2014) [4-64] about damping ratio in pitch mode (about 1.5%). These matrices are integrated in the HAWC2 model as superelement [4-65]. Then, simulations (details are provided below) are re-performed with the superelement and the new mooring system. From these analyses, representative load scenarios are extracted and they are presented in Table 4.3-3.

As well, damage equivalent loads for 25 year lifetime have been calculated based on:

$$S_L = \left( \frac{\sum_i t_i \sum_j n_{ij} S_{ij}^m}{N_{eq} T_s} \right)^{1/m} \quad \text{Eq. 4.3-3}$$

Where  
 $m = 4$  is the Wohler factor;  
 $N_{eq} = 10^7$  is the equivalent number of cycles during lifetime;  
 $T_s = 10 \text{ min} = 600 \text{ s}$  is the simulation duration;  
 $t_i$ : is the occurrence of a scenario,  $i$  in 25 years;  
 $S_{ij}$ : is the stress range,  $j$  for scenario,  $i$  as obtained from rainflow counting;  
 $n_{ij}$ : is the number of cycles of stress range bin,  $j$  for scenario,  $i$ .

Equivalent damage loads for 25 years at interface and at joint top are collected in Table 4.3-4

**Table 4.3-3 – Representative loads at the universal joint**

		DLC	Fx [kN]	Fy [kN]	Fz [kN]	Fres [kN]	Mx [kNm]	My [kNm]	Mres [kNm]
Fx	Max	6.2a	8.30E+03	3.40E+02	1.20E+04	8.30E+03	-1.10E+04	3.00E+05	3.00E+05
	Min	6.2a	-8.40E+03	4.30E+00	1.30E+04	8.40E+03	1.30E+03	-2.80E+05	2.80E+05
Fy	Max	6.2a	1.60E+03	6.50E+03	1.20E+04	6.70E+03	-1.80E+05	3.80E+04	1.80E+05
	Min	6.2a	6.00E+02	-6.80E+03	1.30E+04	6.80E+03	1.60E+05	5.80E+04	1.70E+05
Fz	Max	6.2a	-2.40E+02	-2.30E+03	1.90E+04	2.30E+03	-2.60E+04	3.80E+03	2.70E+04
	Min	6.2a	-1.80E+03	2.90E+02	9.10E+03	1.90E+03	9.40E+04	-3.10E+04	9.80E+04
Fres	Max	6.2a	-8.40E+03	4.30E+00	1.30E+04	8.40E+03	1.30E+03	-2.80E+05	2.80E+05
	Min	6.2a	2.30E-01	8.60E-02	1.40E+04	2.40E-01	1.30E+04	-8.50E+04	8.60E+04
Mx	Max	1.3	2.80E+02	-2.80E+03	1.40E+04	2.90E+03	2.90E+05	-6.20E+03	2.90E+05
	Min	6.2a	-8.80E+02	3.80E+03	1.20E+04	3.90E+03	-2.00E+05	-3.20E+04	2.00E+05
My	Max	6.2a	5.00E+03	-1.30E+03	1.10E+04	5.20E+03	-1.80E+04	3.30E+05	3.30E+05
	Min	6.2a	-1.90E+03	4.20E+02	1.00E+04	2.00E+03	2.90E+03	-3.20E+05	3.20E+05
Mres	Max	6.2a	5.00E+03	-1.30E+03	1.10E+04	5.20E+03	-1.80E+04	3.30E+05	3.30E+05
	Min	6.2a	4.80E+02	3.80E+02	1.60E+04	6.10E+02	-1.50E+01	-4.10E+00	1.60E+01

**Table 4.3-4 – Damage equivalent loads**

	Fx [kN]	Fy [kN]	Fz [kN]	Mx [kNm]	My [kNm]	Mz [kNm]
Interface	768.7	2069.1	1066.9	146510.0	62140.0	18580.0
Joint top	1908.2	4382.8	1937.1	119740.0	49973.0	-

Next, new elastic analyses are carried out in Abaqus to determine stresses in shells and elastomeric pads, and strains in rubber. Attention has been given to ensure that the joint stays in its elastic behavioral range. Shells' thicknesses have been fitted to have reasonable utilization factor in ultimate limit state but having in mind reserve for fatigue limit state. Although the bulk dimensions have not been altered, it could have been worthy to check this fine-tuning's influence on the stiffness matrix.

The maximal strain in the elastomeric pads is 0.10% (unfactored value). The ultimate von Mises stress results are given in Table 4.3-5. They are obtained on the sheath.

**Table 4.3-5 – Ultimate stress results**

	Characteristic value [MPa]	Partial safety factor	Design value [MPa]	Utilization factor
Stress	1.443	1.1	1.587	0.84%
Strength	235	1.25	188	

Fatigue analysis is not regarded in details in the present design process. However, some considerations are worthy to be presented.

Sedillot and. Stevenson (1983) [4-57] experimentally showed after fatigue tests on three different shape rubber specimens that the relation between the tearing energy and the crack growth rate is a material property. They established a minimum life time of 180 years for the elastomeric pads. This result suggests that this component is not the weakest link of the structural system. On the other hand, the robustness given to the joint's steel shell is expected to cover fatigue effects that could damage it. It is important to provide a high reliability to the universal joint because the structure has little redundancy.

### Reinforced concrete base

Once the universal joint has been completely designed and hydro-aero-servo-elastic (HASE) analyses have been carried out in HAWC2, seven pairs of representative scenarios have been



selected to design the reinforced concrete base. The scenarios correspond to the situations where respective extrema (maxima and minima) of load components are realised at the joint's rod top. Actual loads applied at the base top are obtained as the reactions developed under the joint's socket. CEB-FIP Model Code [4-67] proposes some properties for concrete: (i) density 2400 kg/m<sup>3</sup> (2500 kg/m<sup>3</sup> is used for reinforced concrete); (ii) Poisson's ratio 0.2; and (iii) compressive yield stress 18 MPa. The soil properties are extracted from Ref [4-73]: internal angle 35° and effective unit weight 9 kN/m<sup>3</sup>. In addition, Ref [4-68] completes with cohesion of 25 kPa. IEC 61400-3 [4-66] recommends a roughness parameter lesser than 1.0; it is taken as 0.5.

Four failure modes are considered to justify the base: overturning of the structure due to excessive moments, bearing capacity of the soil-structure interface, sliding on the seabed and punching of the universal joint into the reinforced concrete base. Ref [4-58] is used to assess bearing capacity and sliding, while Ref [4-68] is considered for punching, assuming that the punching effect only originates from the lower elastomeric pad.

A cylinder of diameter 6.00 m with 2.50 m height as depicted in Figure 4.3-5 is found to satisfy all the requirements. Table 4.3-6 which presents the overview of these analysis results for the critical scenarios, shows that the base dimensions are not driven by the failure criteria but by the joint size.

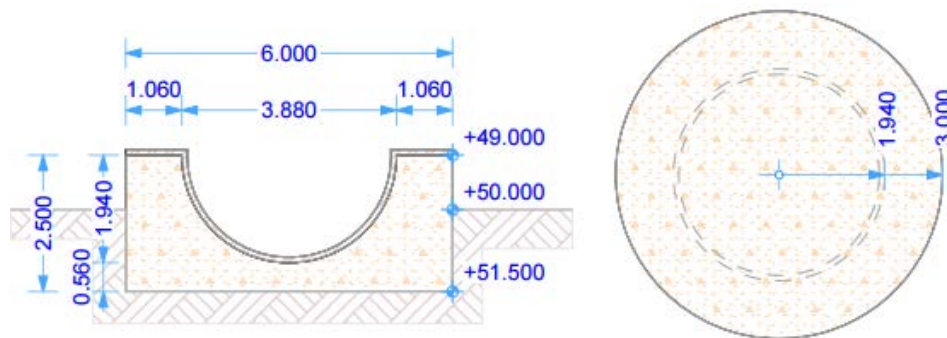


Figure 4.3-5 – Planform of the reinforced concrete base

Table 4.3-6 – Results of base design

	Overtuning (X-Direct.)	Overtuning (Y-Direct.)	Bearing	Sliding	Punching
	[kNm]	[kNm]	[kPa]	[kN]	[kPa]
Critical scenario	Max Mx	Max Fres	Max Fres	Max Fres	Max Fz
Resisting	6773.12	6779.42	864.55	915.22	5586.21
Driving	22.37	44.68	80.05	14.42	1.77
Safety factor	302.84	151.73	10.80	63.47	3150.33

### Design load cases

Design load cases as defined by IEC 61400-3 [4-66] are considered: 1.2 for fatigue limit state, and 1.3 and 6.2a for ultimate limit state.

**DLC 1.2:** 11 wind speed bins (5 m/s, 7 m/s, 9 m/s, 11 m/s, 13 m/s, 15 m/s, 17 m/s, 19 m/s, 21 m/s, 23 m/s, 25 m/s) with six wind seeds each have been applied each with yaw errors  $\pm 10^\circ$  from the normal to the rotor plane. Pierson-Moskowitz waves were misaligned to wind direction by  $\pm 10^\circ$ . That makes  $11 \times 6 \times 3 \times 3 = 594$  scenarios.

**DLC 1.3:** six wind seeds for each of 11 wind speed bins have been applied each with no yaw error. Waves of JONSWAP type were aligned along wind direction. That makes  $11 \times 6 = 66$  scenarios.

**DLC 6.2a:** 42.73 m/s wind has been applied along 24 directions:  $0^\circ, 15^\circ, 30^\circ, 45^\circ, 60^\circ, 75^\circ, 90^\circ, 105^\circ, 120^\circ, 135^\circ, 150^\circ, 165^\circ, 180^\circ, 195^\circ, 210^\circ, 225^\circ, 240^\circ, 255^\circ, 270^\circ, 285^\circ, 300^\circ, 315^\circ, 330^\circ$  and  $345^\circ$ . A JONSWAP wave was directed along wind direction with  $\pm 30^\circ$  yaw error. With no active controller, the structure was loaded with an extreme current (1.2 m/s) of parabolic type at

0°. Blades were pitched a 90° with no dynamic induction. This leads to a total of  $24 \times 3 = 72$  scenarios.

Metocean conditions are given by Ref [4-73] and are presented in Table 4.3-7.

**Table 4.3-7 – Sea states [4-73]**

Wind speed [m/s]	Turbulence Intensity [%]	Significant height, Hs [m]	Peak period, Tp [s]	Occurrence [hrs/yr]
5	18.95	1.140	5.820	933.7500
7	16.75	1.245	5.715	1087.3000
9	15.60	1.395	5.705	1129.0500
11	14.90	1.590	5.810	1106.7500
13	14.40	1.805	5.975	1006.4000
15	14.05	2.050	6.220	820.1500
17	13.75	2.330	6.540	633.0000
19	13.50	2.615	6.850	418.6500
21	13.35	2.925	7.195	312.7000
23	13.20	3.255	7.600	209.9000
25	13.00	3.600	7.950	48.9612
42.73	11.00	9.400	13.700	-

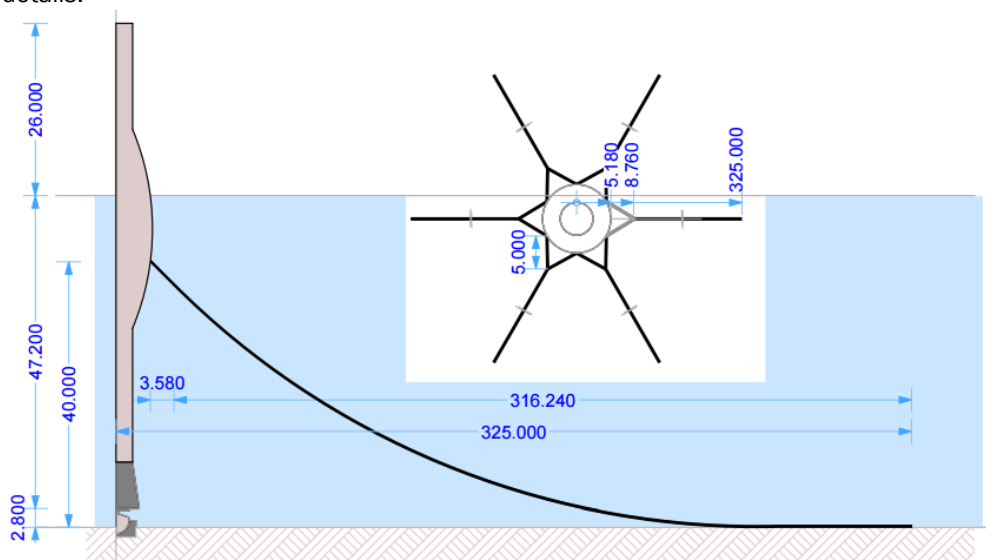
### 4.3.3 Results of the performed studies of innovations on component level

The carried out detailed design leads to important results both at the component level and at the global level. At the component level, defined shape and dimensions are clearly set; and at global level, general performance is found to be satisfactory. Finally, an installation process is proposed. It is designed to be aligned with the well-established practices in wind energy industry.

#### At component level

Representative mean and dynamic loads are found on the critical line to be 2319.6 kN and 910.16 kN, respectively. The utilization factor is therefore calculated from Eq 4.3-1:  $u = 0.3238 \leq 1$ .

As the universal joint sustains the maximum stresses and the base has been proven to comply with the failure modes, the final design is illustrated by Figure 4.3-5, Figure 4.3-6 and Figure 4.3-7 with details.



**Figure 4.3-6 – Mooring system layout**

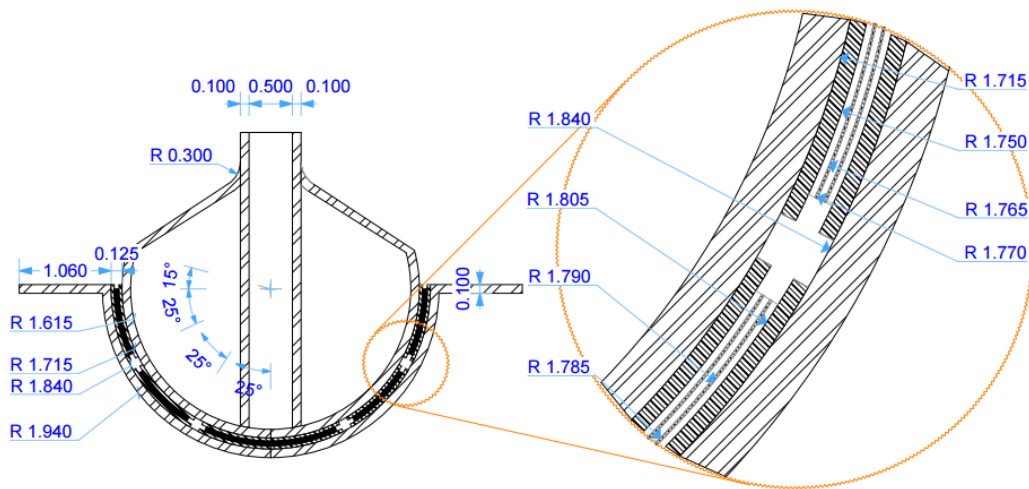


Figure 4.3-7 – Universal joint dimensions

#### At the global level

In order to investigate the performance of the structure at the global level, three criteria will be handled: modal frequencies, global platform's motion and some characteristic curves (power curve, thrust force curve, rotor rotational speed curve and blade pitch angle curve).

Table 4.3-8 shows the natural frequencies and the logarithm decrement of the whole structure. The first tower modes have their natural frequencies at about 0.065 Hz which is out of the 1P excitation range, [0.10 Hz, 0.16 Hz] and at the lower tail of the wave spectrum (lower than 3% of the wave energy during production phase).

Table 4.3-8 – Natural frequencies of the whole turbine

Mode	Natural frequency [Hz]	Logarithmic Damping [%]
1st Tower side-side mode	0.06483	11.44
1st Tower for-aft mode	0.06540	11.37
1st fix-free rotor mode	0.15108	0.002
1st Tower yaw mode	0.19001	0.065

On the other hand, Figure 4.3-8 illustrates the chosen characteristic curves of the structural system. By comparing to those of the DTU reference turbine [4-69], it is found that the new system supported by the innovative component globally performs as good as the reference. However, it should be noted that for the rotor rotational speed, the controller allow a slight slope once the rated rotor speed is reached. Detailed discussion of this subject is out of the scope of the present report.

In addition, the averages of offset means are 2.50 m (for storm case) and 2.10 m (for production regime); or 1.9° (for storm case) and 1.6° (for production regime). As well, the averages of offset maxima obtained are 5.12 m (for storm case) and 4.01 m (for production regime); they are below the admissible offset set above. These displacements correspond to floating cylinder's pitch angles of 3.9° (for storm case) and of 3.0° (for production regime).

#### Installation process

The installation process is primarily made of six steps. Figure 4.3-9 depicts each step of this route.

- (a) **Seabed preparation and cutting.** The first step consists of removal of marine biota following by excavation. The displaced marine biota is taken elsewhere for ecosystem preservation.
- (b) **Foundation setting.** The universal joint mounted on the reinforced concrete base is prefabricated and assembled ex-situ. The whole set is settled inside the excavation.

- (c) **Backfill and scour protection.** Then, the remaining spaces around the reinforced concrete are backfilled, and scour protection is provided.
  - (d) **Floating system sink.** The floating system constituted by the floating cylinder and the buoyant chamber is transported above the base. Its shaft is plugged into the joint sheath.
  - (e) **Ballast addition.** Ballast is added at the floating cylinder foot. This step can also be done during Step (d) to help sinking the floating system.
  - (f) **Mooring system.** The mooring lines are added and anchored to seabed.
- Finally, the turbine (tower plus rotor and nacelle assembly) can be mounted on the semi-floater structure using classical run-through.

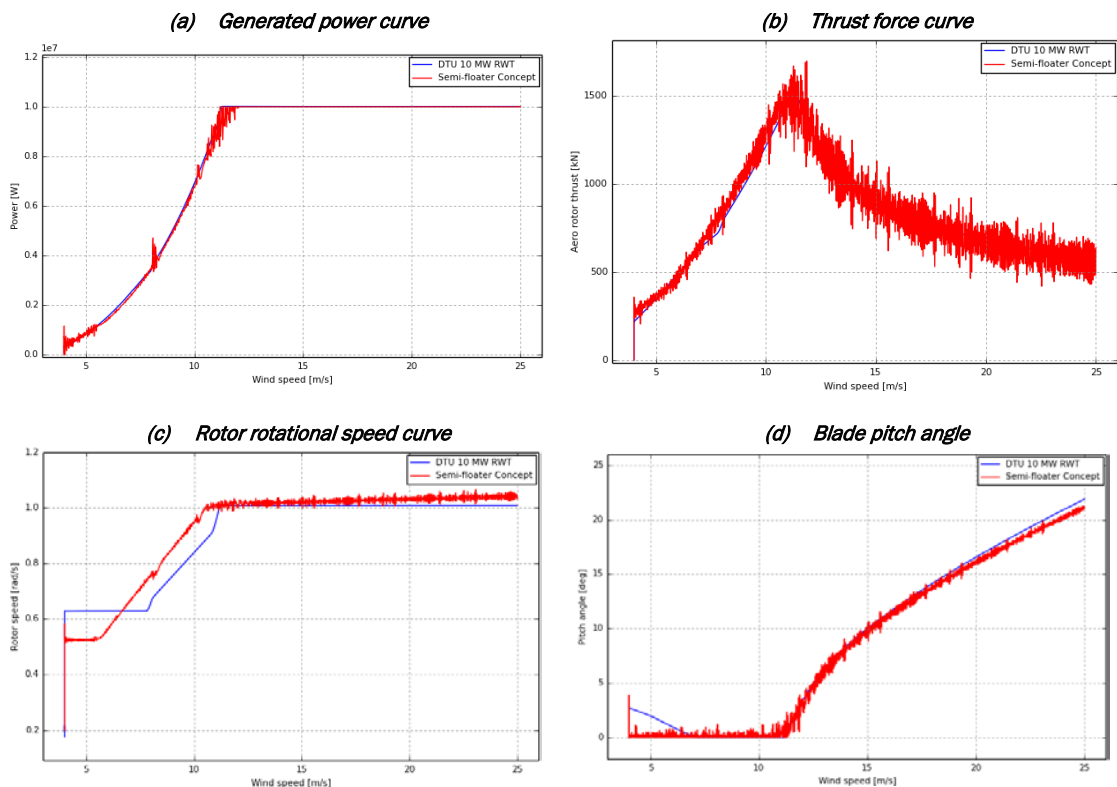


Figure 4.3-8 – Characteristic Curves

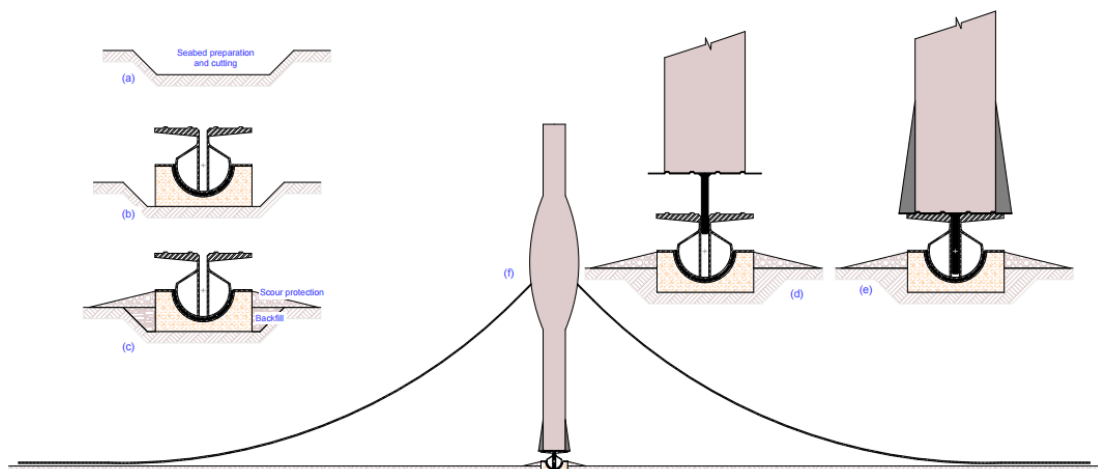


Figure 4.3-9 – Installation Process

#### 4.3.4 Current TRL of innovations and recommendations for their further development

The semi-floater concept as presented here is a subtle combination of classic gravity-based foundation and traditional spar floater. The buoyant system and the mooring lines are found in the spar floater, while the reinforced concrete base is similar to the footing in gravity-based foundation. In this respect, wind energy industry already has good experience to handle this new concept.

However, the universal joint and the elastomeric pad technology can be found unfamiliar to wind energy industry. But it can take advantage of oil and gas industry's practice which has studied this concept since 1969 [4-70] and is still continuing nowadays [4-71]. In addition, the elastomeric pad technology has been thoroughly studied and extensively used as bearings in bridge engineering and as base isolation in earthquake engineering. On the other hand, the spherical ball and the socket can be easily manufactured using cast steel or rolled sheet.

All these considerations supplement the design proposed here to show that the Technology Readiness Level for this concept is in the order of 3: "technology concept formulated" [4-72]. All the components have been designed in details: materials, geometry and dimensions are well determined. At this stage, a small-scale model can be built and tested in wave tank in order to carry this design to a more mature level: "TRL 4 - experimental proof of concept" [4-72].

Two levels can host further developments of this concept: global and local. First, an important advancement can be the adaptation of this concept in large water depths or for more powerful turbines like 20 MW. To achieve this upscaling, the present results can serve as initial guess. Then, the algorithms as presented here can be used for preliminary design of the mooring system and the universal joint. The suggestions addressed below can also be considered to adjust the floating system.

Second, a close focus can be given to the joint design in order to tackle tiny details such as: (i) connections (welds, bolts...) between shell parts; (ii) local buckling and possible internal frame; (iii) more realistic boundary conditions and load transmissions; (iv) optimization in order to increase its utilization factor. Naturally, shrinking the universal joint will lead to the diminution of the reinforced concrete base's geometry.

Similar improvement can also be done on other structural components. For example, the mooring system can be revised to allow larger offsets and support larger axial forces. Also, a coupled reduction of the buoyant system and the ballast can be possible; this will permit that the mooring system and the joint receive more loads.

#### 4.3.5 Cost reduction potential of innovations on component level

Both the material cost and the total cost of the present design are presented. The former is compared to those of jacket and monopile solutions, respectively. The unit costs are employed as shown in Table 4.3-9. The structure's transportation to the installation site is not accounted because of its reliance on the distance that is project dependent.

**Table 4.3-9 – Material unit cost**

Material	Unit	Unit cost [€]	References
Hull steel	kg	3.00	[4-50]
Hull reinforced concrete	kg	0.25	[4-50]
Ballast	kg	0.07	[4-50]
E-glass polyester fibre	kg	6.00	Adapted from [4-75]
Steel chain	m	250	[4-76]
Anchor + connector	U	125 000	Adapted from [4-76]
Elastomeric pad	m <sup>3</sup>	76 900	[4-77]
Wind Turbine Installation In Shipyard	Turbine	6 860	[4-76]
Wind Turbine Installation at Sea	Turbine	256 350	[4-76]
Drag Embedment Anchors	Anchor	9 471	[4-76]



Ref [4-73] proposes a jacket solution as turbine support for 50 m water depth. The total structure weighs 2120 t; it can be deduced a material cost of 6,360,000 euros. Ref [4-74] estimates a material cost of 8,100,000 euros for a monopile solution at similar environment. The material cost of the semi-floater concept is estimated at 3.2 million euros. This amount is half of the jacket's cost and almost two fifth of the monopile's one. This is a substantial cost reduction that can be further capitalized at deeper sea environment.

This sum is higher than the one obtained in Ref [4-50]. This is mainly due to the new mooring system used here, to the correction brought on floating system dimensions, and to the use of the actual universal joint geometry. Table 4.3-10 breaks down this cost into respective parts corresponding to different structural components. It shows that the most expensive parts are the floating cylinder and the mooring system. As seen above, possible optimization of these parts may significantly contribute to cost reduction of this semi-floating concept.

**Table 4.3-10 – Material and total cost of semi-floater concept**

Component	Cost [€]
Floating cylinder + Ballast	1,097,428.78
Buoyant chamber	396,770.41
Mooring system	1,245,000.00
Universal joint (shell + elastomeric pads)	381,893.85
Reinforced concrete base	34,170.88
<b>Material cost</b>	<b>3,155,263.92</b>
Wind Turbine Installation In Shipyard	6,860.00
Wind Turbine Installation at Sea	256,350.00
Drag Embedment Anchors	56,826.00
<b>Total cost</b>	<b>3,475,299.92</b>

## 4.3.6 Appendixes

### Appendix 4.3-A: Preliminary design of catenary lines

Let be a mooring line of catenary type with linear weight,  $w$  hung at a vertical height,  $h$  above the seabed as depicted in Figure 4.3-A1. It is anchored at a radial distance  $Rad$  away from the fairlead. Its total length  $L$  can be decomposed into a suspended part of length  $s$  and a straight part laying on the seabed of length  $B$ . Before or after deformations,  $s$  and  $B$  respectively take the values  $s_1$  and  $s_2$ ,  $B_1$  and  $B_2$ . It is assumed a minimal ratio  $\theta = B_2/s_2$ . The horizontal scopes of the catenary part are  $x_1$  and  $x_2$ , corresponding to before and after deformations, respectively.

Deformations consist of a horizontal displacement of the fairlead by  $\Delta x$ . At the fairlead, the tensile force  $T$  has a vertical component,  $V$  and a horizontal one,  $H$ . Each of these forces has two states 1 and 2 for before and after deformations, respectively.

The aim of the present algorithm is to determine the initial geometry given parameters  $w$ ,  $h$  and  $\Delta x$ .

**After deformations**, the line supports a tension  $T_2$ . Its suspended length can be calculated by

$s_2 = \sqrt{\frac{2hT_2}{w}} - h^2$ . Then, a system of two nonlinear equations with two unknowns,  $H_2$  and  $x_2$ , is set and simultaneously solved:

$$\begin{cases} s_2 = \frac{H_2}{w} \sinh\left(\frac{w x_2}{H_2}\right) \\ h = \frac{H_2}{w} \left[ \cosh\left(\frac{w x_2}{H_2}\right) - 1 \right] \end{cases} \quad \text{Eq. 4.3-1}$$

**During deformations**, the total length conservation is assumed:  $B_1 + s_1 = B_2 + s_2$ . Horizontally along the seabed, it can be written  $B_1 + x_1 + \Delta x = B_2 + x_2$ . Both equations combine to  $s_1 - x_1 = s_2 - x_2 + \Delta x$ .

**Before deformations**, a system similar to Eq.4.3-1 is also set:

$$\begin{cases} s_1 - x_1 = s_2 - x_2 + \Delta x = \frac{H_1}{w} \sinh\left(\frac{w x_1}{H_1}\right) - x_1 \\ h = \frac{H_1}{w} \left[ \cosh\left(\frac{w x_1}{H_1}\right) - 1 \right] \end{cases} \quad \text{Eq. 4.3-2}$$

Eq.4.3-2 can be simultaneously solved for  $H_1$  and for  $x_1$ . Therefore, the radial distance from the fairlead to the anchorage can be obtained by  $Rad = B_1 + x_1 = x_1 - s_1 + (1+\theta)s_2$ , and the total length  $L = Rad - x_1 + s_1$ .

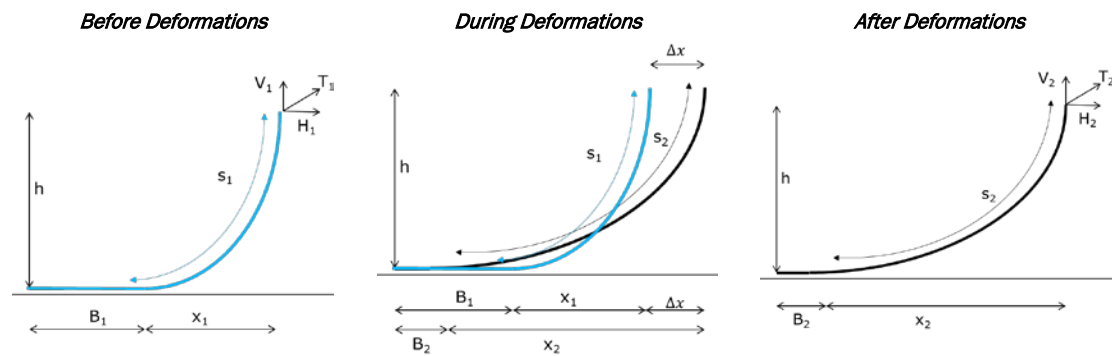


Figure 4.3-10 – Steps of the preliminary design algorithm

### 4.3.7 Conclusions

A more mature design is successfully proposed for three components of the semi-floater concept. Their implementation results in a performance as good as that for the reference. Cost analysis shows the superiority of this concept over other possible solutions such as jacket and monopile. This success encourages further developments on both global and component levels. These include more detailed modeling of the components and consideration of deeper water environments.



## 4.4 Conclusions

The Chapter „Soil and Foundations“ includes three contributions regarding possible cost-saving solutions for sub-components of jackets structures.

Bucket foundations are firstly presented. The pros of this sub-component are by now well-known. By having zero noise emission during the installation no costs for noise reducing technology must be spent. Since offshore wind turbine systems present very peculiar load configurations, bucket foundations have to be adapted and have to prove their reliability. Some advancement in this regard is illustrated in the contribution where an experimental campaign is presented and experimental data is interpreted. Various methods to estimate the tensile capacity of piles are compared to each other. The experimental results are also interpreted with existing methods. Cyclic loading tests are however still missing and must be carried out to complete the experimental campaign. In the contribution it is highlighted that the cost saving might be between 15 and 20% in comparison to monopiles or jackets founded on piles.

The second contribution concerns piles for jacket installed with vibratory hammer. Vibro-piles have a great potential for becoming cost-effective foundations since noise and time of the installation are relevantly reduced in comparison to impact-driven piles. In the report a large-scale test of a pile under tensile monotonic loading is interpreted by means of analytical and numerical methods in order to assess the bearing behavior of the foundation. Standard CPT-methods are used to evaluate the ultimate bearing capacity of the pile. As in part expected, the experimental results fall by 60 to 80% in comparison to the CPT-method predictions. A 2D numerical model is developed to capture the initial axial stiffness of the pile, which is really important for design purposes. The numerical model is fitted to the experimental curve by changing the elastic modulus of the sand. Overall it was demonstrated that vibro-driven piles have lower bearing capacity than impact-driven piles and therefore a lower margin for cost savings than expected. This however must be proved by testing a second pile which is going to be subjected to pre-loading. Furthermore, the setup effects will be investigated by performing ne large-scale experiments.

The last contribution deals with the further development of a semi-floater concept founded on a concrete base. Mooring lines, universal joint and concrete base are the focuses of the analysis. Load and maximum displacement were defined and line length and horizontal anchorage distance from fairlead were calculated. The joint is designed so to not apply torque on it and is pre-dimensioned by means of analytical formulas. Refined analysis is carried out with a numerical model with which relevant design cases are simulated. By means of that the stresses in the different parts of the joint are calculated. The pre-design of the reinforced concrete base is also completed. Global level analysis is documented in which the general behavior of the innovative component is found to perform appropriately with respect to the reference. Also the installation process is considered and more importantly cost analysis and current TRL of the system are outlined.

## References

- [4-01] Byrne, BW (2000). “Investigations of Suction Caissons in Dense Sand,” PhD Thesis, The University of Oxford.
- [4-02] Terzaghi, K (1943). “Theoretical soil mechanics”, New York: Wiley.
- [4-03] Prandtl, L (1920). “Über die Harte plastischer Körper, Nachr.D.Ges.D. Wiss.” Gottingen
- [4-04] Larsen, K.A (2008). Static Behaviour of Bucket Foundations. PhD Thesis, Aalborg University, Denmark.
- [4-05] Ibsen, LB, Barari, A, and Larsen, KA (2014a). “Adaptive Plasticity Model for Bucket Foundations,” Journal of Engineering Mechanics, Vol. 14, Number 2. American Society of Civil Engineers. ISSN 0733-9399, CODEN: JENMDT.
- [4-06] Ibsen, LB, Barari, A, and Larsen, KA (2014b). “Evaluation of Vertical Bearing Capacity of Bucket Foundations in Saturated Sand,” International Journal of Geomechanics, ISSN 1532-3641.

- [4-07] Ibsen L.B., Hanson, M Hjort, T. and Taarup, M. (2009) "MCPParameter Calibration for Baskarp Sand No. 15" DCE. Technical Report No.62. (ISSN 1901-726X), Aalborg University, Department of Civil Engineering, Aalborg, Denmark
- [4-08] Ibsen, LB, Barari, A, and Larsen, KA (2012). "Modified vertical bearing capacity for circular foundations in sand using reduced friction angle," *Ocean Engineering* 47 (2012) 1-6, Elsevier Ltd.
- [4-09] Ibsen, LB, Barari, A, and Larsen, KA (2013). "Calibration of Failure Criteria for Bucket Foundations on Drained Sand under General Loading," *Journal of Geotechnical and Geoenvironmental Engineering*, American Society of Civil Engineers.
- [4-10] DNV (1992). Foundations. Classification Notes No.30.4, Det Norske Veritas, Norway, pp 13.
- [4-11] Brinch-Hansen, J (1970). "The Revised and Extended Formula for Bearing Capacity," *Geotechnisk Institut, Bulletin No. 28, Copenhagen*, pp 5-11.
- [4-12] Caquot, A, and Kerisel, J (1953). "Sur la Terme de Surface dans le Calcul des Fondations en Milieu Pulverult," *Proc. of the 3rd International Conference on Soil Mechanics and Foundation Engineering, Vol. 1, Zurich*.
- [4-13] EC-7 (2004). EN 1997-1:2004, Eurocode 7: Geotechnical Design – Part 1: General rules. Dansk Standard.
- [4-14] Bolton, M. D., and Lau, C.K.(1993)."Vertical bearing capacity factors for circular and strip footings on Mohr-Coulomb soil". *Canadian Geotechnical Journal*, 30(6).
- [4-15] Randolph, M, and Gourvenec, S (2001). *Offshore Geotechnical Engineering*. Spon Press and imprint of Taylor & Francis, ISBN13: 978-0-415-47744-4(hbk), ISBN13:978-0-203-88909-1(ebk), pp 265-266.
- [4-16] Davis, EH, and Booker, JR (1971). "The bearing capacity of strip footings from the standpoint of plasticity theory," *Proc. Australia-New Zealand Conf. Geomech., Melbourne, Australia*, pp 276-282.
- [4-17] Ovesen, NK, Fuglsang, LD, Bagge, G, and Krogsbøll, A (2012). "Lærebog i Geoteknik", Polyteknisk Forlag, Lyngby, Denmark. ISBN10 87-502-1042-4, ISBN13 978-87-502-1042-9, pp. 223-230.
- [4-18] Schanz, T, Vermeer, PA, and Bonnier, PG (1999), "The hardening soil model: Formulation and verification", *Beyond 2000 in Computational Geotechnics – 10 Years of Plaxis*, Balkema, Rotterdam. ISBN 90 5809 040 X.
- [4-19] Senders, M (2008). *Suction caissons in sand as tripod foundations for offshore wind turbines*. PhD Thesis, The University of Western Australia.
- [4-20] Houlsby, G.T. and Byrne, B.W. (2005a). Design procedures for installation of suction caissons in sand. *Proceedings of the ICE, Geotechnical Engineering* 158, No. 3, 135-144.
- [4-21] Houlsby, G. T., Kelly, R. B. & Byrne, B. W. (2005b) The tensile capacity of suction caissons in sand under rapid loading. *Proc. International Symposium on Frontiers in Offshore Geotechnics (ISFOG)*. Perth, Australia, Taylor Francis Group.
- [4-22] Houlsby, G.T., Ibsen, L.B., and Byrne, B.W.(2005c) " Suction caisson for wind turbines" Department of Civil
- [4-23] Byrne, B.W. and Houlsby, G.T. (2002) "Experimental investigations of the response of suction caissons to transient vertical loading" *Proc. ASCE, Journal of Geotechnical Engineering* 128, N° 11, November, pp 926-939
- [4-24] Vaitkunaite, E, Devant Molina, S, and Ibsen, LB (2012), "Comparison of Calculation Models for Bucket Foundation in Sand", *DCE Technical Memorandum No. 17*, Aalborg University, Denmark, ISSN 1901-7278, 2012.
- [4-25] Fisker, L.B., and Kromann. K. (2004). "Cyklisk Belastning af Bøttefundament i Tryktank", *Speciale ved Aalborg University*.
- [4-26] Kelly, R. B., Houlsby, G. T. & Byrne, B. W. (2006). A comparison of field and laboratory tests of caisson foundations in sand and clay. *Getotechnique*, 56, No. 9, 617–626.
- [4-27] Lehane, B. A., Schneider, J. A. & Xu, X. (2005) The UWA- 05 method for prediction of axial capacity of driven piles in sand. *Proc. International Symposium 'Frontiers in Offshore Geotechnics'*. Perth, Australia, Taylor & Francis Group.

- [4-28] Randolph, M.F., Jamiolkowski, M. B. & Zdravkovic, L. (2004) Load carrying capacity of foundations. Proc. Skempton Memorial Conf. London.
- [4-29] Mørch, C.B (2014): The suction bucket jacket – a new wind turbine foundation concept. Dong Energy
- [4-30] INN WIND.EU: Validation of innovations by tests on component level. Deliverable 4.1.4, 2015.
- [4-31] Randolph M.F., Gourvenec S.: Offshore geotechnical engineering. Spon Press, 2011.
- [4-32] Haigh, S. K.: Foundations for offshore wind turbines. In Proceedings of the 8<sup>th</sup> International Conference of Physical Modelling in Geotechnics (ISFOG), 2014.
- [4-33] INN WIND.EU: Innovations on component level (Interim report). Deliverable 4.1.2, 2014.
- [4-34] Matlock B.G.W.M.: Comparison of the lateral bearing capacities of hammered and vibrated piles. 5<sup>th</sup> International Conference Offshore Foundations, 2015.
- [4-35] Igoe D., Gavin K., O’Kelly B.: An investigation into the use of push-in pile foundations by the offshore wind sector. International Journal of Environmental Studies, 2013.
- [4-36] Achmus M., Lemke K., Abdel-Rahman K., Kuo Y.-S.: Numerical approach for the derivation of interaction diagrams for piles under cyclic axial loading. Proceedings of the Twenty-fifth International Ocean and Polar Engineering Conference, 2015.
- [4-37] Viking K.: Vibro-driveability – A field study of vibratory driven sheet piles in non-cohesive soils. PhD thesis, Royal Institute of Technology Stockholm, 2002.
- [4-38] Lammertz P.: Ermittlung der Tragfähigkeit vibrierter Stahlrohrpfähle in nichtbinigem Boden. PhD thesis, Universität Duisburg-Essen.
- [4-39] Braaker: Rammgeräteeinfluss auf die Tragfähigkeit. Pfahl-symposium, 1986.
- [4-40] Borel S., Bustamante M., Rocher-Lacoste F.: The comparative bearing capacity of vibratory and impact driven piles. International symposium on vibratory pile driving and deep soil vibratory compaction, 2006.
- [4-41] LeBlanc, C., Liingaard, M.A., Shajarati, A., Kallehave D., Skov Gretlund J.: Vibro-driving of monopiles-experience from Anholt Offshore Wind Farm, Offshore EWEA, Frankfurt 2013.
- [4-42] Deutsche Gesellschaft für Geotechnik e.V., Empfehlungen des Arbeitskreises "Pfähle" - EA-Pfähle, Berlin: Ernst & Sohn Verlag, 2012.
- [4-43] Achmus M., Müller M.: Evaluation of pile capacity approaches with respect to piles for wind energy foundations in the North Sea. 2nd International Symposium on Frontiers in Offshore Geotechnics, 8-10 November 2010, University of Western Australia, Perth.
- [4-44] Lehane B.M., Schneider J.A. and Xu X: A review of design methods for offshore driven piles in siliceous sand. UWA Report GEO 05358.
- [4-45] API 2011: ISO 19901-4:2003 (Modified), Petroleum and natural gas industries-Specific requirements for offshore structures, Part 4-Geotechnical and Foundation Design Considerations.
- [4-46] ABAQUS 6.14 User’s Manual. Simulia, Providence, USA, 2014.
- [4-47] Bolton M.D.: The strength and dilatancy of sands. Géotechnique 36, 1986.
- [4-48] INN WIND.EU Deliverable 4.1.1 – “State of the art on component level”, October 2013
- [4-49] INN WIND.EU Deliverable 4.1.2 – “Innovations on component level for bottom based structures (Interim Report)”, August 2014
- [4-50] INN WIND.EU Deliverable 4.3.3 – “Innovative Concepts for Floating Structures”, August 2014
- [4-51] Bulder B.H., van Hees M.Th., Henderson A., Huijsmans R.H.M., Pierik J.T.G., Snijders E.J.B., Wijnants G.H., Wolf M.J.: Studie naar haalbaarheid van en randvoorwaarden voor drijvende offshore windturbines. ECN, MARIN, Lager- wey the Windmaster, TNO, TUD, MSC, 2002.
- [4-52] Lefebvre, S., Collu, M.: Preliminary design of a floating support structure for 5 MW offshore wind turbine, Ocean Engineering 40:15–26, 2012.
- [4-53] Benassai G., Campanile A., Piscopo V., Scamardella A.: Ultimate and accidental limit state design for mooring systems of floating offshore wind turbines, Ocean Engineering 92:64–74, 2014
- [4-54] Det Norske Veritas: Position mooring, Offshore Standard DNV-OS-E301, 2013.
- [4-55] Det Norske Veritas: Offshore mooring chain, Offshore Standard DNV-OS-E302, 2008.

- [4-56] Brown D.T.: Mooring Systems in “Handbook of Offshore Engineering” Ed Chakrabarti S, Elsevier, 2005
- [4-57] Sedillot F., Stevenson A.: Laminated rubber articulated joint for the deep water gravity tower, Transactions of the ASME, Vol 105:480-486, 1983.
- [4-58] Det Norske Veritas: Design of Offshore Wind Turbine Structures, Offshore Standard DNV-OS-J101, 2014.
- [4-59] Cremer L., Heckl M.: “Structure-Borne Sound”, Springer-Verlag, New York, 1988.
- [4-60] Abaqus. “Lecture 3 - Materials” in “ABAQUS/Explicit: Advanced Topics.” 2005.
- [4-61] Abaqus, “Keywords Reference Manual”, Dassault Systèmes, 2012.
- [4-62] South J.T.: “Mechanical properties and durability of natural rubber compound and composites”, PhD Thesis, Virginia Polytechnic Institute, 2001.
- [4-63] American Association of State Highway and Transportation, “AASHTO LRFD Bridge Design Specifications.” Ed 6, 2012.
- [4-64] Kim J.H., Hong S.Y., Kim H.J.: The shape design and analysis of floating offshore wind turbine structures with damper structure and shallow draft, Journal of Ocean and Wind Energy, Vol. 1, 3:170-176, 2014.
- [4-65] Larsen T.J., Hansen A.M.: “How 2 HAWC2, the user’s manual”, DTU Risoe 2014
- [4-66] The international Electrotechnical Commission: Wind Turbines – Part 3: Design requirements for offshore wind turbines, IEC 61400-3 Ed 1, 2009.
- [4-67] Comite Euro-International du Beton. “CEB-FIP Model Code 1990, Design Code”. London: Thomas Telford Services Ltd., 1993.
- [4-68] Thonier H.: Conception et calcul des structures de batiment, Ponts et chaussees, 1992.
- [4-69] Bak C., Zahle F., Bitsche R., Kim T., Yde A., Henriksen L.C., Andersen P.B., Natarajan A., Hansen M.H.: Design and performance of a 10 MW wind turbine, J. Wind Energy, To be accepted.
- [4-70] Mott G.: Marine platform foundation structure, patent US 3710580 A, 1973.
- [4-71] Zaheer M.M., Islam N.: Reliability analysis of universal joint of a compliant platform, Fatigue Fract of Engng Mater Struct 33:408-419, 2010
- [4-72] Horizon 2020: “Work programme 2014 – 2015, General Annexes” European Commission Decision C (2014)4995 of 22 July 2014.
- [4-73] INN WIND.EU Design report – Reference Jacket, “INN WIND Design Report Reference Jacket Rev00.docx”, Internal teamsite, uploaded 2014-01-16, accessed 2014-08-12.
- [4-74] Njomo W.W., Natarajan A., Dimitrov N., Buhl, T.: Design of monopiles for multi-megawatt wind turbines at 50 m water depth, EWEA 2015 Conference Proceedings, to be published.
- [4-75] Shah D.U., Schubel P.J., Clifford M.J.: Can flax replace E-glass in structural composites? A small wind turbine blade case study, Composites Part B 52:172–181, 2013.
- [4-76] Wayman E.N., Sclavounous P.D., Butterfield S., Jonkman J., Musial W.: Coupled dynamic modelling floating wind turbine systems, Offshore Technology Conference, 2006.
- [4-77] Massachusetts Department of Transport, Highway Division: “2005 MHD bridge section weighted average unit prices - guidelines for the use of the weighted average unit price tabulation sheets”, 2005.

## 5 LOAD MITIGATION (FHG-DA, UOL, FHG-KS)

Another innovation on component level is specific load mitigation strategies which are further dealt with in this chapter split into four sections. The first two sections elaborate the application of passive damping devices, i.e. passive tuned vibration absorbers (TVA) at the platform level (Section 5.1) and passive tuned mass dampers at the tower top (Section 5.2). These contributions relate to Fraunhofer LBF Darmstadt (FHG-DA) and ForWind – University of Oldenburg (UOL) respectively. The origin of the strongly increased fatigue loads, which is a major challenge for the design of the large reference wind turbine support structure is investigated. As main reason the natural frequency excitation of the tower by the blade passing frequency is described in detail and possible concepts and their effect are evaluated. The third section also written by UOL briefly reports on the prospects of semi-active and active dampers.

The last section 5.4 prepared by Fraunhofer – IWES Kassel (FHG-KS) is focussing on different control and regulation concepts to mitigate loads, namely the peak shaving of the thrust and the speed exclusion window to avoid resonances during operation. In addition, an outlook is given on the effect of more advanced strategies such as active tower damping.



## 5.1 Passive damping devices

Novel 20MW Offshore wind turbines need to have a light-weight design to reduce material cost. Their place of installation is in an increased water depth of round 50m. That goes coincide with an increased size of the turbines diameter and tower. Then the surface area, that flows through the OWT increases as well as the induced wind speeds. Therefore the OWT dynamics need to be reconsidered when upscaling the structure. These two requirements for larger OWTs increase the maximum amplitudes that need to be reduced.

The classification of vibration absorber depends on the amount of automated adaptivity and the required energy consumption. The first chapter discusses passive tuned vibration absorbers (TVA) as they are already used in many civil engineering structures. Generally, passive TVAs mitigate vibrations that are induced by, e.g. wind. They work in narrow frequency bands to cancel only one operational eigenmode. To work properly, the TVA position must be chosen to have maximum controllability. Than they decrease large deflections in the OWT, which can cause material stresses. The latter lead to long-term claims, like material fatigues that are responsible for structure damages.

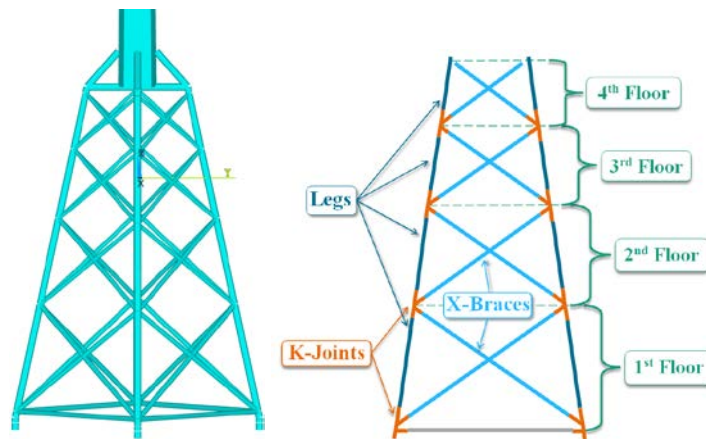
The vibration reduction of several eigenfrequencies in a broadband frequency range leads to the application of multiple distributed vibration absorbers which influence each other and have interactions with the main structure.

### 5.1.1 Discussion of the considered innovations on component level

The considered innovations are treated numerically. The numerical simulation model is implemented in ANSYS as well as the implementation of the single passive vibration absorber. The model fitting to the reference structure is investigated. A first passive vibration absorber design is surveyed in the end of this subchapter.

#### Simulation Model

The numerical simulation model consists of a tower, the jacket structure with same dimensions than the reference structure. The nacelle is modelled in the same way within ROSAP: as a lumped mass. The transition piece modelling fulfills functional aspects (see Figure 5.1-2). The tower is supported through the transition piece and pipes to the jacket. The here shown transition piece still differs from the final vision at the end of this report. In total the model is built with beam189 and mass21 elements and it consists of around about 12,000 nodes. The jacket and transition piece part of the finite element model is shown in Figure 5.1-1.



**Figure 5.1-1 - Jacket structure and transition piece in ANSYS (left) and schematic jacket structure (right)**

The anchoring of the jacket feet in the seabed is implemented as a fixed mounting in ANSYS. The numerical material parameters for steel are assumed for the whole structure. The used parameters are the E-modulus, Poisson's ratio, density, material damping, element length, length of the tube section, inner and outer radius.

The structure is made of steel and consists therefore of very low damping. A more detailed description of the reference structure can be found in [5-02].

To fit the modal behaviour of the OWT the eigenmodes and frequencies are compared. A possibility to fit the eigenfrequencies is to reduce the stiffness. The geometry and material data have influence on the stiffness of the structure. Thus, in numerical considerations there are two possibilities to fit the model, when boundary conditions are already the same:

- 1) fitting geometries (e.g. integrate more details into the geometry formulation integrate fitting parameters that can be adapted) and/or
- 2) fitting material parameters in a narrow band.

Since the geometry parameters are already settled and the ROSAP model is also modelled with Timoshenko beam theory, the material parameters are fitted to tackle the reference model behaviour. A detailed description of the fitting is given in the interim report [5-05]. The deviation of the overall structure model is shown in Table 5.1-1. A comparison of the tower models can be found also in the interim report [5-05].

**Table 5.1-1 - Comparison of the eigenfrequencies of the overall structure with the reference model**

Mode Number	Mode Shape	Reference Model [Hz]	ANSYS Model [Hz]	Deviation [%]
1	1 <sup>st</sup> bending	0.2867	0.2846	0.73
2	1 <sup>st</sup> bending	0.2885	0.2864	0.71
3	Torsion	0.9358	0.9797	1.78
4	2 <sup>nd</sup> bending	1.1003	1.1175	1.56
5	2 <sup>nd</sup> bending	1.1133	1.1388	2.29

### Passive Vibration Absorber Design

In the following the passive vibration absorber design is illustrated. It consists of large braces to guarantee a distance the tower and the transition piece. The effective mass is modeled symmetric as a circular absorber. The mass is attached to the brace via a spring element. In the numerical considerations it is realized with a combine14 element formulation.

The first idea was to attach the effective mass via a damping element as it can be fabricated in [5-06]. Then the passive vibration absorber would result in a viscous Lanchester damper, which only



consists of a damping and effective mass element. That would also increase the damping in the whole structure.

The geometric scheme leads to a large static load to keep the effective mass. Since also dynamic loads occur, the design was implemented with a spring, which is able to keep the effective mass. Constructively it can be implemented with a steel construction. Implementing a spring increases the amount of load reduction in comparison to a damping device.

For a second design approach the implementation of a pendular TVA can be considered.

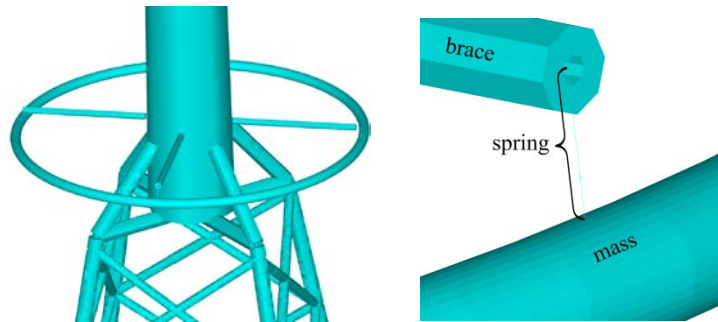


Figure 5.1-2 - Design concept of the simulated TVA

## 5.1.2 Description of the performed studies of innovations on component level

### Positioning

Already in the beginning on numerical investigations on the dimensioning of passive vibration absorbers, the positioning of the device was planned to be realizable. Even when the construction of the nacelle, the tower, the transition piece and the jacket structure are not finalized yet, there are limitations in the available space. In discussions over existing OWT and available space it turned out, that the nacelle itself is very compact. Of course, from the positioning point of view it is the best location to mitigate loads.

For a single TVA the controllability correlates with the position of the largest amplitude in a specific eigenmode. Influencing operational modes by wind loads the nacelle would therefore be the best position.



Figure 5.1-3 - Idea of passive vibration absorber at double flues (see [5-01])

However nearby the nacelle as well as in its interior, the available space is limited. The nacelle design is in a process of adjustment and no additional space is designated to include vibration absorbers. Form the nacelles position the torsional mode could also be influenced best, since the deflections are large. The largest deflections of the second eigenmode occur in the middle of the

structure. Thus the application at the transition piece has best observability. The design leans to an idea that was already successfully installed to smokestacks.

Due to the process of the design of the transition piece and because of the available space, the TVA is applied at the transition piece to influence the first bending and torsional eigenmode.

### Numerical Analyses

The first five eigenfrequencies of the structure are two times the first bending eigenmode, the torsional mode and twice the second eigenmode. The first and second bending eigenmodes appears twice, because of the centre of the nacelle is not in the towers centre. Further eigenmodes show an oscillation of the x-braces at the floor nearby the sea.

For the model, two different types of damping are considered. One takes account of the material damping and the other is a perceptual damping of the overall structure. The damping of the entire structure is missing. The modified damping used to achieve the required response of the structure is defined as material damping. The material damping ratio  $\xi$  for welded steel parts lies approximately between the value of 0.002 and 0.02 [5-03]. With this guideline, a default material damping of the model is realized with  $\xi = 0.0025$ , as this is the material damping of structural steel. With knowing that the fact that the structure has a higher damping in water than in the medium of air, the higher damping factor of water is considered within the material damping. About three-quarters of the jacket are in the water. In this section, the material damping is set to  $\xi = 0.5$ . This relates to the two floors at the bottom and half of the 3rd floor.

### 5.1.3 Results of the performed studies of innovations on component level

#### Results Modal Analysis

The inference on the load mitigation by the application of TVA to the numerical structure can only be guaranteed when using a validated simulation model. Therefore the Modal Assurance Criterion (MAC) is given [5-04]. For this propose the geometry origins and orientations in the ANSYS model are chosen similarly to the reference model. The result is given in Figure 5.1-4. It shows that the comparison of the eigenvectors shows good correlation for the first five eigenmodes. The first three eigenmodes are depicted in Figure 5.1-5 (in the 1<sup>st</sup>, 3<sup>rd</sup> and 5<sup>th</sup> picture). It shows the fore-aft, the side-to-side and the torsion of the tower.

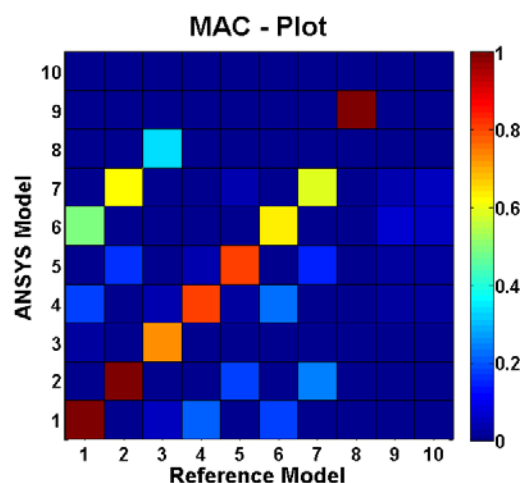


Figure 5.1-4 - MAC values plotted comparing ANSYS and reference model in ROSAP

Only the global modes are essential to the overall dynamic response. Due to missing information about the eigenmode shapes six to ten of the reference model, no statement concerning the comparison of the models above 1.5 Hz can be made.

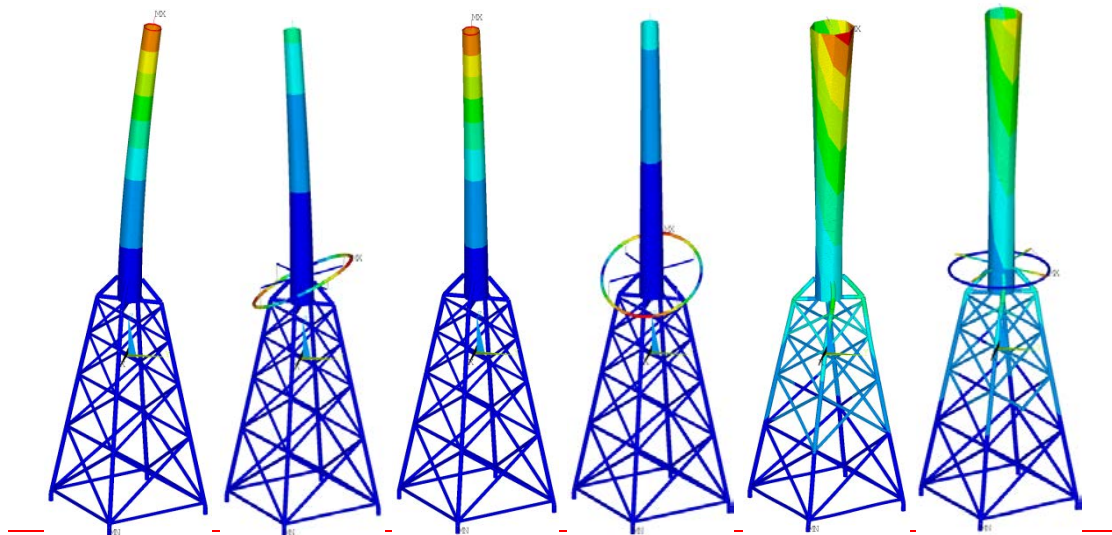


Figure 5.1-5 - Comparison of first 3 mode shapes without and with vibration absorber, respectively

Figure 5.1-5 shows the behaviour of the eigenmodes without and with the circular vibration absorber. The scaling of the 1<sup>st</sup>, 3<sup>rd</sup> and 5<sup>th</sup> picture is unequal to these of the 2<sup>nd</sup>, 4<sup>th</sup> and 6<sup>th</sup> picture.

Of course the amplitudes of the operating modes depend on the excitation of the OWT. Also the damping and the interaction with fluid and aerodynamic behaviour must be taken into account. The presented numerical results are obtained using a Dirac impulse with 10 kN. The loads are applied at the tower.

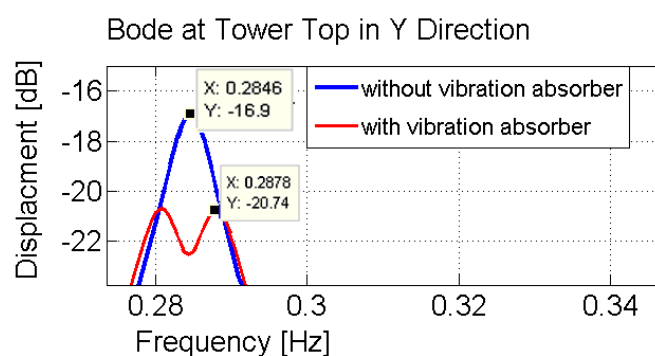
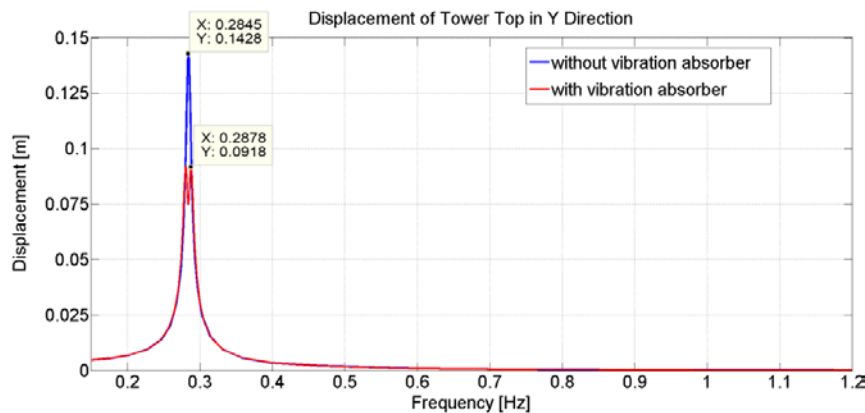


Figure 5.1-6 - Deviation of the response with and without vibration absorber on tower top in y-direction

The displacement's deviation of 35.8% is also seen in Figure 5.1-7. Because of the stimulating force the top of the tower is displaced without vibration absorber to 0.1428 m. In contrast, the top of the tower is displaced only by 0.0918 m if constructed with the vibration absorber.



**Figure 5.1-7 - Deviation of the displacement with and without vibration absorber on tower top in y-direction**

The mass of the TVA should be at most – as a rule of thumb – 10% of the overall mass. For large and heavy applications the additional mass should lie between 2-5% of the overall mass (see [5-07]). Thus, the presented design adds too much additional mass to the structure which also increases the overall costs for the OWT enormously.

The shown vibrations absorber performance can be improved with including more damping. In the shown design the springs have to stand a large static load. When harmonic excitations adjoin, the durability of the presented TVA need to be more investigated.

#### 5.1.4 Current TRL of innovations and recommendations for their further development

The technology readiness level for single passive vibration absorbers are in general TRL 9, since these kinds of devices are well known in construction and manufacturing and are applied at several real world constructions.

Nevertheless for every system where TVAs are applied, there need to be made 3 steps to ensure that the devices work properly [5-07]:

- 1) At first, there need to be measurements of the structure to know the exact excitation loads.
- 2) In a second step the TVA need to be positioned, dimensioned and constructed.
- 3) The last step depends on the fine tuning in frequency and probably mass of the TVA when applying to the structure.

For the reference structure and the 20 MW wind turbine generator the design is made only numerically. The passive TVA for the reference structure only exists on a numerical and analytical level. There are no realizations of the specific design of the passive TVA and therefore no experiments in a laboratory environment. Thus the technology readiness level of the here presented passive TVA for the 10 MW OWT is TRL 3.

#### 5.1.5 Cost reduction potential of innovations on component level

The possibilities of the presented vibration absorber are the mitigation of occurring loads. The device already reduces the resonance of the first bending mode. A vibration absorber can increase the operating range of the system, involving longer power generation. In addition, a TVA helps to increase the lifetime of the OWTs, which reduces the current costs of generating electricity. Furthermore a TVA or a system of TVAs can help to improve the structural behaviour. Thus, a TVA makes the system more economical and helps to enhance generating power at the ratio of costs. By usage of a vibration absorber, the durability of the material of the entire structure can be improved, since large deflections are downsized. In the shown computations the displacements are decreased by nearly 10 cm. The deflections lead to stresses in the material that cause fatigue. In addition, it is expected to reduce the prevailing deflections and vibration speed of the nacelle to extend the operating range.

Besides the possibilities of tuned vibration absorbers, there are some risks, when applying these devices. If the TVA is mistuned and has a low damping ratio, the structural amplitudes can be increased and excite the structure. The deflection amplitudes would be increased in this case.

The mistuning of a TVA can be caused by unexpected excitations in the environment, changes in the main structure regarding mass and stiffnesses or the TVA can be mistuned in the fine tuning step (see section 5.1.4, step 3)). This disadvantage can be lowered by integrating damping elements.

One risk for this specific setting is the concentration on an ideal impulse. Clearly, the former investigations are done in the modal domain, where all eigenmodes of the system are respected. The exact forecasts in reduction of displacements depend highly on the excitation location, amplitudes, directions and their characteristics. Up to now the excitation differs from real excitations and is thus a risk in the tuning perspective.

The introduced assembly adds mass of about 12% of the main structure to the reference 10 MW OWT, without saving material. Also the fabrication (formally welding), in-situ execution and the transportation need to be taken into account. All this just increases the initial costs of the OWT. A rough estimation on the material lead material costs at least 12% more (excluding fabrication, transport and installation costs).

The lowering in the costs only appear over time, when the maintenance of the OWT is elongated and the frequency range in which the OWT is able to harvest energy is extended.

#### **5.1.6 Required further development of innovations (with a focus on challenges related to the upscaling from 10 MW to 20 MW wind turbine)**

The mass ratio of the presented TVA is 12,3% while reducing the displacement by nearly 36%. The mass ratios need to be decreased for the load mitigation assemblies. There are chances to increase also the vibration reduction level.

The vibration reduction via TVA can be forwarded with different research scopes. In all cases it would be best to achieve a broadband frequency range. Therefore it is useful to consider distributed tuned vibration absorbers. There all single devices itself work in a narrow band frequency range and in combination the attached devices have broadband impact to the structure. An advantage is the reduction of the effective used masses in every single device. A disadvantage is still the needed design space in the nacelle, tower and TP components. Another disadvantage can be the interaction between the devices. The interaction has to be considered in numerical simulations.

Since disturbances and changes in the excitations as well as the boundary conditions are likely, the devices should be semi-active or active. In combination with distributed vibration absorbers the control scheme has to handle different distributed devices at once. This leads to interesting research questions like central and decentral sensor networks and control schemes.

It is unlikely to develop a precise design of a distributed network that can be simply upscaled. It is more useful to investigate in common simulation methods that are based on modal descriptions of simulation models. Then the application of schematic descriptions in a modular way is possible. Now the modal parameters of the presented TVA are implemented in ROSAP to show the load mitigation.



## 5.2 Tuned Mass Dampers at Tower Top

The relative large displacement and acceleration amplitudes both in fore-aft and sideways direction at the tower top or nacelle of an offshore wind turbine make this location interesting for the employment of tune mass dampers. The mechanical principle of such devices is similar to the tuned vibration absorbers described in the previous section. Tune mass dampers are further investigated in this chapter from the viewpoint of the overall dynamics and the fatigue loads of the offshore wind turbine. Prior to an extensive parameter study on the massed dampers in Sub-Sections 5.2.2 to 5.2.5 the dynamics of the reference wind turbine with respect to the resonance between the first natural frequency and the blade passing frequency is discussed. A redesign of the rotor speed control characteristics partly solved some resonance problems described in report D.1.2 [5-08].

### 5.2.1 Discussion of the considered innovations on component level

In the reports D4.1.1 [5-08] and D4.1.2 [4-49][5-09] the usage of different optimization principles for mitigating loads of the INN WIND.EU support structure and tower design have been discussed. In a first step, also dealt with in this sub-section, the relevant load situations, loads, and critical components have been identified. Fatigue load situations in normal operational conditions have been identified as the relevant load situations which can be influenced by passive, semi-active or active damping devices. Due to the particular reference design of the wind turbine and the control system the first eigenfrequency of the support structure and the blade passing frequency, which equals three times the rotational speed, coincide within the partial load region. This leads to an increased acceleration amplitude in the upper part of the support structure, to corresponding high inertia loads and to increased fatigue loads. This is seen both in fore-aft and sideways direction.

#### Change of frequency relation

The relation between first tower eigenfrequency and rotational speed of the turbine dominates the excitation of the structure. A complete separation of the two frequencies is not possible. The Campbell diagram (Figure 5.2-1) shows the interaction between the blade passing frequency and the first tower eigenfrequency at 0.3 Hz. A decrease of first tower eigenfrequency or an increase in the rotor speed would reduce this problem.

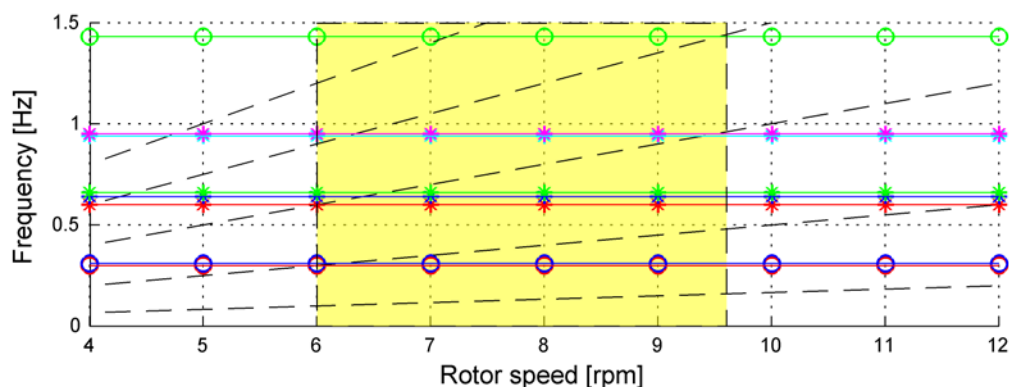


Figure 5.2-1 - Campbell diagram for the INN WIND.EU reference turbine and support structure including coupled tower (circles) and blade (star) modes - operational region indicated by the yellow box [5-09]

### Usage of speed exclusion window

The definition of a speed exclusion window is another possible solution to reduce the excitations. Actually this has been realised for the INN WIND.EU reference turbine. Figure 5.2-2 shows the selected exclusion window.

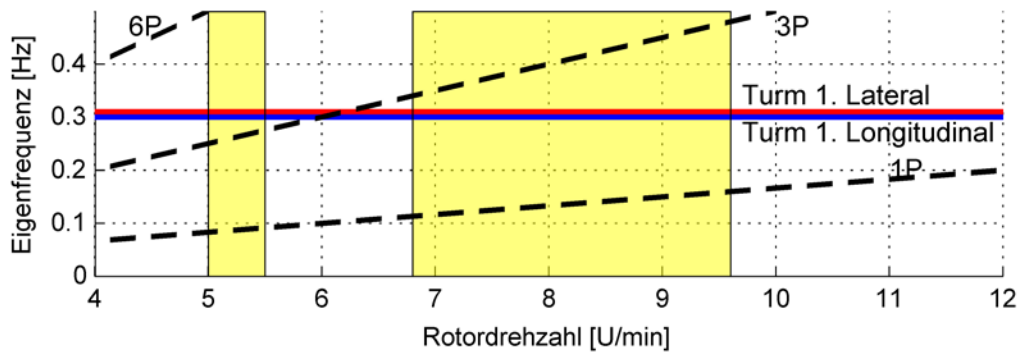


Figure 5.2-2 - Campbell diagram of the INN WIND.EU reference turbine with exclusion window between 5.5 and 6.8 Hz [5-011]

## 5.2.2 Description of the performed studies of innovations on component level

### Boundary conditions

The performed studies on the mass damper at the tower top are based on the INN WIND.EU reference design [5-05]. The aeroelastic simulation tool DNV GL Bladed has been used to perform the simulations in the time domain. The site parameters are chosen according to wind turbine class IA. The wave characteristics wave period and height are taken from the UpWind.eu design basis for the deep water site [5-013]. The values are shown in Table 5.2-1.

Table 5.2-1 - Environment conditions for wind turbulence and sea state parameters

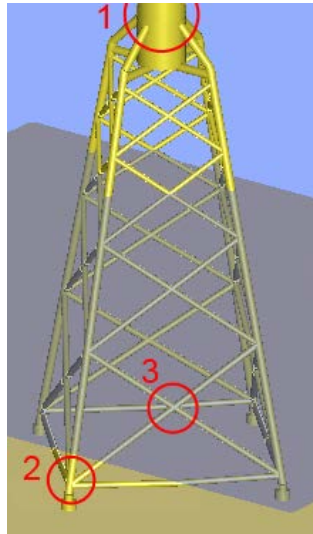
V [m/s]	2	4	6	8	10	12	14	16	18	20	22	24
TI[%]	29.2	20.4	17.5	16	15.2	14.6	14.2	13.9	13.6	13.4	13.3	13.1
Hs [m]	1.07	1.1	1.18	1.31	1.48	1.7	1.91	2.19	2.47	2.76	3.09	3.42
Tp [m]	6.03	5.88	5.76	5.67	5.74	5.88	6.07	6.37	6.71	6.99	7.4	7.8

The simulations have been made with respect to different orientation of wind and wave to the jacket structure.

### Identification of critical components

Relevant components for load mitigation by damping devices have been identified at the tower bottom for the longitudinal and the lateral bending moments as well as the lower part of the jacket structure in the K and X joints. Figure 5.2-3 illustrates the investigated spots of the structure.





**Figure 5.2-3 - Jacket structure and investigated sections**

The relevant components of the load envelope have been identified as the fatigue loads. The fatigue loads are mainly driven by the operational load cases in normal environment conditions. They have been calculated by aeroelastic simulation in the time domain for different wind speeds and sea states. The effect of the load is weighted according to the steel material of the structure with rainflow counting and in respect to the relevant SN-slope.

#### **Structural damping by tuning the ratio between eigenfrequency and excitation frequency**

The influence of the relation between structure eigenfrequency and rotational speed has been analysed in detail. The damage equivalent loads have been calculated for a set of frequencies from 0.21 to 0.35 Hz and the whole operational range of the wind speed from 4 to 24 m/s.

#### **Parameter study for mass damper**

A parameter study has been carried out for the tuned mass dampers which takes in account different values of the damper mass, the tuning frequency as well as the effect to different location of the structure. The analysis is made for the whole operational range with turbulent wind fields with different wind directions. Figure 5.2-4 and Table 5.2-2 display the used parameters.

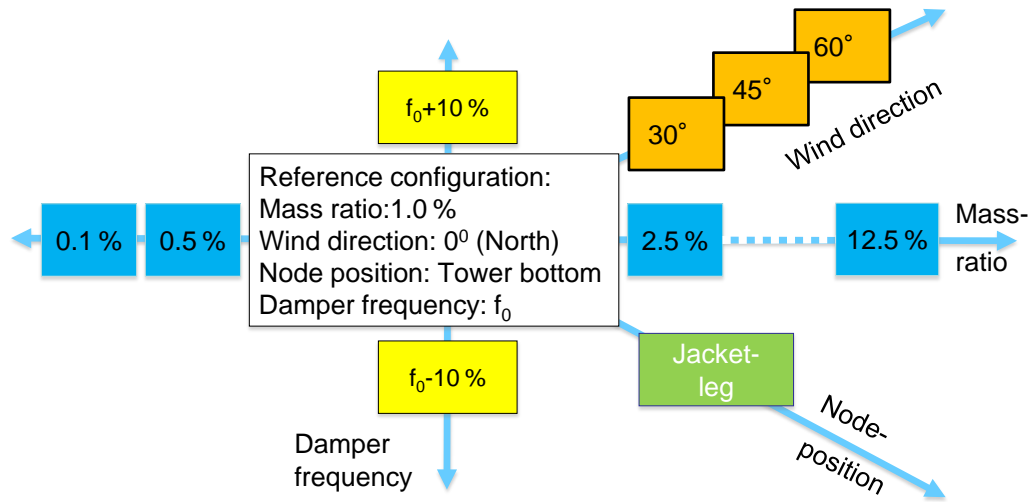


Figure 5.2-4 - Degrees of freedom of parameter study [5-011]

Table 5.2-2 - Parameter values for study of tuned mass dampers

<b>Damper mass:</b>		
Mass ratio	%	0,1; 0.5; 1.0; 2.5; 4.0; 7.5; 10; 12.5
Damper mass	ton	0.86; 4.31; 8.63; 21.6; 43.1; 64.7; 86.3; 108
<b>Tuned frequencies:</b>		
Frequency	Hz	0.30; 0.27; 0.33
<b>Analysed load spot:</b>		
Spot		Tower bottom (1); Jacket bottom k-Node (2); Jacket bottom x-Node (3)

### 5.2.3 Results of the performed studies of innovations on component level

#### Optimization of the ratio between first eigenfrequency and rotor rotating frequency

The following Figure 5.2-5 and Figure 5.2-6 illustrate the damage equivalent tower base bending moments extracted from simulation results in for-aft direction and in sideways direction respectively.

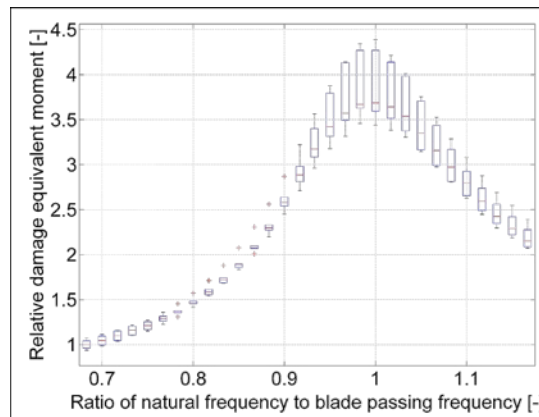


Figure 5.2-5 - Tower base fore-aft damage equivalent load normalized with the lowest load value for a wind speed of 8 m/s (6 rpm) over the ratio of the first natural frequency and the blade passing frequency [5-011]

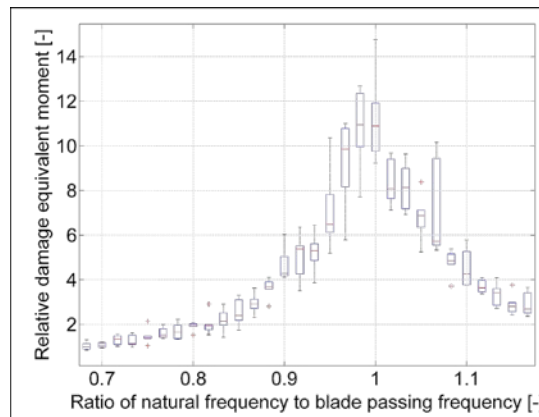


Figure 5.2-6 - Tower base sideways damage equivalent load normalized with the lowest load value for a wind speed of 8 m/s (6 rpm) over the ratio of the first natural frequency and the blade passing frequency [5-011]

The results highlight an increase of the tower base damage equivalent moment in both directions. There are relevant differences between the fore-aft and sideways direction. While a damped resonance peak is found in the fore-aft direction (Figure 5.2-5) a high resonance due to the missing aerodynamic damping of the rotor occurs in the sideways direction (Figure 5.2-6). The resonance peak in the fore-aft direction is spread more widely due to the higher damping. An operational point 10 % apart of the natural frequency results in only 30 % load reduction in supercritical and 25% reduction in subcritical operation in fore-aft direction whereas the sideways moment already decreases by 60 % for a 10 % safety margin. The overall amplification ratio is 3.7 in fore-aft and 10.9 in sideways direction.

The analysis was extended to the full range of wind speeds, ranging from 4 m/s to 24 m/s and natural frequencies from 0.21 Hz to 0.35 Hz. The analysis took into account the damage equivalent bending moments of the tower base in the fore-aft as well as side-to-side direction and the blade root bending moments. No significant influence on the blade root bending moments was found for the different natural frequencies of the tower. In contrast the fatigue loads of the tower are heavily influenced. Figure 5.2-7 and Figure 5.2-8 plot the tower bottom bending moments for this analysis. The damage equivalent loads are normalized in each figure to the lowest value for the considered loading direction. The straight vertical lines mark from left to right the wind speed at 6 m/s from where the results in Figure 5.2-5 and Figure 5.2-6 have been extracted, the start of pitching region below rated wind speed and the point of rated power respectively. The line on the top left indicates the blade passing frequency of the turbine, the dashed lines give a 10 % margin

around. Crosses mark the simulated combinations of wind speed and natural frequency of the structure. The area between the crosses is interpolated.

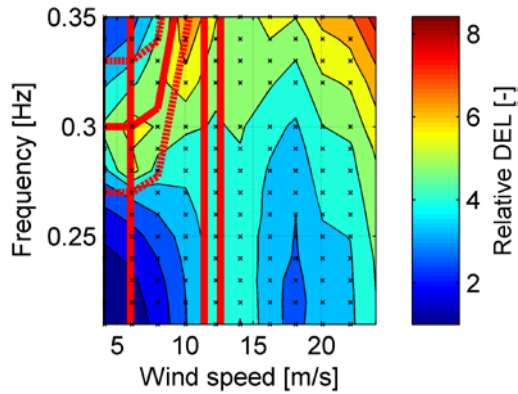


Figure 5.2-7 - Relative damage equivalent loads for  $N_{ref}=10^7$ , SN-slope  $m = 4$  over wind speeds and natural frequency for fore-aft tower base direction [5-012]

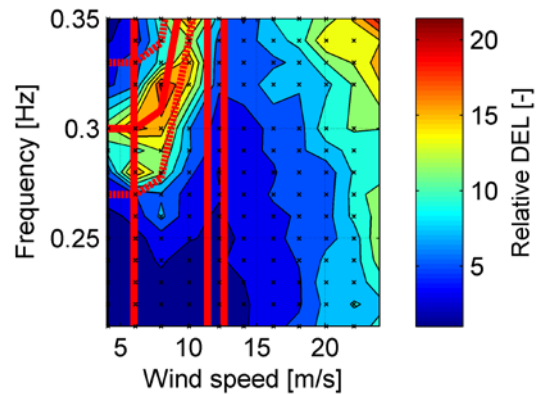


Figure 5.2-8 - Relative damage equivalent loads for  $N_{ref}=10^7$ , SN-slope  $m = 4$  over wind speeds and natural frequency for sideways tower base direction [5-012]

It can be observed, that the fatigue damage is highly amplified for a first eigenfrequency of the structure in the region around the blade passing frequency (3P). The results show significant higher values starting from low to high wind speeds. In addition, an increase of fatigue loads from low to high natural frequencies of the system can be seen too. Even for a 10% margin around the 3P excitation (dashed lines), the damage equivalent moments are still significantly higher.

Another interesting aspect is found around rated wind speed, where the load effect differs between the fore-aft compared and the sideways direction. Whereas the response in the sideways direction is not influenced by the transition region, a strong effect is found in fore-aft direction. As seen in Figure 5.2-7, the fatigue damage rises significantly in the area right above rated wind speed. This area is marked with the vertical solid lines. The DELs are up to four times higher compared to the lowest value.

The initial design of the reference turbine led to these resonance issues. The combination of a relatively stiff structure with an excitation by the blade passing frequency results in largely increased fatigue loads and therefore in very short life time expectations. The absolute reduction in life time depends also on the wind speed distribution, which is, however, not evaluated in this study.

As a consequence the control system has been modified to exclude the most significant excitation part of the blade passing frequency (Figure 5.2-9).

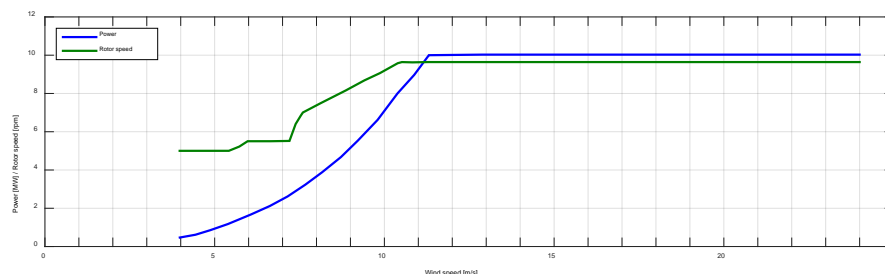


Figure 5.2-9 - Rotor speed and power with speed exclusion window from 5.5 to 6.8 m/s [5-011]

The speed exclusion window has been selected to prevent the high tower excitations especially in partial load. The rotational speed is kept constant below 6 m/s at 5 rpm, accelerates to 5.5 rpm at 6 m/s and is kept constant till 7.5 m/s. At this speed the rotational speed is rising rapidly to

6.8 rpm. This is realized by control of the generator torque. From 7.5 m/s on the blade tip speed is kept constant till 11 m/s, where the pitch control starts for constant rotational speed. Above 11.4 m/s the generator torque is kept constant too. The associated Campbell diagram has been shown already in Figure 5.2-2.

Figure 5.2-10 shows the actual damage equivalent moments at tower bottom for the reference configuration with the speed exclusion window in fore-aft (blue) and sideways (green) direction. Especially between 6 and 8 m/s wind speed higher loads are observed. In combination with the distribution of the wind speeds at the specific site, e.g. by a Rayleigh distribution, the wind speed region of 6-8 m/s occurs more often than the wind speeds above rated wind speed. Hence, the influence of this region will even increase.

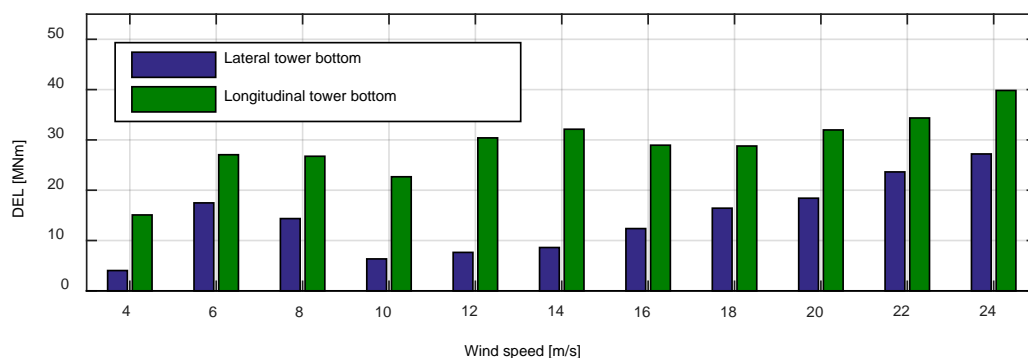


Figure 5.2-10 - Damage equivalent loads at tower bottom for the reference design with speed exclusion window; SN-slope 4;  $N_{ref}=10^7$ ; 20 years design lifetime, [5-011]

#### Parameter study on tuned mass dampers

Tuned mass dampers have been addressed as promising concepts to some extent in the reports D4.1.1 [5-08], D4.1.2 [5-09] and D4.3.2 [5-010]. The influence of adjustable parameters of different designs have been analysed in another study by simulations with the aeroelastic simulation tool DNV GL Bladed which models the dynamic behaviour of the system in turbulent wind conditions. .

Figure 5.2-11 and Figure 5.2-12 compare the damage equivalent moments at the tower bottom for different wind speed and mass relation in fore-aft and sideways direction respectively. In fore-aft direction the influence of the damper mass on the reduction of the fatigue moments is marginal, whereas in sideways direction a high influence is clearly seen. The total damping in this direction is given by the combination of structural damping and the supplement damper mass. The aerodynamic damping is negligible in side-to-side direction. Load reduction for some wind speeds can be till 50 %. The damping effect is not only seen at 6-8 m/s but likewise over the whole operational range.

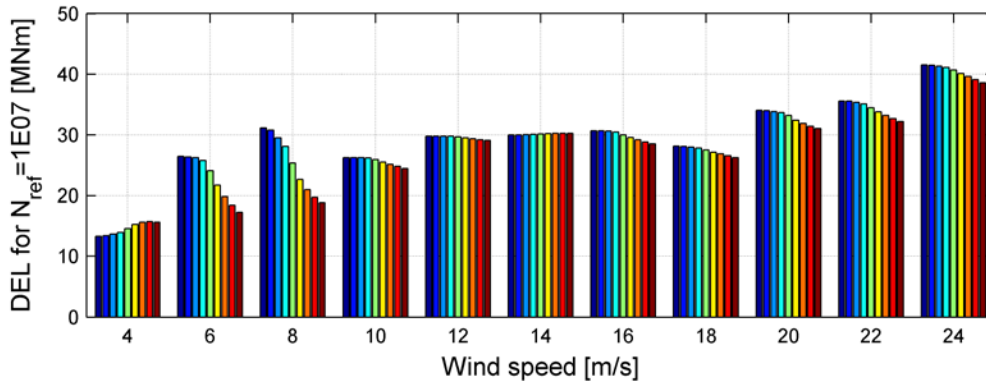


Figure 5.2-11 - Damage equivalent bending moments at tower base in fore-aft direction with integrated dampers, reference in dark blue, additional bars for mass ration from 0.1 % to 12.5% (from left to right); tuned frequency 0.30 Hz, [5-010]

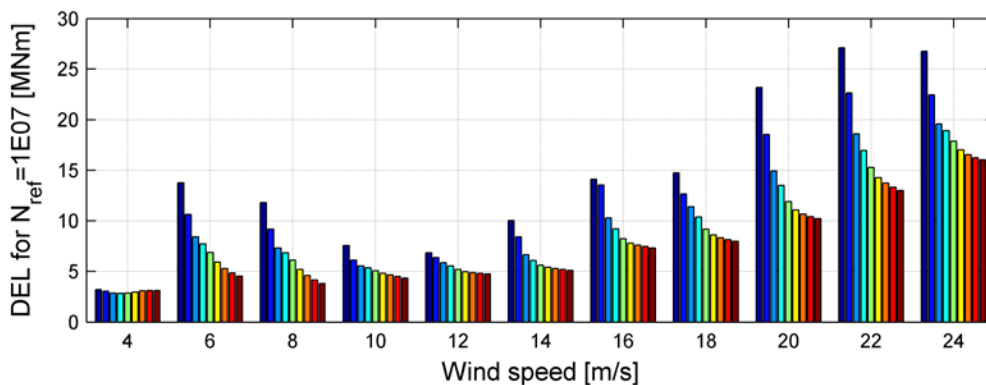


Figure 5.2-12 - Damage equivalent moments at tower base in sideways direction with integrated dampers, reference in dark blue, additional bars according to the damper mass ratio for 0.1 % to 12.5 % (from left to right); tuned frequency 0.30 Hz, [5-010]

The influence of different damper masses on the loads in the jacket structure is mainly seen in the sideways direction similar to the effect on the loads at the tower bottom. The influence is larger when the wind direction is from the north.

Figure 5.2-13 illustrates the damage equivalent force at the K-Joint for 0° wind direction. The influence is as larger as seen at the tower bottom. The effect is reduced when the wind direction is perpendicular to the flat side of the jacket, i.e. 45° wind direction, as seen in Figure 5.2-14.



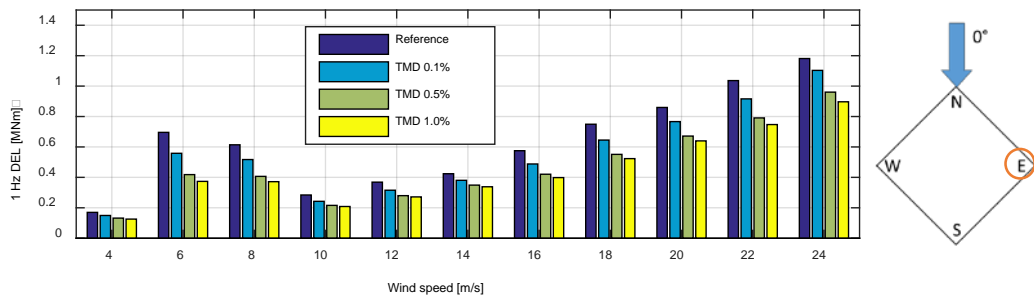


Figure 5.2-13 - Damage equivalent load at the eastern jacket bottom K-joint with different damper masses; wind direction 0°, [5-011]

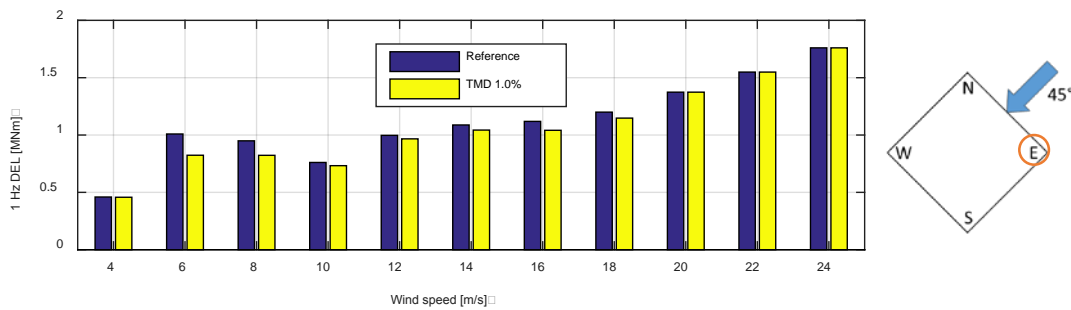


Figure 5.2-14 - Damage equivalent load at the eastern jacket bottom K-joint with damper masses 0.1%; wind direction 45°, [5-011]

Next the analysis of the influence of uncertainties in the frequency design of the damper and of the eigenfrequencies of the system itself is discussed. Especially the influence of false tuning on the effectiveness of the damping system has been shown. The damper mass ratio has been selected as 1% while a mistuning of +/- 10% of the reference eigenfrequency of 0.30 Hz has been considered.

Whereas the damper with a too low tuning frequency has almost the same damping effect compared to an optimum tuning, a higher damper frequency leads to less load mitigation. In full load operation almost no or only little load reductions are observed for a too high tuning frequency almost since the load magnitudes approach the undamped reference case. For a conservative design and corresponding tuning of the damper the eigenfrequency of the system should be slightly underestimated.

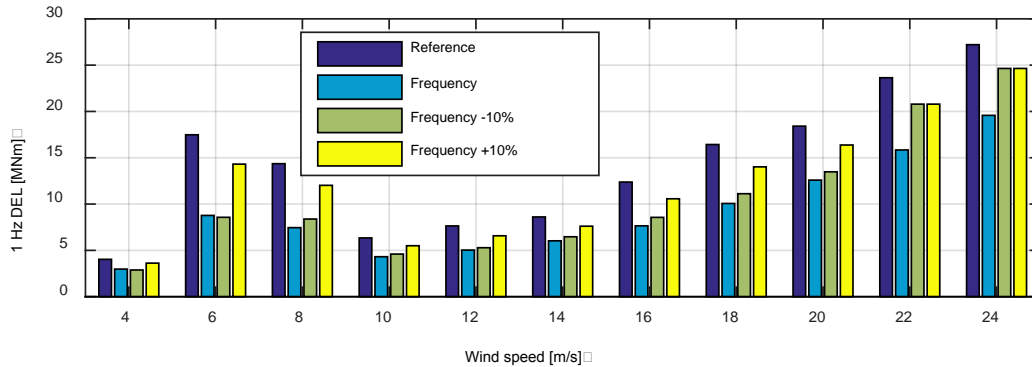


Figure 5.2-15 - Damage equivalent moment at tower bottom for reference design and damper solution with +/- 10% mistuning, [5-011]

Figure 5.2-16 summarizes the findings of the parameter study for variation on the damper mass, the effect of mistuning the systems and the different effects on tower bottom structure in fore-aft and sideways direction as well as the influence of the wind direction on the different damper systems on the Jacket K-joint.

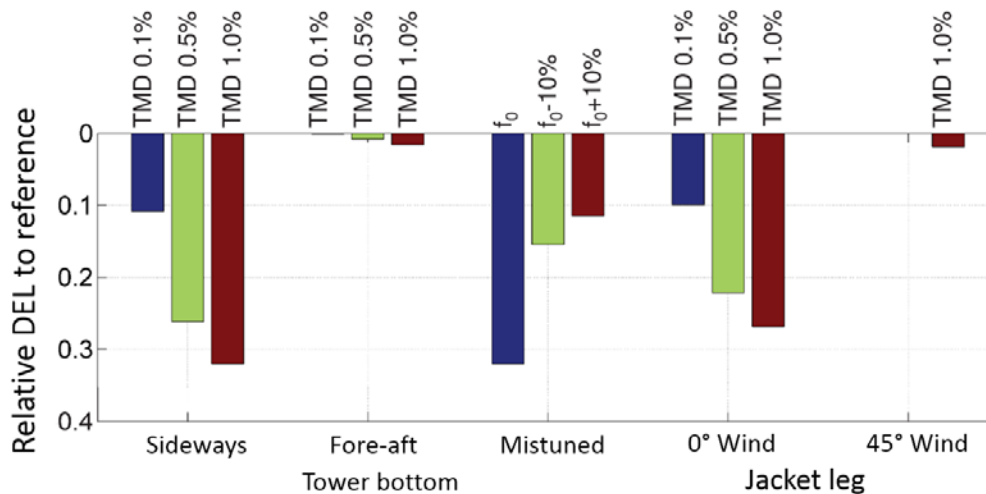


Figure 5.2-16 - Mitigation of fatigue loads w.r.t. reference design; left: Tuned mass damper with mass ration 0.1 % to 1.0 % on tower base; center: misstuned mass damper; right: effect for different wind direction of jacket leg; lifetime weighted Damage Equivalent Load, [5-012]

### 5.2.4 Conclusion and assumed impact of innovations on component level

The analysis has shown that the usage of tuned mass dampers placed at the tower top can have positive effects on the lifetime extension of the tower and jacket structure at a deep water site. A damping mass of 0.5 % of the modal mass of the structure has already a significant influence on the fatigue loads. The fatigue loads on certain subcomponents like the cross section at the tower bottom and the jacket bottom can be reduced especially in partial load operation which is the most recognized load situation. Mainly the vibrations in sideways direction can be reduced. The analysis showed as well that the loads can be significant reduced also without a damper system

by a slightly change of the support structure eigenfrequency or a change of the rotational speed in the partial load region.

If a tuned damper is included in the structure an additional weight of 0.5% of the modal mass of the fundamental support structure frequency, i.e. approximate 4.3 tons, has to be taken into account for the 10 MW reference design. While some fatigue load component e.g. the sideways bending moment near the tower base can be reduced by up to 25% the effect on the overall mass and CAPEX will be significantly lower and will depend on the load component governing the local hot spot design. The installation of the damper can already been done onshore in the upper tower segment or in the nacelle, depending on the design principle. Extra offshore work is needed for removing the transport fixations. Extra commissioning time is required to tune the damper system on site. A rather limited amount of extra maintenance time offshore is necessary as well to inspect the system and maintain bearings. Nonetheless such systems are considered to be robust and to be easily and cheap to maintain.

### **5.2.5 Required further development of innovations (with a focus on challenges related to the upscaling from 10 MW to 20 MW wind turbine)**

Tune mass damper at the tower top can be upscaled to the 20 MW class. The required mass and associated cost will still be moderate in comparison to the rotor-nacelle assembly.

The need for load mitigation concepts and measures to deal with the resonance between the fundamental structural mode and the blade passing frequency will become even more important for turbines in the 20 MW class since it is expected that the resonance frequency will shift towards the blade passing frequency at rated rotational speed. Therefore it will be more difficult to consider a speed exclusion zone close to the rated rotational speed and a tuned mass damper could offer to narrow down the width of the exclusion zone. A similar trend on the resonance between the fundamental structural mode and the rotating frequency has been recently observed at turbines with slender blades and rather tall towers in the 3 MW class onshore. A resonance range close to the rated speed is corresponding with even more frequent values of the mean wind speed and will cause higher energy losses when the rotor has to operate with a lower aerodynamic efficiency.

However, basic scaling laws will act slightly against the efficiency of tuned mass dampers. The lower first eigenfrequency of the support structure – rotor-nacelle assembly system governed by a taller structure and the higher mass of the rotor-nacelle assembly will result in a lower damping energy at constant mass ratio. Hence a larger damper mass and dimensions will be required and a more compact design has to be fit into the upper tower section in order to provide sufficient clearance between the damper mass and the tower shell even at large vibration amplitudes. Therefore the employment of semi-active or active damping systems might become more attractive in relative terms for larger offshore turbines.

So far structural dampers are only designed for more or less prescribed turbine concepts. In order be able to gain more benefit form structural damper systems a more proactive approach with an integrated design of the entire wind turbine systems including all relevant aspects of the support structure and the rotor-nacelle-assembly is desirable.

### 5.3 Semi-active and active damping devices

After analysing passive dampers the employment of semi-active and active damping systems are considered as the evident alternative proposal for structural control of wind turbine structures. Previous publications indicate interesting prospects [5-014]. In contrast to passive dampers the intensity of the control, which is exerted on the structure, can be adjusted during operation. Thus, the magnitude of the counter-acting forces is adapted to the respective operating point. This protects both the structure as well as additional components and enables cost-efficient operations. Furthermore, semi-active and active systems can operate effectively over a wide frequency band. Considering the variable rotor speed and corresponding frequency range of excitation in the partial load range this corresponds to a good performance over a broad span of wind speeds. The oscillation of the structure and thus the fatigue loads are also effectively damped over the entire power production range as well as the idling operation. However, open questions are the failure probability and the robustness of the systems which could affect the reliability and availability of the entire turbine. Another disadvantage of an active system could be resonances between the active damper and the wind turbine or its controller. This must be avoided by appropriate controller design.

#### 5.3.1 Discussion of the considered innovations on component level

##### Implementation and analysis of the reference structure in GH Bladed

Prior to any analysis of semi-active and active damping devices for the 10 MW design initially an in-depth analysis of the reference support structure itself, was required. Therefore, the reference support structure, designed by Rambøll, had to be modelled by the aero-elastic simulation tool GH Bladed. Next the design integration of rotor-nacelle-assembly and the effect of the reference controller in different operational points could be studied. The results have been documented in report D4.1.2 ([5-09]).

##### Semi-active damper with liquid in a U-tube or multiple U-tube arrangements with control of the flow

There are several publications dealing with active tuneable liquids in U-tubes for semi-active controlling the motion of the support structure of wind turbines. Practical usage has not been shown yet. First laboratory tests have been performed in literature, although not explicitly for the support structure analysed in this project. The actual TRL is selected with TRL 2. To increase this to TRL 3 with respect to the reference 10 MW WTG or the 20 MW WTG the following steps have to be made:

- 1) Analyse the actual needs for load mitigation of the support structures under specific operational and non-operational conditions. Till now the analysis focused only on the load case in normal operation.
- 2) Develop a model of a semi active liquid damper and include it in the aeroelastic model of the system. The damper system has to be tuned and the interaction with the WTG checked. In several development loops the structure, the control and damping system have to be adapted.
- 3) Draft design the liquid damper system. Scale the system and make a proof of concept of the specific system in the laboratory

##### Semi active viscous dampers

Magneto rheological (MR) dampers are actually used in automotive and defence applications. The usage in wind industry for damping of structural loads is not known. Regarding the height, frequency and load cycles of the application the technology readiness level for the discussed 10 MW and 20 MW WTG will be selected with TRL 2. The necessary steps to get to TRL 3 are:

- 1) Develop a MR system with respect to loads, frequency and size.
- 2) Extract needed parameters for the design of critical subsystems and perform a laboratory test if needed.
- 3) Proof of concept with respect to the parameters.

#### **Active tower damping by Pitch or Torque Control**

Active tower damping, which is described in Chapter 5.3.3 is already introduced in wind industry applications. Table 5.3-1 gives the possible variants of application. The TRL is selected with 4, the main reason for this being the large scale of the reference 10 MW WTG and the 20 MW. No testing in full-scale realistic environment has been done till now. To increase the TRL to TRL 5 the following steps have to be made:

- 1) Implement the systems in full scale simulation environment. Identify and compute all needed load cases according to guidelines. Make a risk analysis for supplement possible load cases and introduce extra design rules if needed.
- 2) Design realistic support elements, like adapted pitch actuation systems, based on the load calculations in 1).
- 3) Test a scaled model in the laboratory with connected simulation environment covering the whole operational range, the so-called Hardware in the Loop test (HiL). The scaled model test is needed as the equipment for 10 MW or 20 MW is too large for a first laboratory test.

#### **5.3.2 Description and results of the performed studies of innovations on component level**

A model of a semi-active liquid damper has been developed and has been included in the aeroelastic model of the system. Next a first parameter study on semi-active and active dampers has been carried out for the 10 MW reference design. Nonetheless the damper system has not been tuned and the interaction with the WTG has not been checked, yet. In several development loops the structure, the control and damping system have to be adapted. At the time of writing the required conceptual iterations, the comprehensive analysis and refinement of the results has not been finished yet.

#### **5.3.3 Conclusion and assumed impact of innovations on component level**

At the moment no firm conclusion and comparison of semi-active and active damper systems with passive dampers can be drawn.

#### **5.3.4 Required further development of innovations (with a focus on challenges related to the upscaling from 10 MW to 20 MW wind turbine)**

As discussed in Section 5.2.5 the need for load mitigation concepts and measures to deal with the resonance between the fundamental structural mode and the blade passing frequency will become even more important for turbines in the 20 MW class since it is expected that the resonance frequency will shift towards the blade passing frequency at rated rotational speed. Relative simple passive mass damper will become less effective and the integration into the available space in the tower top will become more difficult. Therefore the employment of semi-active or active damping systems is becoming more attractive in relative terms for larger offshore turbines. On the other hand it will be more challenging and more costly to provide the required larger damping energy by semi-active or active systems which are needed due to both the large modal mass and the lower fundamental natural frequency.

The primary objective of a wind turbine's control system is to ensure a safe and stable operation while maximizing the overall energy output. Ensuring safety is achieved by keeping electrical and mechanical quantities within admissible ranges. Thus, the control system has a substantial impact on the loads experienced by the turbine during its lifetime. This, of course, also applies to the loads on the support structure. It is useful to distinguish between the operational and the dynamic control level.

The operational control deals with supervisory control tasks, e.g. triggering grid-connection when the conditions for power production are fulfilled. Its main inputs are averaged measurements of the wind field and the rotational speed. Based on these measurements it initiates transitions between the turbine's operational states: idling, start-up, power production, normal shutdown, and shutdown due to a fault.

Choosing operational control parameters like the cut-in and the cut-out wind speed does not only affect the annual energy yield. It has also a substantial influence on the loads. Mainly three dedicated load mitigation concepts are currently available on the operational control level: speed exclusion zones, soft-cut out, and peak shaving.

Dynamic control is related to several feedforward and feedback control strategies. Their primary objective is to ensure proper dynamic responses of the turbine, e.g. to changing mean wind speeds, to gusts, or to safety issues. For actuation, the typical basic controller structure uses the generator torque in the region below rated wind speed and the collective pitch angle in the region above rated wind speed. The rotational speed is used as the control input in both cases.

The basic feedback controllers have a tremendous impact especially on the fatigue loads of the tower. For example, most utility-scale wind turbines exhibit a bandwidth limitation for the closed loop system above rated wind speed due to the first tower mode [5-015], [5-016]. If this is not properly taken into account, the controller design might induce unwanted vibrations that emerge from interaction between controller and tower motion.

The basic control strategy can be enhanced by a large number of methods to actively mitigate loads, see e.g. [5-017]. Different methods are available for active tower damping. Furthermore, active idling is an interesting option for offshore turbines. Load mitigation strategies for the 10+MW offshore turbines are being developed in task 1.4 and further developed here as required for different support structure designs.

### 5.3.5 Discussion of the considered innovations on component level

In the context of the present investigation three concepts are of special interest, i.e. the speed exclusion zone, peak shaving and active tower damping.

#### Speed exclusion zone

This paragraph mainly cites [5-018] speed exclusion zones, also called rotational speed windows or tower resonance bridging, can be useful when the rotor speed (1P) or blade passing frequency (3P) excites a structural resonance at a certain operating point, see e.g. [5-020][5-021]. Such resonances can be avoided by choosing the turbine's natural frequencies outside the operational excitation ranges. However, sometimes this is not possible. This is shown in the Campbell diagram in Figure 5.3-1, where the frequency of the 1<sup>st</sup> tower mode lies within the operational rotor speed range. At the red dot, the 1P-line cuts the dash-dotted line indicating the natural frequency. That is, when the system operates near this operating point, a vibration with the 1<sup>st</sup> tower frequency will be excited.

A speed exclusion zone can be employed in order to avoid this phenomenon. This means that the control system is modified such that the critical speed range includes no stable operating points. Thus, the rotor speed will rapidly drive through the critical speed range without severely exciting the natural frequency. Usually, this is implemented by modifying the speed-torque curve of the generator, see [5-020] and [5-022] for two implementation alternatives.



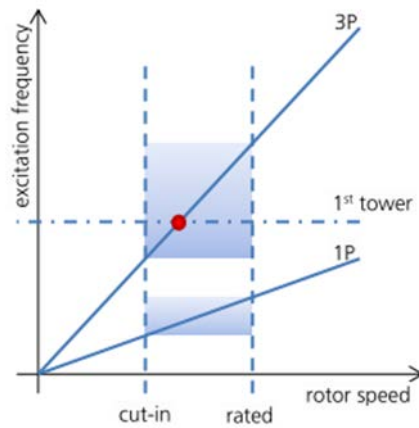


Figure 5.3-1: Campbell diagram. The red dot indicates an operating point where the 1<sup>st</sup> tower mode is excited by the rotor speed (1P).

### Peak Shaving

Following the standard operating strategy (speed-torque curve below rated and speed regulation with collective pitch above rated), the steady state thrust force on the rotor plane peaks at rated wind speed, see the dashed line in the middle plot in Figure 5.3-2. This usually causes high bending moments in the tower bottom and is critical both in terms of fatigue and extreme loads.

Applications so called “Peak shaving” or “thrust clipping” is a strategy that reduces the maximum steady state thrust force. The basic idea is to begin pitching the blades slightly below rated wind speed, see the solid line in the left plot in Figure 5.3-2, which reduces the thrust force in the critical range.

Simultaneously to shaving the thrust force peak the power capture in the transition region is reduced (right plot). Therefore, the design of a peak shaver is strongly subject to the trade-off between load mitigation and energy yield. Since its implementation is very simple it is often used as a last resort e.g. for meeting site-specific requirements. For offshore sites with considerable wave excitation, the reduction of aerodynamic damping must also be taken into account.

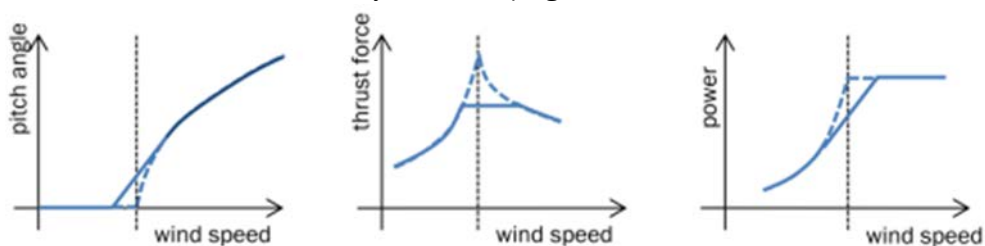


Figure 5.3-2: Steady operating points with peak shaving (solid line) and without (dashed line).

Reducing the maximum steady state thrust force by pitching the blades slightly below rated wind speed is applied as follows. Figure 5.3-3 shows the recommended pitch angle plotted against the generator moment. In this connection two variables are introduced namely the maximum peak shaving pitch angle (value between 0° and 5°) and the peak shaving gain (value between 0.6 and 0.9) multiplied by the nominal generator moment.

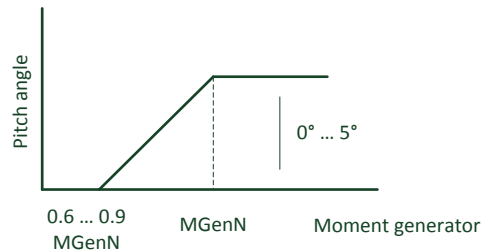


Figure 5.3-3: Recommended pitch angle plotted against the generator moment

### Active tower damping

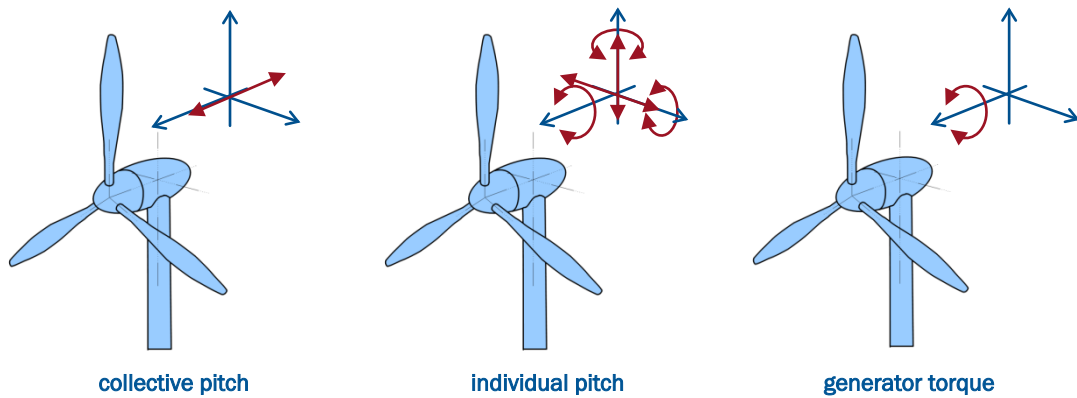
The following sections mainly cite [5-018] and [5-019]. Controlling the pitch angles and generator torque allows for the active damping of vibrations of the support structure. This can be done in the fore-aft as well as in the side-side direction. The actuators are used in a feedback control loop to generate counter-acting forces and moments that reduce the motions of the structure. Usually, the motions are measured by accelerometers mounted on the tower top. To realize a damping effect it is necessary to generate a force that is inversely proportional to the velocity. Hence, the design of the closed loop system includes a filter design to assure an appropriate phasing.

Because the resulting control signals are added to those of the normal operating control loops, the coupling between the different control loops must be taken into account. This is not trivial especially when actuator amplitude and rate constraints are active. Furthermore, active load mitigation is in general subject to a “waterbed effect”: When loads in a certain range in the frequency domain are reduced they will be increased in another range. And, more generally, when loads at a certain part on the turbine are reduced they will be increased on other parts. Consequently, different objectives must be balanced, and the application of mitigation strategies for the support structure requires a broad knowledge of the overall turbine design, see also the subsection on integrated design below.

A classification of different variants regarding actuator and motion direction is given in Table 5.3-1. These are discussed in detail in the following. Figure 5.4-4 shows how the different actuators affect forces and moments on the tower top.

Table 5.3-1 - Different variants for active tower damping

Actuator	Tower fore-aft	Tower side-side
Collective pitch angle	✓	✗
Individual pitch angle	✓	✓
Generator torque	✗	✓



**Figure 5.4-4: - Different actuators for active tower damping and their effective force/moments on the tower top (red arrows).**

The most widely spread variant is the damping of the 1<sup>st</sup> fore-aft tower mode for fatigue load reduction. For that purpose the fore-aft acceleration is fed back to the collective pitch angle using an appropriate filter. Consequently, a counter-acting thrust force on the rotor plane damps the tower vibration, see Figure 5.4-4. Changing the collective pitch angle also has an influence on the normal rotor speed regulation. But, this is usually not a major issue because the frequency of pitch angle variations due to the active tower damping is in most cases greater than the bandwidth of the properly designed rotor speed control loops. More critical is the potential coupling with blade flap modes, see [5-024].

Depending on the specific turbine design, it might be beneficial to mitigate not only the vibrations related to the 1<sup>st</sup> tower mode. For example, in [5-025] it is shown that also tower loads related to 3P harmonic excitation can be reduced using the same feedback structure. Another variant is dedicated to the 2<sup>nd</sup> tower mode. This is especially interesting for offshore turbines because this mode is easily excited by the waves. However, controlling the pitch angles individually is sometimes superior in this case: Depending on the actual shape of the 2<sup>nd</sup> mode, the tilting of the nacelle might be dominant. Then, an individual pitch control strategy that generates a tilt moment is more effective.

The so called “Individual pitch control” (IPC) has been heavily discussed in literature for quite some time, see e.g. [5-026][5-027]. It has been suggested for the reduction of loads on various components, which also includes the support structure. As shown in the middle of Figure 5.4-4 it offers a wide range of forces and moments on the tower top. The measurements used for feedback include tower top acceleration in side-side direction, blade bending moments, or bending moments measured on the mainframe.

The most obvious idea for the support structure is the damping of the side-side motion [5-028]-[5-030]. This motion is being counteracted by a side-side force or a roll moment on the nacelle. For onshore turbines the tower side-side fatigue loads are usually less important as compared to those in fore-aft direction. In contrast, the support structure of offshore turbines can experience significant fatigue loads in the side-side direction. Especially wind-wave-misalignment induces side-side motion because of the low aerodynamic damping [5-023].

From the overall control system’s point of view the coupling with the rotor speed control loop has to be considered. Furthermore, because the blades are actuated independently, either multivariable control design or a preliminary decoupling by a transformation must be carried out. The non-linear mapping, known under different names as “d-q axis-”, “Coleman-”, or “multiblade-” transformation, transforms rotating quantities into a non-rotating frame. In both cases significant amount is necessary for addressing issues like extreme loads induced by rotor asymmetry during shut-downs [5-031] and pitch system amplitude and rate constraints [5-032]. The latter can be an

issue mainly in the operating regime around rated wind speed because large pitch angle variations are necessary.

The active side-side damping is also possible modifying the generator torque [5-035]. To this end, the side-side acceleration is fed back to the demanded generator torque using an appropriate filter. The generator torque is supported by the main frame and, thus, leads to a counter-acting roll moment on the tower top (Figure 5.4-4). Due to the couplings between the various subsystems the interaction with the rotor speed control loop and the tower fore-aft loads has to be taken into account.

The enormous number of papers dealing with results from simulation studies contrasts with the little number of field-tests described in the literature. Some creditable exceptions include [5-031], [5-034]-[5-037]. These studies have been carried out on onshore turbines. Nevertheless, the reported results demonstrate the efficacy of the investigated load mitigation strategies by showing compliance with results obtained from simulations.

Figure 5.3-5 - shows a block schematic of the overall system. There are two distinct control loops:

- The usual rotor speed controller that feeds back the generator speed to the collective blade pitch for the region above rated wind speed, and
- The tower damping controller that feeds back the tower top acceleration in fore-aft direction to the collective blade pitch.

The wind speed is a disturbance input of the closed loop system. Three additional outputs are used for performance evaluation, i.e. the tower bottom bending moment in fore-aft direction, the actual collective blade pitch, and the collective out-of-plane blade bending moment of the blade roots. The user has to provide linear models of the wind turbine and the rotor speed controller for each operating point.

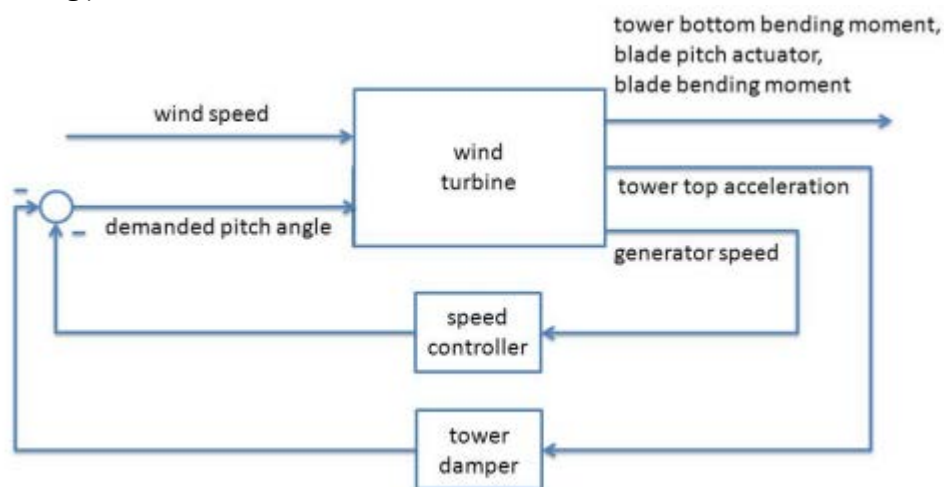


Figure 5.3-5 - Block schematic of the overall control system.

The implemented structure of the tower damping controller consists of a series connection of

- a differentiator,
- three first-order low pass filters,
- a time delay, and
- a notch filter:

$$F_R(s) = k_R \cdot F_{3p}(s) \cdot e^{-T_d s} \cdot \frac{s}{\left(\frac{1}{2\pi f_1} s + 1\right) \left(\frac{1}{2\pi f_2} s + 1\right) \left(\frac{1}{2\pi f_3} s + 1\right)}$$

The bandwidths  $f_i$  of the low pass filters can be used to accurately tune the phase response. The notch filter is used to mitigate 3p activity of the pitch system. While the notch frequency is fixed

$1/T_f$  with respect to the rotor speed at the given operating point, its width and depth is shaped using two parameters:

$$F_{3p}(s) = \frac{T_f^2 s^2 + T_f k_{bw} k_{gain} s + 1}{T_f^2 s^2 + T_f k_{bw} s + 1}$$

The time delay is not a design parameter. It can be used e.g. to reflect delays of the communication etc.

### 5.3.6 Description and results of the performed studies of innovations on component level

In the following two of the concepts introduced before have been analysed by numerical investigations of the INN WIND.EU reference turbine. This includes the peak shaver and the active tower damping.

#### Peak Shaving

Figure 5.3-6 shows the bending moment (tower foot) plotted against wind speed. The array of curves start at peak shaving gain value 0.9 and decrease stepwise with 0.05 to 0.6. At value 0.7 the curve is nearly flat. So, in this example the maximum peak of tower foot bending moment is reduced to 80 %.

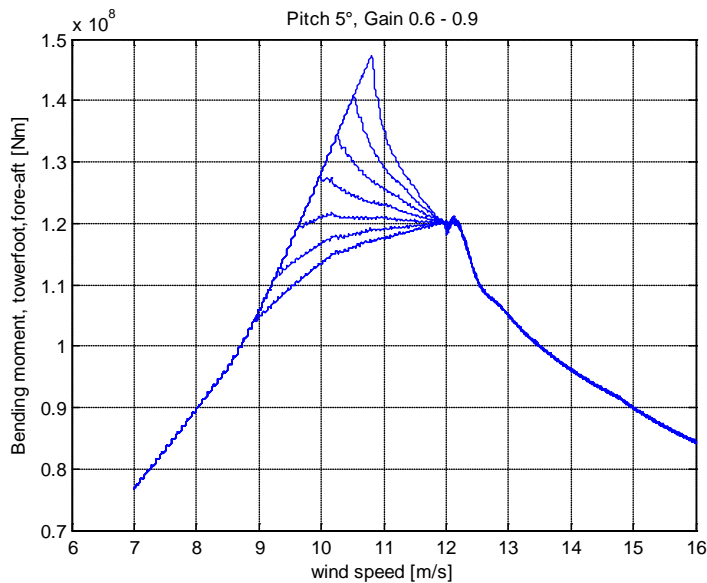


Figure 5.3-6 - Bending moment, tower foot

Figure 5.3-7 shows the numeric results for different pitch angles with peak shaving gains also obtaining peak-free bending moment curves. As mentioned above, the design of a peak shaver is strongly subject to the trade-off between load mitigation and energy yield. Corresponding to Figure 5.3-7, the energy yield is shown in Figure 5.3-8. With knowing the wind conditions at the on- or offshore location one may optimize the peak shaving procedure.

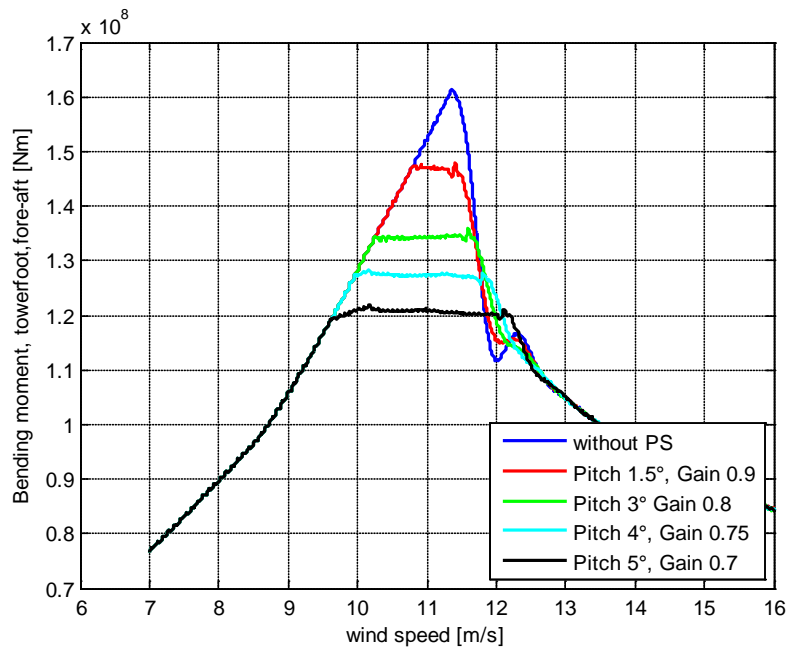


Figure 5.3-7 - Bending moment, tower foot, peak-free

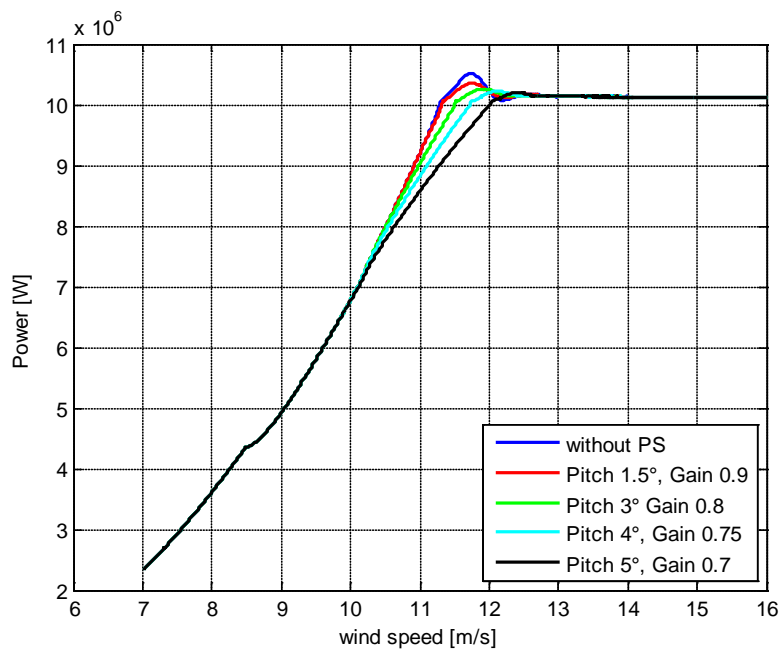


Figure 5.3-8 - Power, peak-free



### Active tower damping

The concept of the active tower damping described in Section 5.4.2 has been implemented in the simulation model of the INN WIND.EU reference wind turbine. In the scope of the numerical simulation with focus on the first tower frequency, three operating points are investigated namely for wind speed 8 m/s (partial load operation), 12 m/s and 16 m/s. The notch filter remains unused because in this case there was no improvement in tower damping achieved.

Figure 5.3-9, Figure 5.3-10 and Figure 5.3-11 show the transfer functions from wind speed to tower acceleration by using an active tower damper. In all three operating points nearly -6 dB magnitude loss is achieved at the frequency range about 0.3 Hz. A further increase of first tower mode damping leads to steady rise of close-by peak at 0.5 Hz.

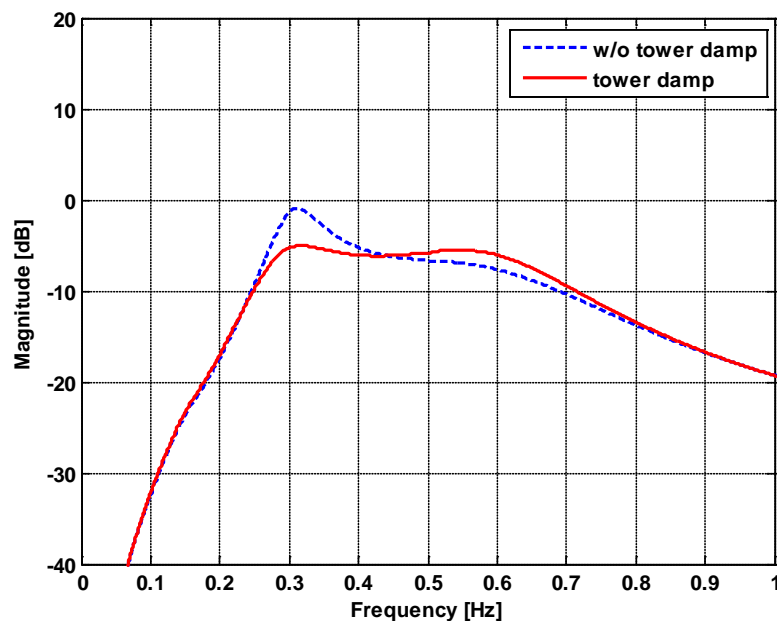


Figure 5.3-9 - Active tower damping, first tower mode, wind speed 8 m/s

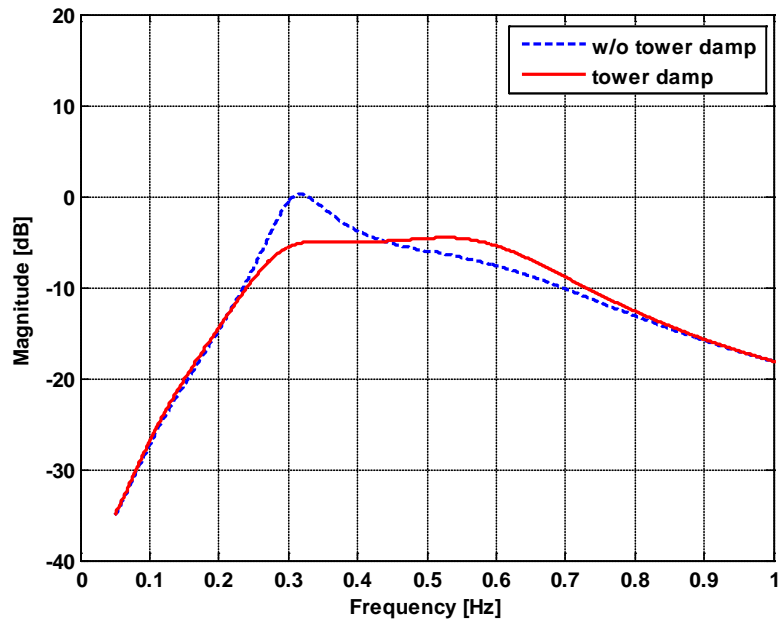


Figure 5.3-10 - Active tower damping, first tower mode, wind speed 12 m/s

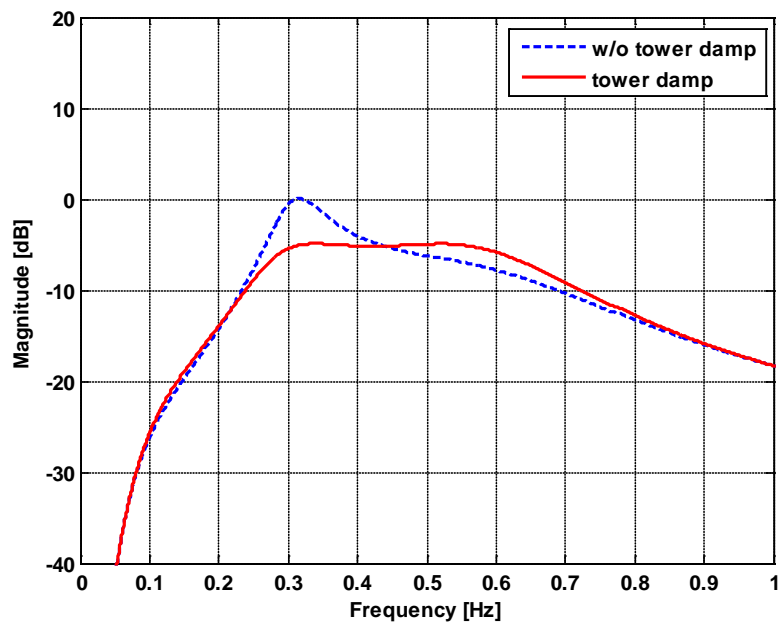


Figure 5.3-11 - Active tower damping, first tower mode, wind speed 16 m/s

## 5.4 Conclusions and Recommendations

Finally, it is confirmed by means of the harmonic response analyse that the passive vibration absorber reduces the amplitude of the displacement of the tower top by 35.8% in Y-direction, which is stated to be the direction of excitation.

However, to get a result an impact of 10 kN is exerted on the top of the tower. Generally acceptable conclusions about the reduction of the displacement by the passive vibration absorber in any other loading case cannot be drawn. Further research concerning the quantities and directions of loads will be essential in order to find out how the overall structure reacts on all kinds of loads. Additional investigation in order to improve the system response could be made regarding the mounting location of the vibration absorber.

Further it has been shown that the complete system is very sensitive to changes of the eigenfrequencies with respect to the driving frequencies of rotor and drivetrain. In conclusion this leads to two different approaches. Firstly a redesign of the rotor and drivetrain with a change on the rotational speed could reduce the necessary load mitigation measures. The second option is the usage of the suggested damping systems, which have to account for the high sensitivity to changes in the eigenfrequencies of the RNA. Tuneable, semi-active or active systems should give a higher safety and effectiveness. In a next step semi-active and active damper systems have to be designed and have to show their potential in the simulation environment. The simulation has to be performed in the frequency but also in the time domain.

Active load reduction technology has been implemented for the reduction of the thrust around rated wind speed by the so called Peak Shaver. The results show the mitigation potential. The effect of the Peak Shaver is a trade-off between load mitigation and capacity factor.

Tower damping in fore-aft directions by active collective pitch control or individual pitch control has been suggested. Tower damping in sideways direction is suggested by usage of individual pitch control and generator control. The effect of the strategies has to be shown by further refining the system. All four active tower damping strategies are already known in wind energy research. The main problem is the lack of reliable full scale implementations in the field. The consequences for the reliability on the used pitch or generator systems have to be analysed.

## References

- [5-01] Figure made by Nawrotzki; GERB Schwingungsisolierungen GmbH
- [5-02] INN WIND.EU Design report – Reference Jacket, “InnWind\_DesignReport\_ReferenceJacket\_Rev00.docx”, Internal teamsite, uploaded 2014-01-16, accessed 2015-08-21
- [5-03] Müller, G.; Groth, C., “FEM für Praktiker – Band1: Grundlagen“, ISBN: 978-3-8169-2685-6, expert verlag, 1993, Renningen.
- [5-04] Ewins, D. J.: “Modal testing: Theory and practice“, ISBN: 0-86380-218-4, Research Studies Press, 2000, Baldock and England
- [5-05] INN WIND.EU Deliverable D4.1.2 – Innovations on component level (interim report), “2014-08-29\_InnwindEU\_D412\_rev03\_tvb\_RN.docx” Internal teamsite, Version 2014-08-29, accessed 2015-08-21
- [5-06] [http://www.gerb.com/de/ueber\\_uns/forschung\\_entwicklung.php](http://www.gerb.com/de/ueber_uns/forschung_entwicklung.php)
- [5-07] Stock, F.; Kammerer, H.: “Nichtlineare Tilger“, Hannover, Berlin: Universitätsbibliothek u. Technische Informationsbibliothek; GERB Schwingungsisolierungen GmbH Co.KG (2001).
- [5-08] INN WIND.EU Deliverable D4.1.1 – State of the art on component level, “DeliverableD411\_20131031.pdf”, Internal teamsite, accessed 2015-09-08

- [5-09] INNWIND.EU Deliverable D4.1.2 – Innovations on component level (interim report), “DeliverableD412\_20150831\_final\_Rev01.pdf”, internal teamsite, accessed 2015-09-08
- [5-010] INNWIND.EU Deliverable D4.3.2 – Innovative Concepts for Bottom-Mounted Structures, “DeliverableD432\_Innovate Concepts for bottom fixed\_final.pdf”, internal teamsite, accessed 2015-09-08
- [5-011] Kuhnle, B., Kühn, M.: “Strukturelle Dämpfer – Ein alter Hut oder Innovation für große Windenergieanlagen?“, 6.VDI-Fachtagung Schwingungen in Windenergieanlagen 2015, Bremen, Germany
- [5-012] Kuhnle, B., Kühn, M.: “Unfavourable trends of rotor speed and systems dynamics for very large offshore wind turbines – Analysis of the 10MW INNWIND.EU reference turbine”, EWEA Offshore Conference 2015, Copenhagen, Denmark
- [5-013] UpWind.EU, Design basis – Upwind K13 deep water site, 2010
- [5-014] Fischer, T.: “Mitigation of Aerodynamic and Hydrodynamic Induced Loads of Offshore Wind Turbines”, Dissertation. Shaker Verlag, Aachen, 2012
- [5-015] Dominguez, S., Leithead, W.: “Size related performance limitations on wind turbine control performance,” in ICC 2006: International Control Conference, 2006.
- [5-016] Sønderby, I., Hansen, M. H.: “Open-loop frequency response analysis of a wind turbine using a high-order linear aeroelastic model,” Wind Energy, 2013.
- [5-017] Bossanyi, E. A.: “Wind Turbine Control for Load Reduction,” Wind Energy, Vol. 6(3), pp. 229–244, 2003.
- [5-018] Fischer, B., Shan, M.: “A survey on control methods for the mitigation of tower loads”, Project report, Kassel, 2013.
- [5-019] Fischer, B.: “GUI for Tower Damping Controller Design”, Kassel, 2013.
- [5-020] Burton, T., Sharpe, D., Jenkins, N., and Bossanyi, E.: Wind energy handbook, 2nd ed. Chichester: Wiley, 2011.
- [5-021] Siegfriedsen, S.: "Method for operating offshore wind turbine plants based on the frequency of their towers" US 6891280 B2. 2001.
- [5-022] Schaak, P., Corten, G.P. and van der Hooft, E.L.: “Crossing resonance rotor speeds of wind turbines,” in EWEC 2003, Madrid, 2003.
- [5-023] Fischer, T. and de Vries, W.: “Final Report Taks 4.1: Integration of support structure and wind turbine design: Deliverable D 4.1.5 (WP4: Offshore Foundations and Support Structures),” 2011.
- [5-024] Leithead, W.E., Dominguez, S. and Spruce, C.J.: “Analysis of Tower/Blade interaction in the cancellation of the tower fore-aft mode via control,” in EWEC 2004, London, 2004.
- [5-025] Shan, W. and Shan, M.: “Gain Scheduling Pitch Control Design for Active Tower Damping and 3p Harmonic Reduction,” in EWEA 2013, Proceedings, 2013.
- [5-026] Caselitz, P., Kleinkauf, W., Krüger, T., Petschenka, J., Reichardt, M. and Störzel, K.: “Reduction of fatigue loads on wind energy converters by advanced control methods,” in EWEC 1997: Proceedings of the European Wind Energy Conference, Dublin, 1997, pp. 555–558.
- [5-027] Bossanyi, E.A.: “Individual Blade Pitch Control for Load Reduction,” Wind Energ, vol. 6, no. 2, pp. 119–128, 2003.
- [5-028] Wortmann, S. and Krüger, T.: "Method for operating a wind energy system" W02009/083085 (A1). 2008.
- [5-029] Duckwitz, D. and Geyler, M.: “Active damping of the side-to-side oscillation of the tower,” in DEWEK 2010: 10th German Wind Energy Conference, Bremen, 2010.
- [5-030] Hess, F. and Buchtala, B.: "Method and Device for Preventing a Lateral Oscillation of a Wind Power Installation" US20130209254 A1. 2011.
- [5-031] Shan, M., Jacobsen, J. and Adelt, S.: “Field Testing and Practical Aspects of Load Reducing Pitch Control Systems for a 5 MW Offshore Wind Turbine,” in EWEA 2013, Scientific Proceedings, 2013, pp. 101–105.

- [5-032] Kanev, S. and van Engelen, T.: “Exploring the Limits in Individual Pitch Control,” in EWEC 2009, 2009.
- [5-033] van Engelen, T., van der Hooft, E. and Schaak, P.: “Development of wind turbine control algorithms for industrial use,” in EWEC 2001, Copenhagen, 2001.
- [5-034] Rossetti, M. and Bossanyi, E.: “Damping of tower motions via pitch control – theory and practice,” in EWEC 2004, London, 2004.
- [5-035] Städler, M.: “Controls for Load Reduction,” in DEWEK 2008: 9th German Wind Energy Conference, Bremen, 2008.
- [5-036] Bossanyi, E., Wright, A. and Fleming, P.: “Controller field tests on the NREL CART2 turbine: Upwind Project, Deliverable 5.6.1,” 2010.
- [5-037] Wortmann, S. and Leweke, H.: “REpower Field Test of Active Tower Damping: Upwind Project, Deliverable 5.6.3,” 2011.

## 6 MANUFACTURING (RAW)

The objective of the first part of this chapter is to describe different jacket transition piece concepts and their advantages as well as disadvantages with respect to fabrication costs. Several studies have been performed in order to determine the governing parameters and their influence on the TP's structural behavior as well as on the jacket. In this final report, the concepts have been further developed. The three different TPs have been designed to transfer the loads of the INN WIND.EU 10MW wind turbine to the reference jacket. ULS and FLS analyses are carried out. Finally, cost evaluations are included to compare the different TP designs.

The second part of this chapter refers to a cost optimisation of the jacket fabrication process. Three examples of possible fabrication strategies are presented and evaluated. Furthermore, the share of the four main fabrication cost contributors – namely material, welding, coating and assembly costs - is shown based on an example jacket structure. It is expected that the ongoing process of improving the developed cost evaluation tool can further decrease the fabrication costs of future jacket structures.



## 6.1 Jacket Transition Piece Concepts

### 6.1.1 Introduction

Jacket foundations are characterized by a number of legs, which are stiffed by braces. The Transition Piece (TP) connects the tower with the jacket and transfers the loads from the tower bottom to the jacket. Consequently, TPs are primarily designed to resist the loads and comply with the Operation & Maintenance (O&M) as well as manufacturing requirements. However, it is a challenge to find the best fit for a given project; different TP concepts influence the structural behavior of the Jacket. Furthermore, the secondary steel and O&M requirements must be taken into account.

In order to compare different TP concepts, several studies have been performed for determining governing parameters and their influence on the structural behavior and on other requirements of the jacket. These parameters have been separated into *hard* and *soft* parameters which are characteristic for the respective TP concept, see Figure 6.1-1. Hard parameters have a measureable effect, e.g. the mass of TP, the total length of the welds and the surface area for coating). Soft parameters have no – at least not a straightforward - measurable effect and are often linked to O&M requirements and the level of manufacturing. Potential patent issues might in some cases play a role as well.

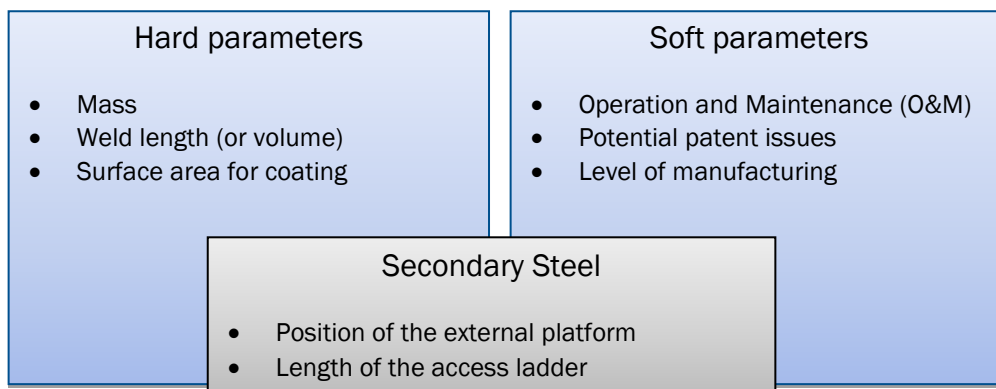


Figure 6.1-1: Identification of different parameters influencing the TP design

In the following, an overview of the most common TP concepts is given followed by a more detailed evaluation of the respective TPs' characteristics. In this evaluation the "box girder model", the "strut model" and the "I-extreme model" will be considered.

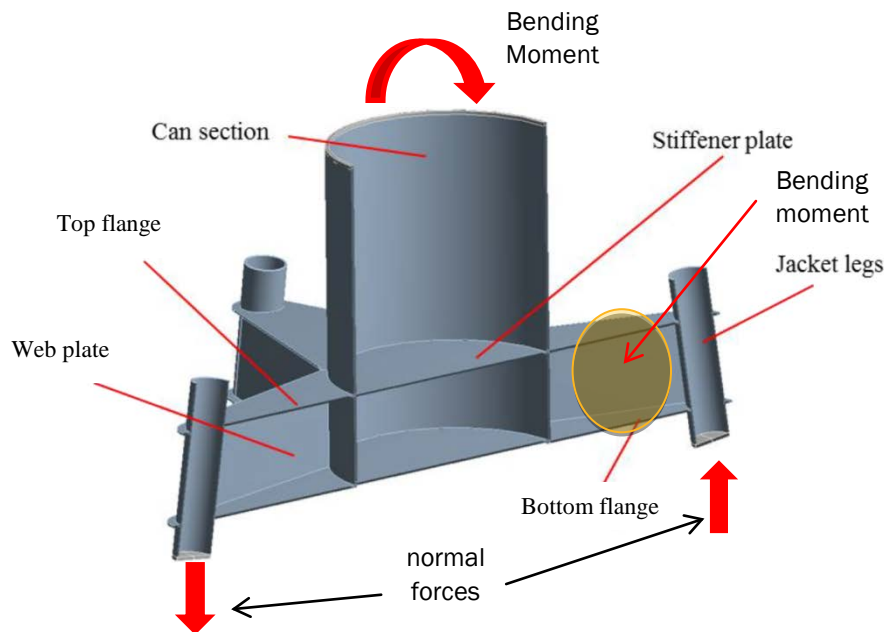
### 6.1.2 Overview

In this section an overview of different TP concepts is given. The most common concepts are the "box girder model", the "strut model" and the "I-extreme model". Each concept can be realized with a considerable amount of variations and subsets. The focus of this evaluation is on the simple concepts, which are described and evaluated in the following.

#### Simple "box girder model"

The simple box girder model relies on horizontal and vertical girders which are connected with the bottom tower section and the jacket legs. The bending moment at the tower bottom is transferred into a pair of axial forces at the upper jacket legs. The connection between the center can section and jacket legs is designed with a box girder consisting of a bottom flange, a top flange and two web plates, see Figure 6.1-2. All connections are welded.

Depending on the height-to-length ratio of the girders, the box girder concept model leads to high bending moments at the girders. This can be regarded as potentially inefficient since the load transfer relies heavily on bending which is the most inefficient way of transferring loads (compared to a load transfer via axial forces).



**Figure 6.1-2: Simple box girder**

The main advantage of the box girder model lies in its O&M characteristics: The external platform is usually placed on the top of the top flange, see Figure 6.1-3; since there are no struts and beams on the top of the external platform, the O&M staff has a larger area for carrying out their work. Furthermore, the crane which is located at the external platform can rotate without constraints.

Regarding the access to the external platform, it has to be considered that the length of the access ladder is determined by the distance measured from the sea level to the external platform. A rest-platform is required if the length of the access ladder exceeds a certain limit. Since the installation of a rest platform raises costs, the positioning of the external platform must be considered thoroughly. Finally, the position and overall concept of the external platform depends on the individual customer's requirements and priorities.

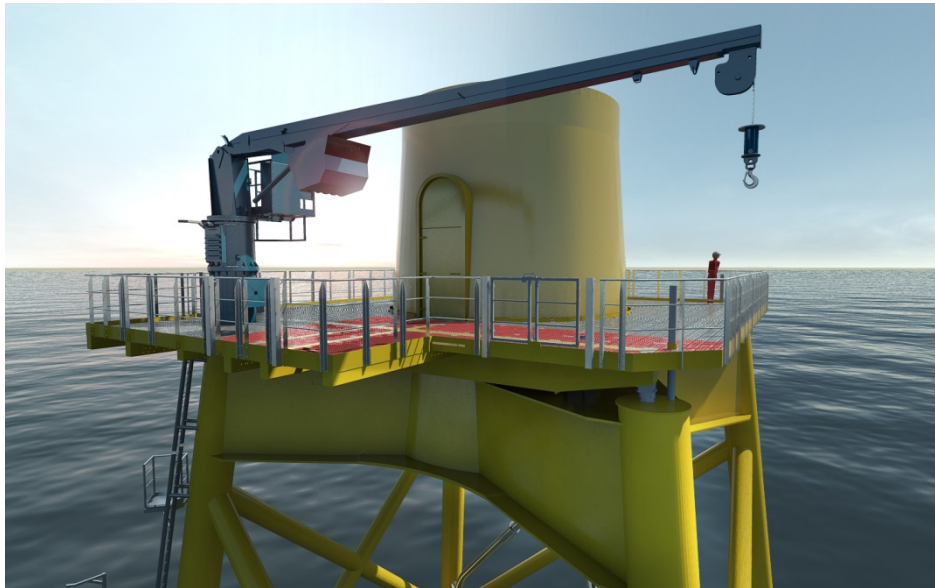


Figure 6.1-3: Box girder model with external platform placed on top of the top girder [Belwind Jacket]

### Simple strut model

The simple strut model consists of horizontal and inclined struts (lower and upper braces), see Figure 6.1-4. The connections to the center can and chords are welded. The connections between the chord and the jacket legs are welded as well. Stiffener plates are usually added at the elevation of the lower braces in order to increase the torsional stiffness of the TP. Ring stiffeners can be introduced at the center can where the upper braces introduce punching shear.

While the overall load transfer of the box girder model is dominated by bending at its girders, the load transfer of the simple strut model is mainly governed by axial loads. Since the load transfer through axial forces is generally more efficient than the load transfer through bending moments, the strut model is expected to yield smaller material costs compared to the box girder model. On the other hand, additional costs may arise due to the stiffener plates and ring stiffeners at the center can.

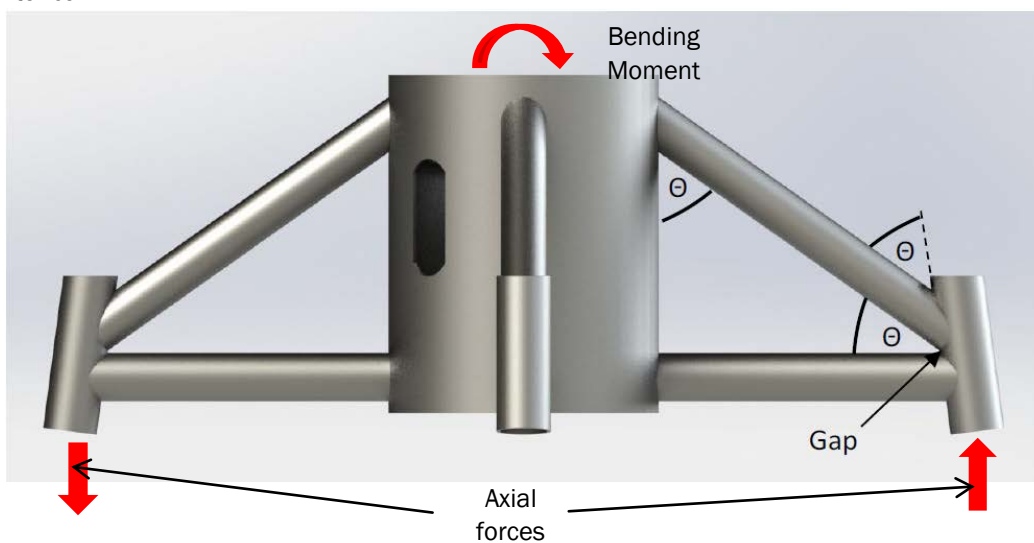


Figure 6.1-4: Simple strut model

There are several options for placing the external platform: One option is offered by positioning the external platform on the top of the chords, see Figure 6.1-5.

In contrast to the box girder model, the strut introduces a major impact on the O&M requirements because there is generally not enough space for a full rotation of the crane due to the presence of the inclined upper braces. Other possible positions of the external platform are on the top of the lower braces and above the ring stiffeners. However, the access distance from the sea level to the external platform should be kept as short as possible in order to avoid additional costs.

Since the connection of the upper brace to the center can must be located above the TP door, there is a minimum angle between the lower brace and upper brace. Consequently, the strut model generally requires a greater height compared to a box girder TP.



**Figure 6.1-5: Simple strut model with external platform to be placed on top of the TP chords [Fife Jacket]**

#### Simple “I-extreme model”

The simple I-extreme model consists of I-cross sections with a horizontal shear plate stiffener at the bottom and an inclined top flange, see Figure 6.1-6. All connections between the steel components are welded. Due to an increase of the girders’ height-to-length ratio the load transfer through the girder relies more on favorable axial forces than on bending, similar to what can be observed for the strut model. Consequently, the I-extreme model offers a solution requiring less steel than the box girder model. Additionally, it is expected that the connection of the girders to the center can is facilitated when compared to the strut model concept.

The external platform is placed on top of the horizontal girder. The position of the external platform could introduce a problem in terms of O&M similar to the strut-model concept because the crane’s rotation might be limited and there is only a small opening inside the I-girder in order to walk around the center can.

By using two web plates instead of only one I-cross section, an extension of the I-extreme model concept is offered (box-extreme). This extension corresponds to a box girder concept with inclined top flanges.

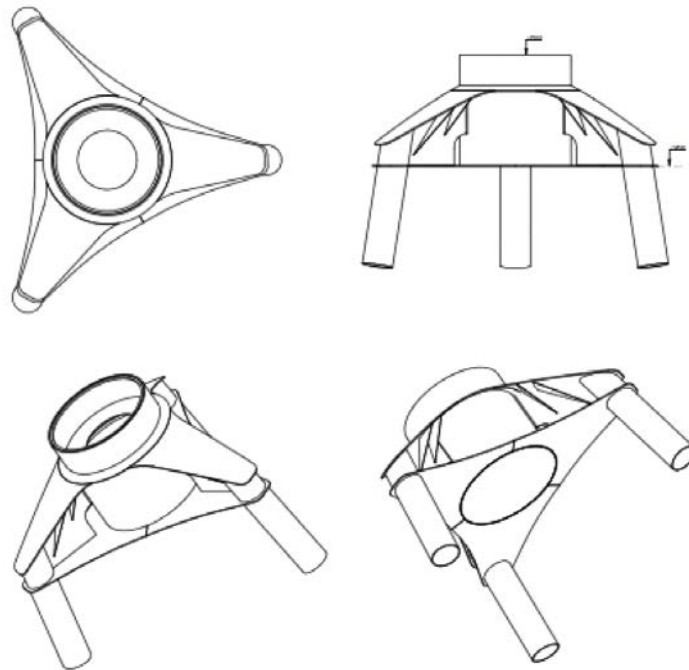


Figure 6.1-6: Simple I-extreme

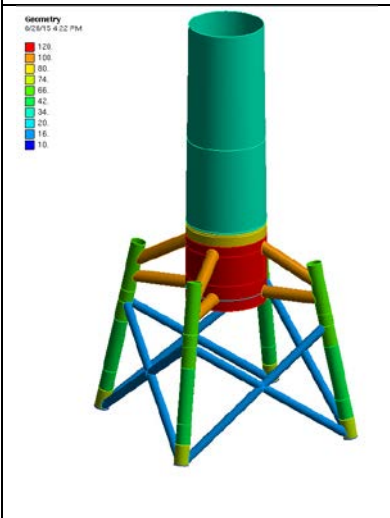
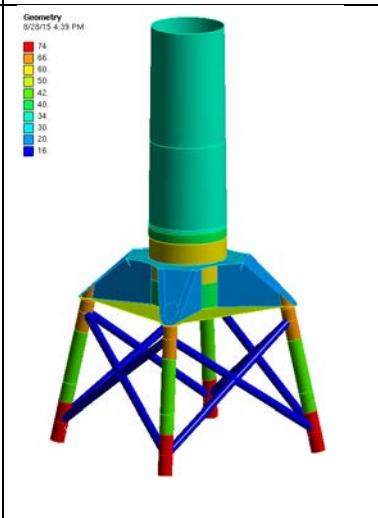
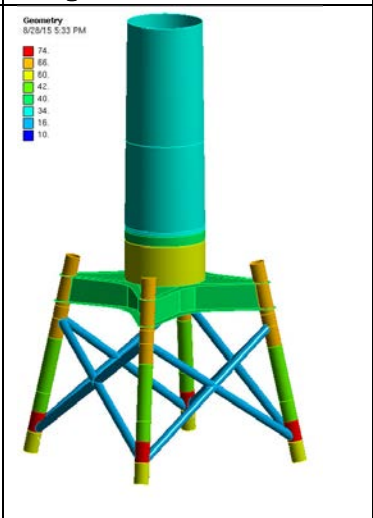


### 6.1.3 Design Study

#### Introduction

In order to evaluate the different TP solutions with respect to primary steel costs, a design study has been performed based on the requirements outlined in the Reference Jacket Design Report, ref. [6-01]. The aim of this study was to find an optimized design for each of the 3 TPs displayed in Table 6.1-1 for a subsequent cost comparison.

**Table 6.1-1 – TPs considered in the design and cost study.**

4-Strut TP	Box-extreme TP	Box-girder TP
		

The main assumptions made in this design study are summarized below:

- Transition to a 4 legged jacket substructure (Reference Jacket)
- Height of all TPs: 7.5 m
- Width of all TPs: 14.0 m (wrt. centerline of legs)
- ULS extreme and FLS damage equivalent loads are applied according to the data provided in the Reference Jacket Design Report, ref [6-01], which have been derived from the INN WIND.EU 10MW reference wind turbine

#### Design Procedure

The objective of this section is to briefly describe the procedures that have been applied in the FE analysis. The finite element discretization used for this analysis is quite detailed and therefore called advanced finite element analysis. The advanced finite element analysis is carried out in ANSYS, including two different analysis types:

- Extreme event analysis of the TP: Two different load cases and two load directions are considered resulting in four individual load cases.
- Fatigue analysis of the TP: One load case and two different load directions have been considered.

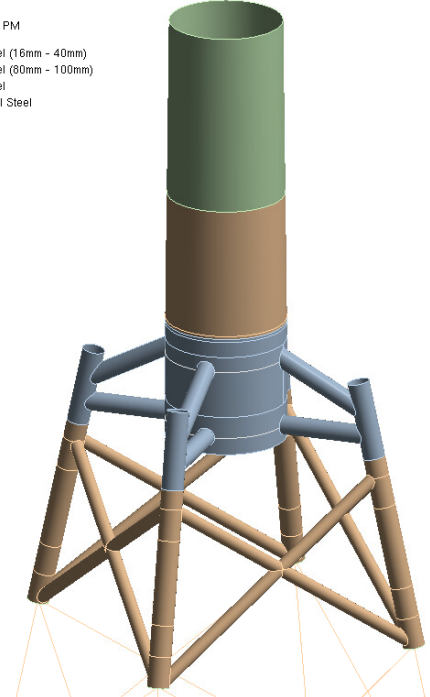
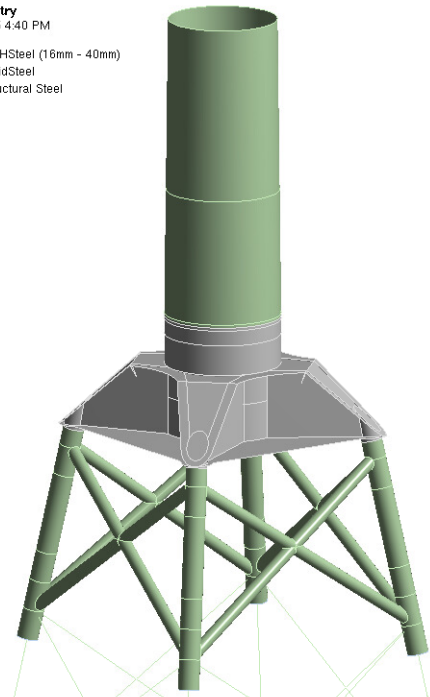
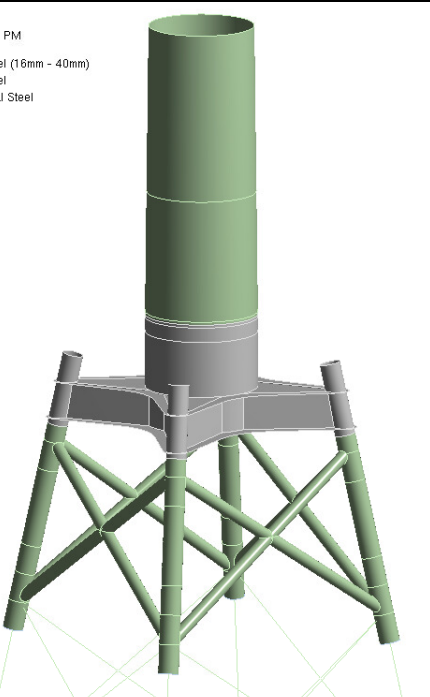

Please note that the load application – especially the damage equivalent FLS loads - performed in this design study is considered a simplified approach as it is only appropriate for conceptual studies. However, this is deemed to be appropriate for the current design phase.

The modeled TP structure, including the upper part of the jacket and the lower tower section, is illustrated in Table 6.1-2. The tower is added to provide a more realistic load distribution from the



tower to the TP. The jacket is added to include the correct boundary conditions. In this design, the tower bottom flange is bolted to the TP flange. Four TP chords are welded on the top of the jacket legs. These connections are modeled fully fixed, which is assumed to represent the most realistic stiffness characteristics.

**Table 6.1-2 – TP structure with tower and jacket (ANSYS model).**

4-Strut TP	Box-extreme TP
<p><b>Geometry</b> 8/28/15 4:23 PM</p> <ul style="list-style-type: none"> <li><span style="display: inline-block; width: 10px; height: 10px; background-color: #cccccc; border: 1px solid black; margin-right: 5px;"></span> MKHSteel (16mm - 40mm)</li> <li><span style="display: inline-block; width: 10px; height: 10px; background-color: #808080; border: 1px solid black; margin-right: 5px;"></span> MKHSteel (80mm - 100mm)</li> <li><span style="display: inline-block; width: 10px; height: 10px; background-color: #90ee90; border: 1px solid black; margin-right: 5px;"></span> RigidSteel</li> <li><span style="display: inline-block; width: 10px; height: 10px; background-color: #d2b48c; border: 1px solid black; margin-right: 5px;"></span> Structural Steel</li> </ul> 	<p><b>Geometry</b> 8/28/15 4:40 PM</p> <ul style="list-style-type: none"> <li><span style="display: inline-block; width: 10px; height: 10px; background-color: #cccccc; border: 1px solid black; margin-right: 5px;"></span> MKHSteel (16mm - 40mm)</li> <li><span style="display: inline-block; width: 10px; height: 10px; background-color: #808080; border: 1px solid black; margin-right: 5px;"></span> RigidSteel</li> <li><span style="display: inline-block; width: 10px; height: 10px; background-color: #90ee90; border: 1px solid black; margin-right: 5px;"></span> Structural Steel</li> </ul> 
<p><b>Box-girder TP</b></p> <p><b>Geometry</b> 8/28/15 5:34 PM</p> <ul style="list-style-type: none"> <li><span style="display: inline-block; width: 10px; height: 10px; background-color: #cccccc; border: 1px solid black; margin-right: 5px;"></span> MKHSteel (16mm - 40mm)</li> <li><span style="display: inline-block; width: 10px; height: 10px; background-color: #808080; border: 1px solid black; margin-right: 5px;"></span> RigidSteel</li> <li><span style="display: inline-block; width: 10px; height: 10px; background-color: #90ee90; border: 1px solid black; margin-right: 5px;"></span> Structural Steel</li> </ul> 	

### Boundary Conditions

In all analyses, the jacket legs are fixed at mudline, in all 6 degrees of freedom. Piles and structural parts below mudline are therefore not considered. Furthermore, appurtenances that are mounted on the jacket and the TP are not modelled. This includes all secondary steel appurtenances like external platform, external ladder boat landing etc. It is assumed that these appurtenances are not influencing the general behavior of the structure significantly. The fixed support at mudline is shown in Figure 6.1-7.

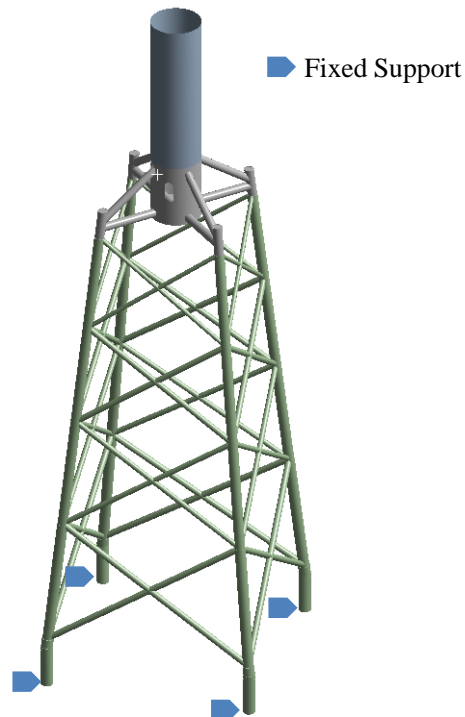


Figure 6.1-7: Jacket fixed support (ANSYS model).

### Load Description for the Advanced Finite Element Analysis of the TP

In order to reduce the load boundary effect, all loads are transferred to the rigid top of the tower. For each load case there is a combined shear force and an axial force applied. In addition to the forces, a combined bending moment and torsion are applied. For each load case two load time steps are considered. The first step contains the combined moment and shear force, acting in an angle of  $45^\circ$  to the axis of horizontal braces, whereas in the second step a degree of  $0^\circ$  is applied. The torsion and axial force are constant in step one and two, see Figure 6.1-8 and Figure 6.1-9.

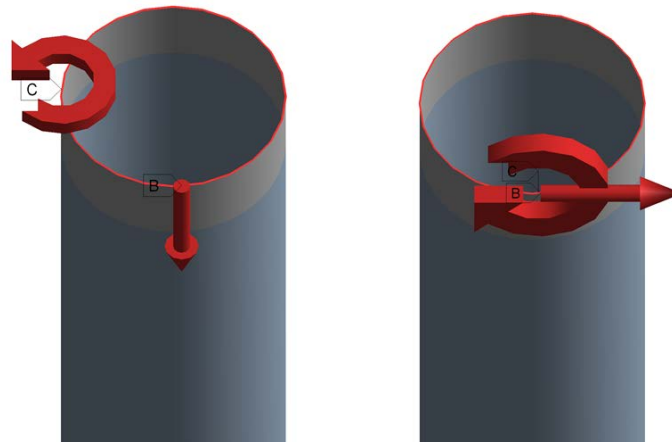


Figure 6.1-8: Applied moments and forces on rigid tower segment (ANSYS model).

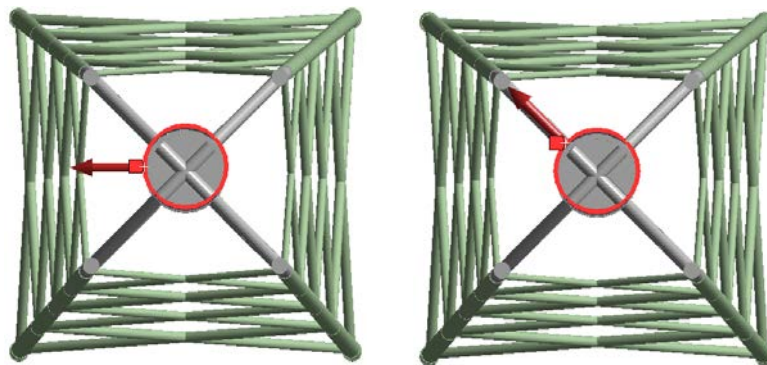


Figure 6.1-9: shear force in load step one (left) and load step two (right) (ANSYS model).

### Discretization

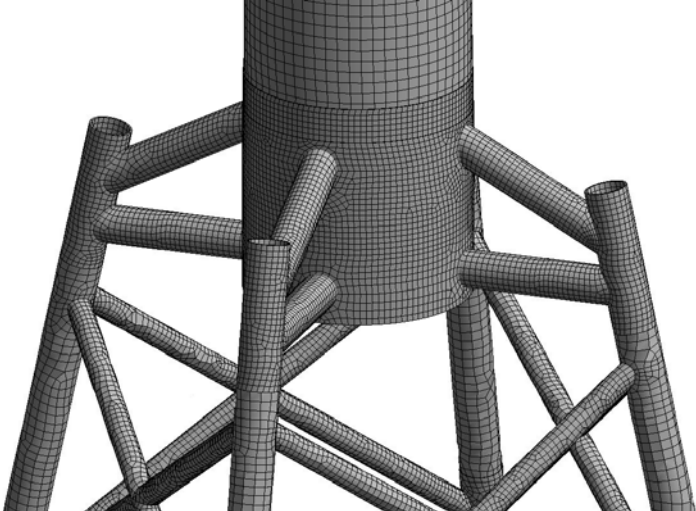
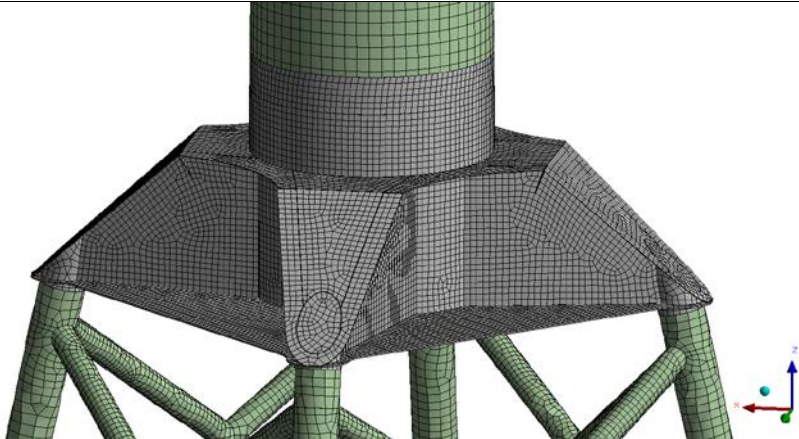
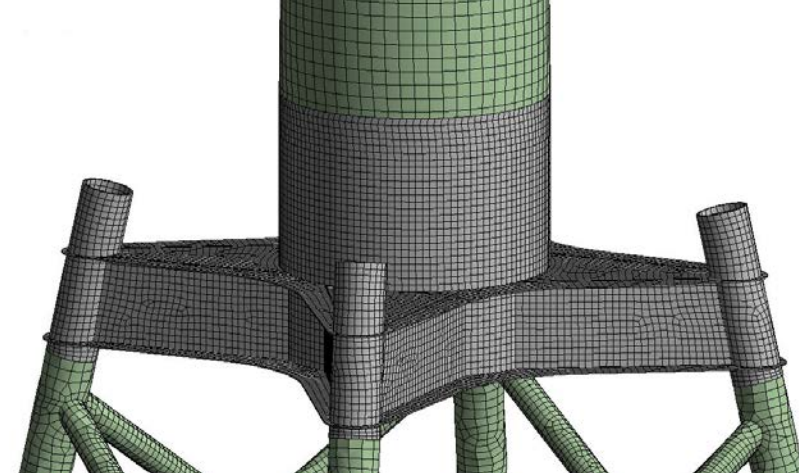
The finite element analyses for this thesis are performed in ANSYS 14.5. The elements used in the calculations are SHELL181 elements and BEAM188 elements. The SHELL181 element is a four-node element with six degrees of freedom (DOF) at each node. The beam element BEAM188 is a two-node element with six degrees of freedom at each node.



Figure 6.1-10: ANSYS elements, BEAM188 (left) SHELL181 (right).

The jacket is modelled completely using beam elements. For the model of the tower and the TP, SHELL elements have been used. The mesh for the tower is automatically generated. The TP has been refined in order to enhance the accuracy. The elements are sized using an element size of approximately 50 mm. A total of about 85000 nodes have been used. The mesh on the TPs is shown in Table 6.1-3.

Table 6.1-3 – Mesh on the TP (ANSYS model).

<p>Detailed Mesh 4 Strut TP Model</p> 
<p>Detailed Mesh Box-extreme TP Model</p> 
<p>Detailed Mesh Box-girder TP Model</p> 

### Material Properties

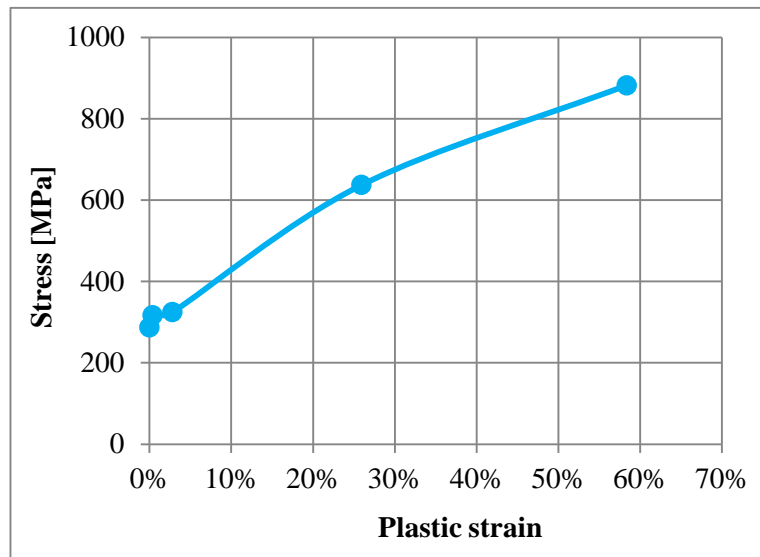
For the advanced finite element simulation, three different material properties have been implemented (see Table 6.1-4). For fatigue analyses the jacket, tower and TP are modelled mainly using linear material properties, in the following named as structural steel. The tower top is modelled with rigid steel, to avoid excessive ovalization and to enable a homogeneous load distribution. For the extreme event analyses, the jacket and the tower are modelled with structural steel. The TP structure is modelled using non-linear steel properties MKH S355, in order to calculate the plastic strain at local hot spots (see Table 6.1-5).

**Table 6.1-4: Material properties used for ULS and FLS calculations.**

Material name	Young's modulus (GPa)	Poisson ratio
Structural Steel	210	0,3
Rigid Material	210000	0,3
MKH S355 steel	210	0,3

**Table 6.1-5: Multi-linear kinematic hardening properties for S355 steel (63 mm to 100 mm plate thickness).**

Plastic strain	Stress (MPa)
0	286,75
0,003977	316,73
0,02801	324,45
0,25933	637,00
0,58359	882,00



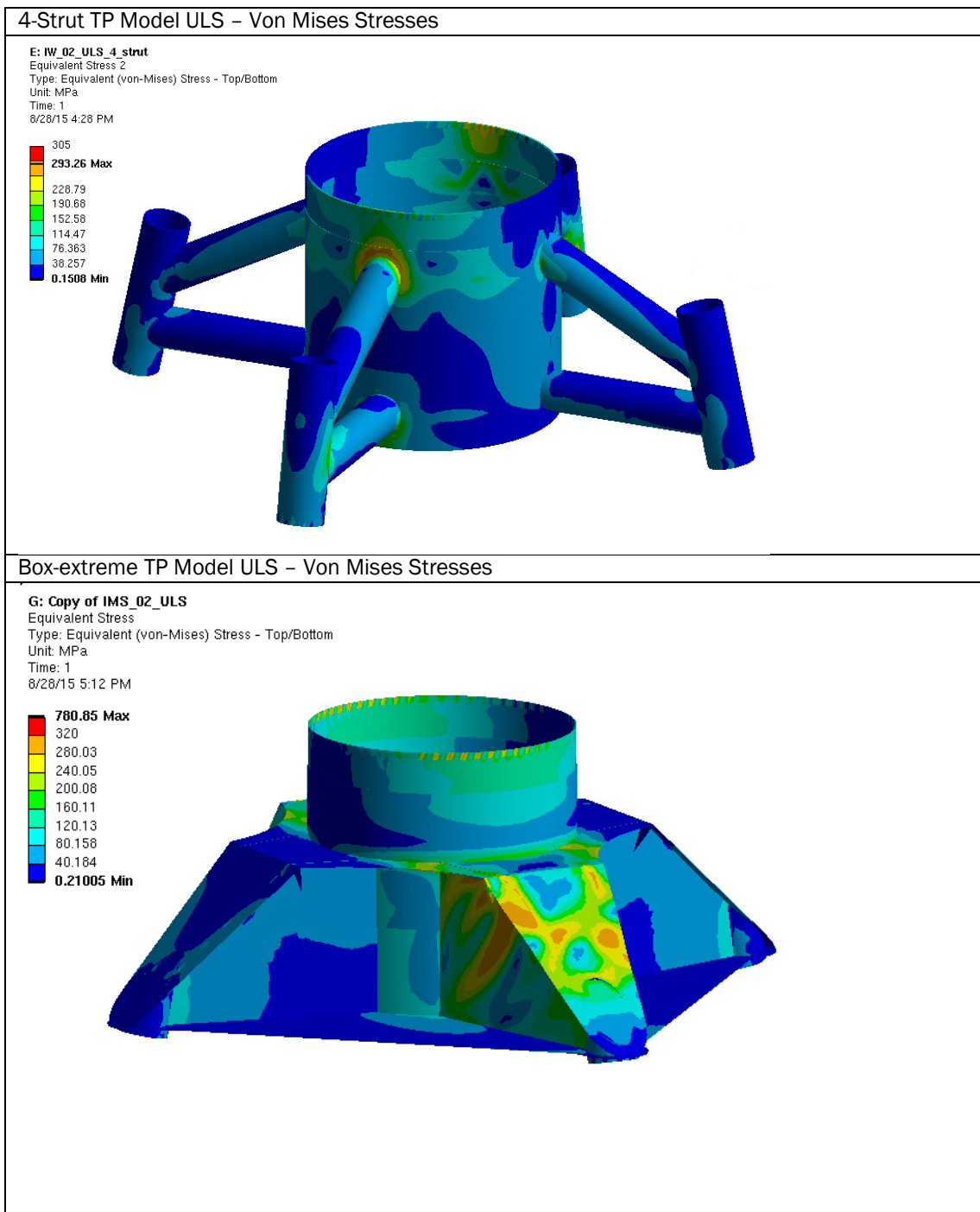


### Results of the TP Design Study

This section briefly summarizes the results derived from the TP design study. All TPs are optimized and designed in order to withstand the ULS and FLS loads.

Table 6.1-6 shows that the equivalent von Mises stresses of the ULS analyses do not exceed the yield strength or that the plastic strain is quite small.

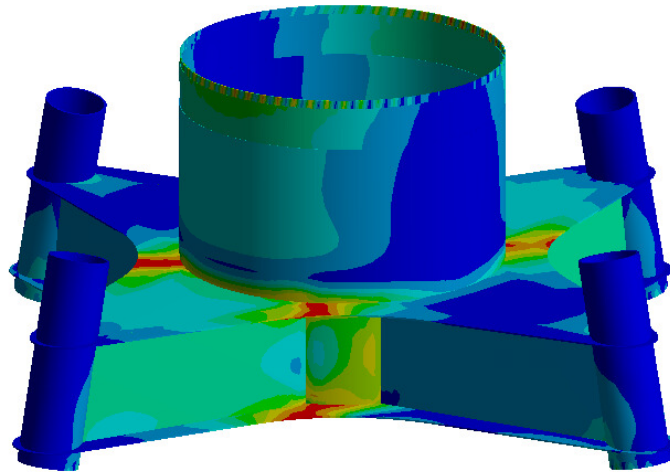
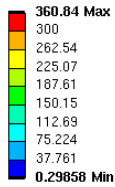
**Table 6.1-6: Von-Mises stresses induced by ULS loads.**





### Box Girder TP Model ULS – Von Mises Stresses

**B: ULS BG\_01**  
 Equivalent Stress  
 Type: Equivalent (von-Mises) Stress - Top/Bottom  
 Unit: MPa  
 Time: 1  
 8/28/15 5:39 PM

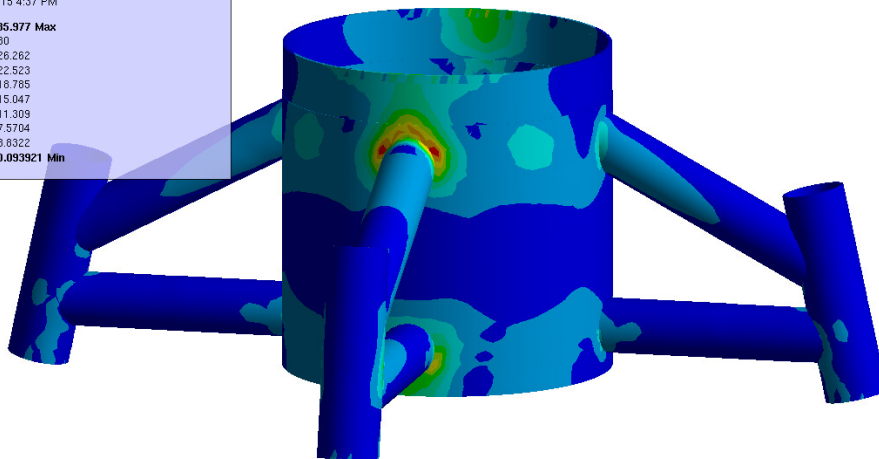
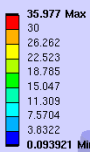


The FLS results are calculated based on damage equivalent loads. In order to withstand the FLS loads, the stresses are not allowed to exceed a von Mises stress limit of 30 MPa at the welds. It can be seen in Table 6.1-7 that only at a small number of welds exceeds the stress limit. In any case, this issue could be solved by individual stiffeners, which is beyond the scope of the present study. Furthermore, the maximum von Mises stresses appear due to singularity effects at hot spot regions. In the course of more detailed analyses it could be shown that these peaks will not occur.

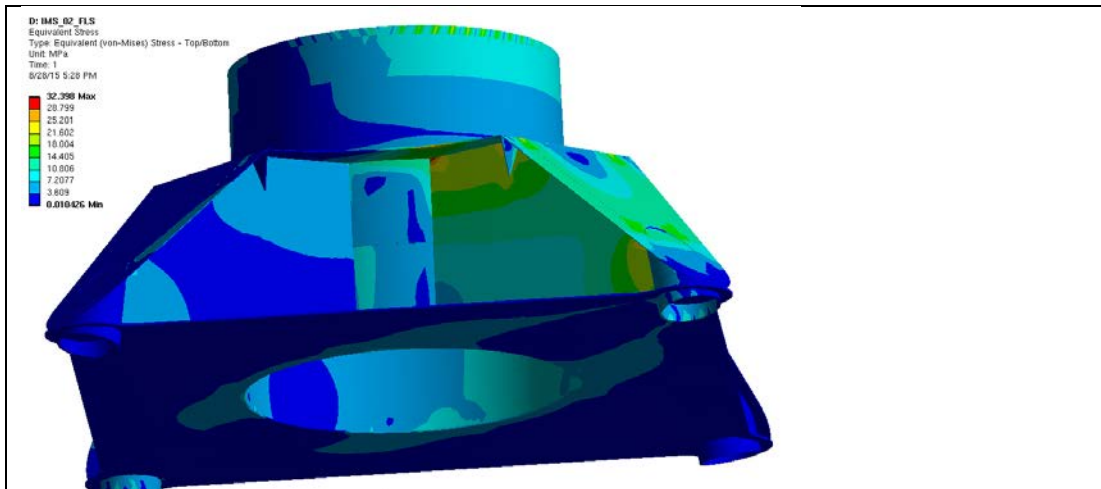
**Table 6.1-7: Von-Mises stresses induced by FLS loads.**

### 4 Strut TP – FLS results – Von Mises Stresses.

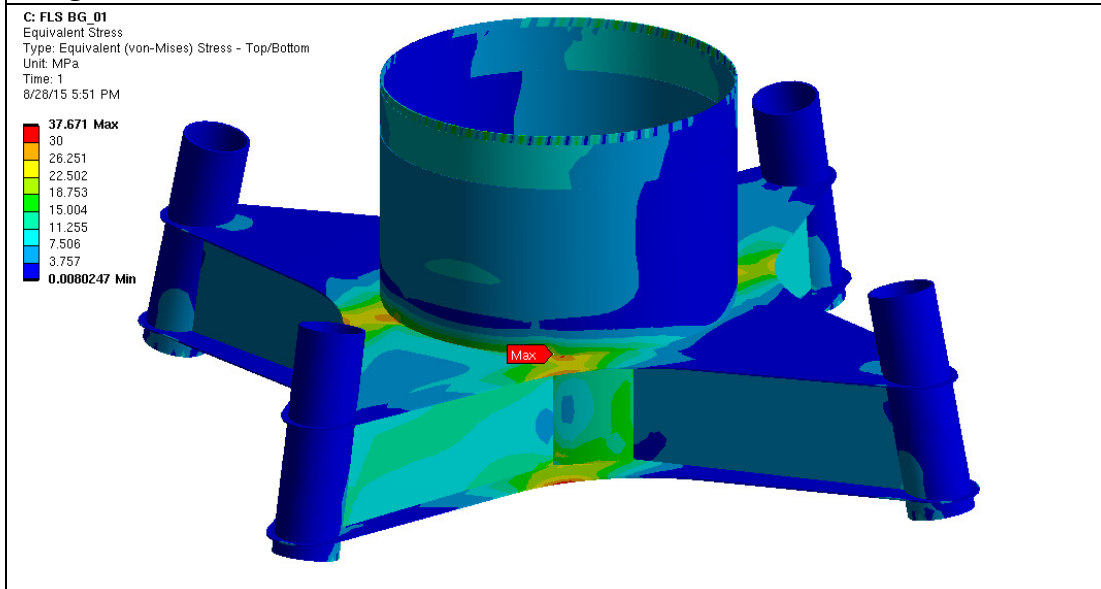
**C: IW\_01\_FLS\_4\_strut**  
 Equivalent Stress 2  
 Type: Equivalent (von-Mises) Stress - Top/Bottom  
 Unit: MPa  
 Time: 1  
 8/28/15 4:37 PM



### Inclined TP – FLS results – Von Mises Stresses.



Box girder TP – FLS results – Von Mises Stresses.



The final properties – mass and welding volume - governing the cost evaluation of the TPs are summarized in Table 6.1-8, Table 6.1-9 and Table 6.1-10. The main conclusion to be drawn from these results is the fact that the 4-strut TP yields a significantly larger mass as well as welding volume. The box girder TP and the box-extreme TP show similar results with respect to mass and welding volume.

It should be noted that the most pronounced drawback inherent in the 4-strut model TP is seen in the fact that the inclined pipes are causing a severe “punch-through” effect at the center can (see stresses displayed in Table 6.1-6Table 6.1-7), This effect needs to be counteracted by strengthening the center can by increasing its wall thickness and introducing a large number of internal ring stiffeners. Both actions significantly increase both the mass as well as the welding volume of the TP.

A more refined version of the 4-strut TP is shown in the OWEC design, used for the Alpha Ventus jackets, where special attention is given to the load transfer between inclined pipes and center can. However, this design has been patented and therefore not evaluated in the course of this study.

**Table 6.1-8: Resulting TP properties – Box-extreme TP**

Item Description	Geometry	Wall thickness [mm]	Mass [ton]	Welding Volume [cm <sup>3</sup> ]
TP-Tower Flange	Plate	34	1.284	19955.55
Can Section 1	Plate	40	7.552	37675.98
Can section 2	Plate	60	45.318	37675.98
Can Section 3	Plate	40	18.887	50319.78
Horizontal Plate 1	Plate	30	11.941	21582.64
Horizontal Plate 1 – fabrication cut				2164.62
Horizontal Plate 2	Plate	50	72.747	37188.16
Inclined Web Plate	Plate	20	11.657	5988.85
Web Plate	Plate	20	27.946	74481.12
Jacket Leg Extension	Pipe	66	13.164	82102.83
			<b>210.496</b>	<b>369135.00</b>

**Table 6.1-9: Resulting TP properties – Box girder TP**

Item Description	Geometry	Wall thickness [mm]	Mass [ton]	Welding Volume [cm <sup>3</sup> ]
TP-Tower Flange	Plate	34	1.284	19955.54
Can Section 1	Plate	40	7.551	37675.97
Can section 2	Plate	60	45.318	37675.97
Can Section 3	Plate	40	18.887	34516.34
Horizontal Plate 1	Plate	40	29.037	34516.34
Horizontal Plate 2	Plate	40	31.321	0.00
Web Plate	Plate	40	37.328	194163.01
Jacket Leg Extension	Pipe	66	46.569	51017.67
			<b>217.297</b>	<b>409521.00</b>

**Table 6.1-10: Resulting TP properties – 4-strut TP**

Item Description	Geometry	Wall thickness [mm]	Mass [ton]	Welding Volume [cm <sup>3</sup> ]
TP-Tower Flange	Plate	80	3.021	60558.18
Can Section 1	Plate	80	15.103	121807.91
Can section 2	Plate	120	90.643	121807.91
Can Section 3	Plate	120	56.674	0.00
Internal Ring Stiffener	Plate	70	8.556	85813.59
Internal Plate Stiffener	Plate	70	7.217	90535.89
Inclined Brace	Pipe	100	64.577	115290.52
Horizontal Brace	Pipe	100	61.892	108126.03
Jacket Leg Extension	Pipe	66	45.530	251673.64
			<b>353.217</b>	<b>955614.00</b>

### 6.1.4 Cost Evaluation of TPs

Based on the results derived from the TP design study outlined in section 6.1.3 a primary steel cost comparison is performed. It should be noted that the cost comparison only considers the material costs for the steel pipes or plates as well as the welding costs. Any further costs, e.g. coating, secondary steel items or equipment are not considered. However, since the primary steel is governing the overall TP costs, this is deemed a sufficient approach in order to evaluate the cost differences of the three TP solutions.

The material costs are calculated based on internally available (however confidential) unit values [€/ton] depending on the wall thickness of each item. For the welding costs a constant unit value [€/cm<sup>3</sup>] has been applied based on Ramboll's internal data base.

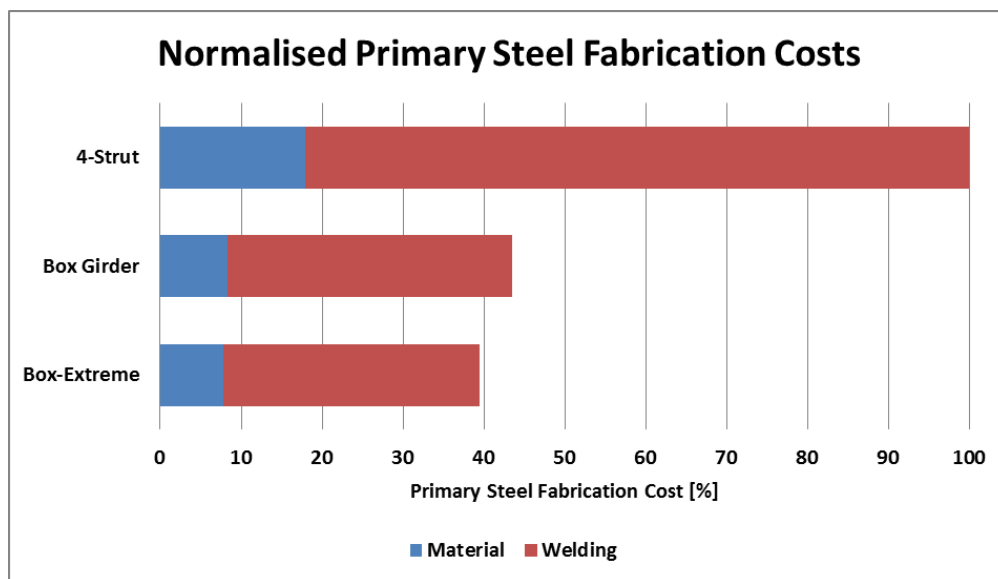


Figure 6.1-11: Normalized primary steel fabrication costs.

### 6.1.5 Current TRL of Innovations and Recommendations for their further Development

The Technical Readiness Level (TRL) can be judged to be at level 9 since the TP innovation is based on typology variations only: TPs similar to the box girder and the strut model have already been fabricated and successfully installed (see *Fife Jacket* and *Belwind Jacket*). TPs similar to the box-extreme are currently being fabricated (*Wikingen Jacket*) and are based on the same analytical and fabrication principles.

### 6.1.6 Conclusion

The transition piece (TP) is an important part of the substructure design connecting the tower to the jacket. This evaluation considers three different TP concepts, namely the box girder model, the strut model and the box-extreme model. The focus of this evaluation is on the advantages and disadvantages of each TP solution with respect to primary steel design. All three models have been optimized based on preliminary loads and assumptions outlined in the Reference Jacket Design Report, ref [6-01].

The box girder shows the most flexible option for placing the external platform. Especially the surface area of the external platform and the crane range are important factors in this respect. It should be noted, that the optimization of secondary steel arrangement is also driven by the O&M

strategies as well as requirements set forth by the wind farm owner and supersedes the optimal primary steel design as the governing premise.

The box girder and the box-extreme solution show an efficient load transfer which avoids pronounced hot spot stresses. Due to the large  $D/t$  ratio of the center can, the center can of the 4-strut TP is prone to severe ovalization caused by the punch-through effect of the inclined pipe connected to the center can. From the designer's perspective, this effect is supposed to be counteracted by increasing the center can's wall thickness, implementation of conical struts as well as by introducing a large number of internal ring stiffeners which minimize ovalization. Consequently, these actions significantly increase both the mass as well as the welding volume of the 4-strut TP.

Based on the evaluated mass and welding volume determined for each TP, a cost estimation has been performed in order to indicate the cost differences of the 3 TP solutions. In terms of primary steel fabrication cost, a more cost efficient TP design can be expected when using a box girder or a box-extreme TP. Both box girder as well as box extreme TP indicate similar costs while the 4-strut yields significantly higher costs. This is mainly due to the punch-through effect caused by the inclined brace connected to the large center can.

Synergies with other innovations discussed in this work-package are identified with respect to *innovative materials*, see chapter 3. In order to reduce TP costs, sandwich materials could offer a cost-saving solution.

## 6.2 Jacket Assembly Concepts and Cost Optimization

The optimization of jacket structures aims at a cost reduction. Three of the main cost contributors for jacket costs are fabrication, installation and transportation. The focus of this section lies on the fabrication costs. The fabrication costs consist of welding costs, material costs, assembly costs and coating costs. The goal is to minimize the fabrication costs by varying the geometry parameters of the jacket and to find the least expensive assembly strategy.

### 6.2.1 Fabrication Cost Model

This fabrication cost model includes the main cost contributors welding costs, material costs, assembly costs and coating costs. Each of the cost contributors has an influential parameter. The influential parameters are depended on geometrical parameters. Hence, it is possible to optimize the jacket by varying its geometrical parameters. An overview of the cost model set-up is shown in Figure 6.2-1.

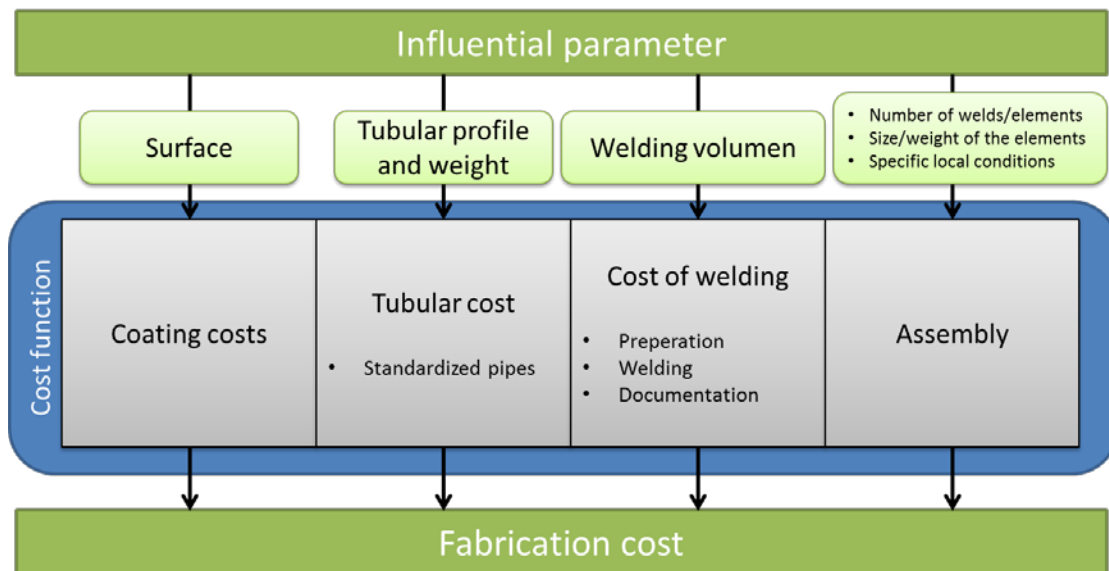


Figure 6.2-1: Structure of the fabrication cost model

#### Costs of tubular members

The costs for tubular members consist of their material and processing costs. Different tubular cross-sections cause different processing costs due to different manufacturing processes, e.g. due to standardize or individual manufacturing. Consequently, each tubular cross-section has a specific cost factor depending on its dimension and manufacturing characteristics. Hence, the tubular cost of each pipe is the product of its weight and a specific cost factor.

#### Coating costs

Coating is for protection from corrosion and depends on the surface area of the jacket. Coating cost is the smallest share of the fabrication costs and remains virtually unchanged by varying the geometrical parameters.

#### Cost of welding

Cost of welding includes the preparation of the welds, the welding, the documentation and the man hours. This cost depends on the welding volume and the welding process. A special distinction must be made between manual and automated welding. Automated welding is less expensive than manual welding, but not every weld can be performed by automated welding. The costs of welding are generally of the same order as the costs for the tubular members. In order to



quantify the welding costs, cost factors are introduced which are multiplied by the volume of the respective weld.

#### **Assembly costs**

Special attention must be paid to the assembly costs. Assembly costs mainly depend on the number of tubular members to be welded. Furthermore there are dependences on the specific local conditions (e.g. size of the assembly hall, location of the assembly hall). The calculation of this cost – which is only indicative - is based on the fabricator's experience.

#### **Assembly strategies**

Assembly strategy describes the assembling in terms of what types of welds are used, the geographical location of assembly and the possibility of pre-assembled elements.

Currently, the construction of jacket structures aims at a weight reduction. Hence, the cross sections of the tubes are as small as possible and thickness transitions are made at tubular joints where utilizations are typically highest. This leads to a lot of different tubular cross-sections and a high number of welds. This assembly strategy is named version A and its main advantage is to be found in the reduction of material costs. Its main drawback can be seen in the fact that the welding and assembly costs are relatively high.

An alternative assembly strategy aims at reducing the number of welds by using the same cross-sections along the whole jacket brace and/or leg. Hence, the mass of the jacket increases while the number of tubular members and the number of welds are decreased.

### **6.2.2 Assembly Concepts**

This section describes three examples of possible assembly strategies. Furthermore, the share of the four fabrication cost contributors – namely material, welding, coating and assembly costs - is shown based on an example jacket structure.

#### **Version A**

Version A is the classical solution and is aiming at a mass reduction of the jacket. Since the design of jackets is mainly governed by the hot spot stresses at the tubular joints, wall thicknesses of chord cans and brace stubs typically require the highest values. In order to reduce the mass of the structure, the adjoining jacket braces and leg members show reduced wall thicknesses. Consequently, this requires intensive welding effort in order to facilitate this high number of thickness transitions and leads to a high number of members which need to be assembled. Typically, all welds are performed manually at the fabricator's site. Figure 6.2-2 shows 3 different assembly strategies; red pipes indicate a larger wall thickness compared to green pipes.

#### **Version B**

The goal of version B is to reduce the number of welds and the number of tubular members in order to reduce assembly costs. On the other hand, the mass of the jacket increases due to the large wall thicknesses used for the entire members. All welds of the jacket are assumed to be welded manually at the fabricator's site.

#### **Version C**

Version C is designed in a similar manner as version A. The difference is that the tubular joints are assumed to be prefabricated by the manufacturer who is using automated welding techniques which reduces costs compared to manual welding. The other connections between the tubular members are assumed to be manually welded by the fabricator. Table 1 shows the share of each of the fabrication cost contributors.

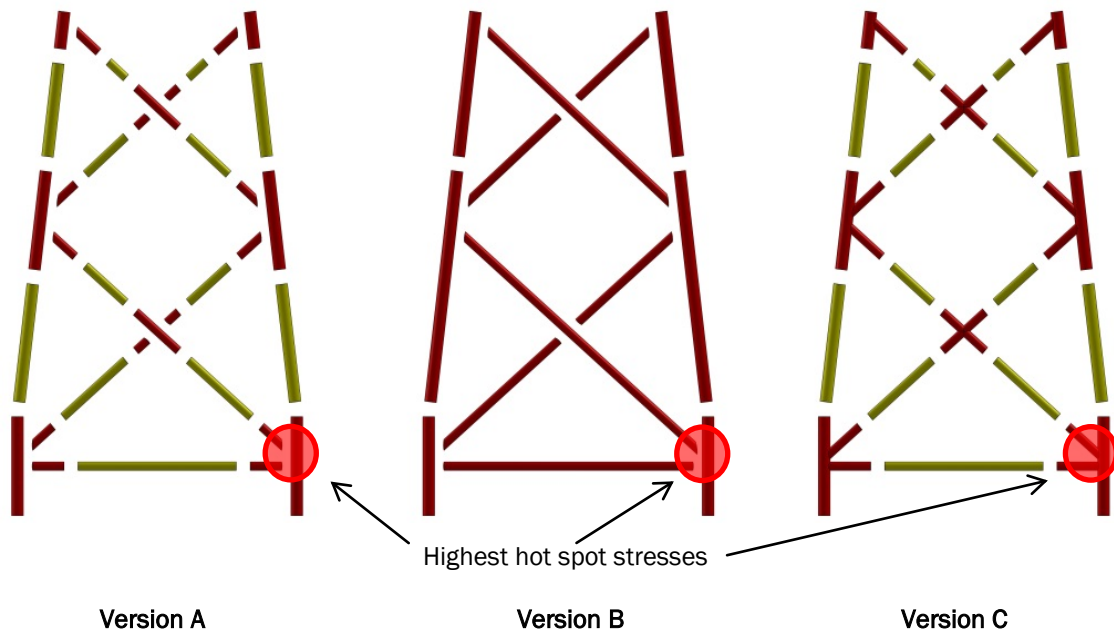


Figure 6.2-2: Three different assembly strategies.

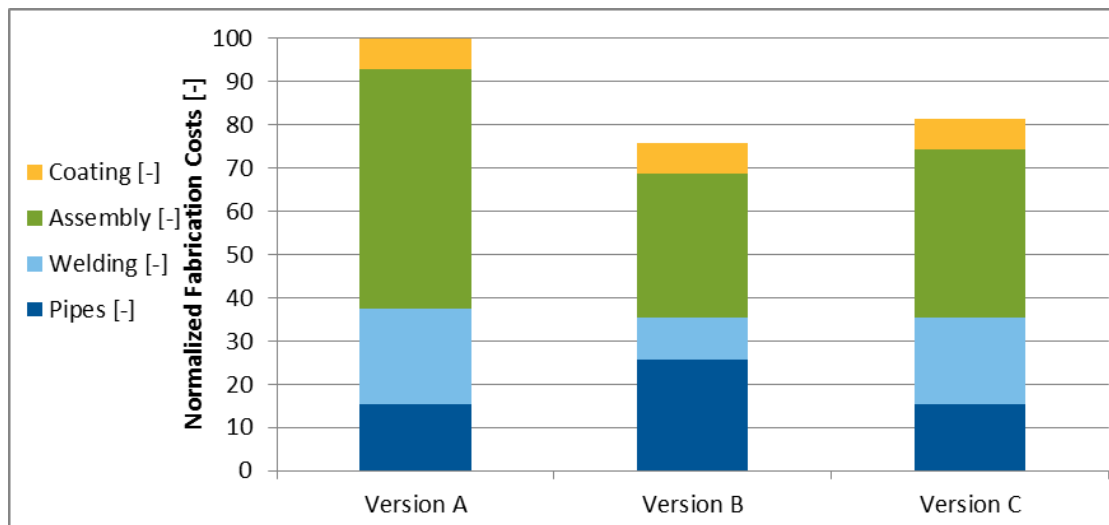


Figure 6.2-3: Fabrication cost distribution caused by different assembly strategies

### 6.2.3 Contribution to Cost Reduction

As shown in Figure 6.2-3, a cost reduction of approximately 20% is expected if more sophisticated assembly strategies are considered. This includes assembly strategies which focus on a reduction of welds as well as automated welding procedures.

It should be noted that the results presented here are based on the current status of Ramboll's cost model tool. Further refinements might be available throughout the next phase.

#### 6.2.4 Technical Readiness Level

The Technical Readiness Level (TRL) of the discussed innovation is considered to be at level 9 since the innovation is mainly based on available technologies which are used for the assembly process. The innovation discussed here is mainly based on the identification of fabrication cost drivers and on transferring the conclusions to the design process.

#### 6.2.5 Conclusions

Fabrication costs are mainly composed of material, welding, assembly and coating costs. The objective of this project is to detect the share of each of these cost drivers by setting up a cost model which enables the designer to find the most cost efficient solution.

From the findings gathered so far, the coating costs seem to be the smallest share of the fabrication costs. Therefore, the main focus of the fabrication cost minimization is on the material costs, the welding costs and assembly costs. A mass reduction of the jacket does not necessarily lead to a cost optimization since a mass reduction also implies a large number of different cross-sections to be welded. This will raise assembly and welding costs.

In general, it is not possible to minimize all of the cost contributors by choosing one assembly strategy. Chapter 6.2.2 shows the result of the fabrication costs for different assembly strategies. The result shows that the reduction of the number of tubular members and welds (version B) is the less expensive strategy, although this raises the structural mass of the jacket. A further investigation of version B shall clarify how the fatigue behaviour – especially of the braces – is influenced by the increased mass of the tubular members. This might lead to a slightly higher mass than the value shown in Figure 6.2 3.

Synergies with other innovations discussed in this work-package are identified with respect to innovative materials, see chapter 3. In order to reduce jacket costs, sandwich materials could offer a cost-saving solution.

#### References

- [6-01] Borstel, T.v., INN WIND.EU Deliverable D4.31, “Design report – Reference Jacket”, Revision 1, 2015

## 7 CONCLUSIONS

In this concluding chapter the main finding on different innovative components presented in this report have been recapitulated. In addition, in Table 7.1 a approximated estimations of the cost reduction potential of each innovation have been summed up. The table is based on Dutch national funding scheme proposals 'TKI-WoZ' (Topconsortium knowledge and innovation Wind at Sea).

As already shown in the Deliverable 4.12 [3-02] and the first part of Chapter 4.1 of the present report, models/approaches describing the load bearing behaviour of sandwich structures already exist. However, they do not consider any load combinations. Namely, jacket as a substructure of an OWEC is characterized by special loading situations. Due to restraint moments a combination of moment and normal force appears in the brace and chord components. A model representing the bearing capacity of sandwich components under this specific load situation has not been established so far. As part of the project Innwind.eu such a model is investigated. To achieve this model, a test plan has been created and specimens of sandwich components are tested statically under eccentric compressive load [3-05]. Using selected experimental tests accompanied by numerical investigations the structural behaviour of sandwich components under eccentric compressive load is described and an interaction N-M diagram has been established. Further studies with modified geometric cross-sectional configurations and different core materials should be carried out in order to exploit the advantages from lower steel sheet thicknesses of sandwich components as much as possible. The current TRL of the sandwich tubes shall be set at level 3. The cost saving aspects for sandwich tubes shows a substantial potential regarding the necessary steel tubes with respect to the standard steel jacket with the savings up to 50 % of the manufacturing time. The impact of the filling in of the sandwich components with core material on the overall cost of the sandwich tubes is difficult to estimate as there are no industrial scale productions of such elements. A rough estimation can be made by assuming that this process would require an additional 25 % of the overall manufacturing time. The potential of bonding as a joining technique for tubular steel structures was evaluated in Subchapter 3.2. The results of the experiments described in Deliverable 4.12 [3-02] and Deliverable 4.14 [3-05] indicate that bonding could be a viable joining technique but a large effort in the development of the bonding process and to select the adequate bonding paste needs to be done. Further research in the selection of the adhesive is required in order to ensure processability and stability of the mechanical properties. In addition, further research is recommended in relation with the manufacturing process aiming to ensure the stability of the bonding line properties and the surface treatment via automation. In order to improve the adhesive properties and design allowable an adhesive benchmarking tests campaign is recommended for further research, in which static and fatigue properties are evaluated. In a later stage, also the fracture energy density of the adhesive-steel interface will need to be further investigated.

Possible innovative cost-saving solutions for foundation of jackets structures are presented in Chapter 4. In Subchapter 4.1 it has been shown that bucket foundation, although rarely used for wind turbine sub-structures, shows certain advantages with respect to piles for supporting jacket structures. The advantages may be observed in the installation phase where noise during the installation is reduced to zero as well as in the decomposition of these kinds of foundation, which can potentially be fully decommissioned. In the contribution it is highlighted that the cost down potential is 15 -20 % if using a suction bucket jacket compared with a standard jacket with piles. The main issue is the adaptation of the bucket foundations for the peculiar load configurations of the offshore wind turbine systems. Some advancement in this regard is illustrated in the contribution where an experimental campaign is presented and experimental data is interpreted. Cyclic loading tests are however still missing and must be carried out to complete the experimental campaign. The second contribution (Subchapter 4.2) concerns piled foundations. The suggested innovation of this part is vibro-driven piles which could be used instead of the traditional impact-driven piles. In the report a large-scale test of a pile under tensile monotonic loading is interpreted by means of analytical and numerical methods in order to assess the bearing behavior of the foundation. Overall it was demonstrated that vibro-driven piles have lower bearing capacity than impact-driven piles and therefore a lower margin for cost savings than expected. This however must be proved by testing a second pile which is going to be subjected to

pre-loading. Furthermore, the setup effects will be investigated by performing large-scale experiments. Currently the expected cost reduction is between 5% and 10%. The third contribution (Subchapter 4.3) deals with the further development of a semi-floater concept founded on a concrete base. A more mature design is successfully proposed for three components of the semi-floater concept. Their implementation results in a performance as good as that for the reference. Cost analysis shows the superiority of this concept over other possible solutions such as jacket and monopile. The material cost of the semi-floater concept is half of the jacket's cost and almost two fifth of the monopile's one. This success encourages further developments on both global and component levels. These include more detailed modeling of the components and consideration of deeper water environments.

Chapter 5 focuses on load mitigation strategies. In Subchapter 5.1 the application of passive damping devices is discussed. The torsional passive vibration absorber is applied at the transition piece. It increases the weight of the support structure with +12,3% mass. In the additional costs only the material is respected. Fabrication (formally welding), in-situ execution and the transportation costs are not taken into account. The lowering in the costs only appear over time, when the maintenance of the OWT is elongated and the frequency range in which the OWT is able to harvest energy is extended. Following, in Subchapter 5.2 an in-depth analysis of the reference support structure, the design integration of rotor-nacelle-assembly and the effect of the reference controller in different operational points are carried out. Therefore, the reference support structure, designed by Rambøll, had to be imported into the aero-elastic simulation tool GH Bladed. It has been shown that the complete system is very sensitive to changes of the eigenfrequencies with respect to the driving frequencies of rotor and drivetrain. In conclusion this leads to two different approaches. Firstly a redesign of the rotor and drivetrain with a change on the rotational speed could reduce the necessary load mitigation measures. The second option is the usage of the suggested damping systems, which have to account for the high sensitivity to changes in the eigenfrequencies of the RNA. Tuneable, semi-active or active systems should give a higher safety and effectiveness. In a next step semi-active and active damper systems have to be designed and have to show their potential in the simulation environment. The simulation has to be performed in the frequency but also in the time domain. Active load reduction technology has been implemented for the reduction of the thrust around rated wind speed by the so called Peak Shaver. The results show the mitigation potential. The effect of the Peak Shaver is a trade-off between load mitigation and capacity factor. Tower damping in fore-aft directions by active collective pitch control or individual pitch control has been suggested. Tower damping in sideways direction is suggested by usage of individual pitch control and generator control. The effect of the strategies has to be shown by further refining the system. All four active tower damping strategies are already known in wind energy research. The main problem is the lack of reliable full scale implementations in the field. The consequences for the reliability on the used pitch or generator systems have to be analysed.

Finally, Chapter 6 deals with overall manufacturing costs of the jacket support structure, mainly composed of material, welding and assembly costs. The objective was to detect the share of each of these cost drivers by setting up a suitable cost model. It has been shown that a mass reduction of the jacket does not necessarily lead to a cost optimization since a mass reduction also implies a large number of different cross-sections to be welded. This will raise assembly and welding costs. Another important cost influencing factor is the choice of assembly strategy which can generate cost reduction of approximately 20% for more sophisticated assembly strategies as stated in Chapter 6.2.2. The results show that the reduction of the number of tubular members and welds (version B, see Chapter 6) is the less expensive strategy, although this raises the structural mass of the jacket. A further investigation of version B shall clarify its fatigue behaviour. The presented cost estimations are referred to the reference steel jacket. Synergies with other innovations discussed in this work-package such as innovative materials in Chapter 3 may allow an additional cost reduction. Different transition piece (TP) concepts have been also studied in Chapter 6 with the focus on the evaluation of the advantages and disadvantages of each concept. Based on the evaluated mass and welding volume determined for each TP, a cost estimation has been performed in order to indicate the cost differences of the 3 proposed TP solutions (see Chapter 6). In terms of primary steel fabrication cost, a more cost efficient TP design can be expected when using a box girder or a box-extreme TP. The results indicate that the fabrication

costs of the TP can be reduced by approximately 20% if the TP is further optimized. As well as for the manufacturing of the jacket a reduction in TP costs may be achieved by using innovative sandwich materials described in Chapter 3.



Table 7.1: Estimated potential for cost reduction [in % Cost or Time decrease] due to innovations

Cost element		Sandwich tubes	Adhesively bonded joints	Suction-bucket foundations	Vibro-driven piles	Tuned vibration absorbers (TVA)	Passive damper	Semi-active and active dampers	Transition piece optimisation	Jacket assembly optimisation	Universal Articulated Joint
CAPEX	Consenting/development										
	Project Management										
	Turbine										
	Support structure	25% T	1 %			-12,3%	10%		20%	20%	50%
	Array electrical/shore connection										
	Installation		20 % T	20%	5-10%						
	Decommissioning										
OPEX	Operations and Maintenance		25%			tbd	tbd				
	Insurance										
	Transmission charges										
	Other										